Copyright

By

Michael Findlater

May 2008

The Dissertation Committee for Michael Findlater certifies that this is the approved version of the following dissertation:

Adventures in Main Group Chemistry: From Molecules to Materials

Committee:

_____
Alan H. Cowley, Supervisor

_____
Richard A. Jones

_____
Bradley J. Holliday

_____
Alan Campion

_____
Colin Abernethy

Adventures in Main Group Chemistry: From Molecules to Materials

by

Michael Findlater, B.Sc. Hons

Dissertation

Presented to the Faculty of the Graduate School of

The University of Texas at Austin

in Partial Fulfillment

of the Requirements

for the Degree of

Doctor of Philosophy

The University of Texas at Austin

May 2008

Dedicated to:

My Family, with whom I credit anything and everything that can be said to be good about me

Acknowledgements

The first and most important person I must thank is, of course, Professor Alan H. Cowley. Boss, your boundless enthusiasm for science was both encouraging and contagious in equal measure while your knowledge and insight made me (for better or worse!) the chemist I am today. The colleagues with whom I had the pleasure and privilege to work with in my time in the Cowley group all played important roles in my development in one way or another and I would be remiss without thanking you all. In particular I would to express my everlasting gratitude to Dr Nick Hill for his instruction, help, mentoring and all round 'great bloke-edness'. Dr. Christopher Entwistle, Dr Leonardo Apostolico and Dr Gregor Reeske (who performed the original synthesis of compound **47**) were sources of constant information and I was happy to have such helpful post-doctoral researchers at my disposal. My thanks also go to my fellow graduate students: Lucille Mullins, Dr Jamie N. Jones, Dr Zheng Lu (who successfully isolated the bridged dimer, **55**), Dr Jennifer Moore, Dr Dragoslav Vidovic, Kalyan Vasudevan, Clint Hoberg, Adam Powell, Lauren Gehman, Rachel Butorac and Sarah Swingle. It is unimportant to list your many qualities now, as you all know the high regard in which I hold all of our friendships. It would also be exceedingly churlish of me to ignore the very important role played in my life by Christina Gomez, she remains one of my dearest friends and someone for whom I will always hold the deepest affections. During their unrelenting friendships Kristen and Monica have been sources of laughs, drinks, food, you name it at varying times, my sincerest thanks to you both.

Finally, but perhaps most importantly I want to thank my family. Everything I know most surely about morality and obligation I owe to them, though some may say that is no praise! My mother has been and continues to be an enduring force in all that I believe in about how one should conduct oneself in relation to others and in faith. My brothers have molded the man I have become through gentle guidance and forced attention! My sister, in large part, raised me and is something of a surrogate mother – though I doubt she will thank me for saying so. To my nephews and beautiful niece, I love you all. A special place is however reserved for my Father, who left me all too soon. At no point have I ever felt his absence as keenly as I do now, he was, without a doubt the smartest person I ever met and it saddens me to think he was unable to see me achieve such academic success.

Adventures in Main Group Chemistry: From Molecules to Materials

Publication No._____

Michael Findlater, Ph.D.

The University of Texas at Austin, 2008

Supervisor: Alan H. Cowley

Three synthetic methods have been explored for the preparation of several novel boron-substituted amidinates and guanidinates. The extension of heterocumulene insertion chemistries to boron-aryl, boron-metallocene and boron-transition metal moieties has also been achieved and the mechanism of such insertions is addressed via density functional theory modeling techniques. The reactivity of these complexes is also explored, mainly through halide abstraction methodologies to generate boron

cations, which are potent Lewis Acids and may be useful in promoting organic transformations or in the polymerization of ethylene.

The synthesis and characterization of the elusive monomeric low valent carbenoid boron(I), a compound with a formal lone pair located upon the boron center, has been lacking. The suitability of the guanidinate ligand system to support such a species is also discussed and a combined experimental and theoretical approach to this highly topical problem is also presented.

Thirdly, the use of photovoltaics (devices which convert solar energy directly into electricity) as an alternative source of energy outwith fossil fuel technologies is a rapidly growing area of interest. Initial efforts to use a novel approach, which incorporates inorganic nanocrystals wired into a conducting polymer matrix, are also presented. Successful synthetic approaches to the gallium, aluminum and indium monomeric precursors suitable for electropolymerization were developed. These compounds proved to be effective starting points for the generation of conducting polymers with embedded III/VI (Ga_2S_3) nanocrystals with further studies currently underway as to their III/V (InP, GaAs) compatriots.

Finally, a retrospective of projects that may best be described in terms of the moniker “Loose Ends and Future Directions” will be presented. The aim of which will be to serve as a useful guidepost for further studies in the fields and topics discussed.

Table of Contents:

List of Figures

List of Schemes

List of Tables

CHAPTER 1: Synthetic Approaches to Amidinate and Guanidinate Complexes of Boron

INTRODUCTION

Amidinate Ligands

A major advantage of the use of the amidinate ligand is the ability to tune, with minimum synthetic effort, the steric and (to a lesser extent) the electronic environment of the resulting complex. This flexibility affords a degree of control over the chemistry at the metal center and is responsible for the widespread use of amidinates as supporting ligands in main group, transition metal, lanthanide and actinide chemistry [1].

Amidinate anions function typically as four-electron, N-donor bidentate chelating ligands and have the general formula $[RNC(R')NR'']^-$. Early work in this field was focused on the benzamidinate derivative $[PhC\{NSiMe_3\}_2]^-$ [1(b)], which is readily synthesized *via* the reaction of $LiN(TMS)_2$ with benzonitrile [2]. More recently, amidinate chemistry has witnessed a significant expansion in the number and types of ligands by elaboration of both the N- and C-substituents. Moreover, several new methods have emerged for the synthesis of metal amidinate complexes, including: (i) protonolysis reactions employing neutral amidines; (ii) insertion of carbodiimides into metal alkyl bonds (iii) reaction of metal halides with N,N,N′-tris(trimethylsilyl)amidines and (iv) salt metathesis reactions of lithium amidinates (prepared by treatment of alkyl lithium reagents with carbodiimides) with metal halides.

Amidinate complexes featuring group 13 metal-alkyl and metal-halide fragments have been the subjects of sustained interest during the last decade [3, 4] due to the discovery of a number of useful applications in key technological areas. For example, gallium amidinate complexes represent promising single-source precursors for nitride materials [4(c)] while amidinate-supported alkylaluminum cations have proved to be active catalysts for olefin polymerization [5]. However, despite this increased attention to and development of the field in general, the chemistry of boron-substituted amidinates remains relatively unexplored.

Considering the rich chemistry displayed by these group 13 species and their relative ease of synthesis, the paucity of boron-substituted amidinate ligands in the literature borders on negligence. Indeed, examples of such compounds obtained by rational synthetic routes are confined to the dibromo compound **1** [6] and the chloro-phenyl derivative **2** [7]. A related example is the vinylidene-amidinate compound **3**, which was obtained serendipitously via the *in situ* generation of an amidinate fragment, followed by displacement of Cl^- from BCl_4^-, during reaction of the propylidyne complex $[Cp(CO)_2Mn{\equiv}CEt][BCl_4]$ with $^tBuN{=}C{=}N^tBu$ and NEt_3 [8]. The bis(trifluoromethyl)-substituted amidinate **4** was formed by rearrangement of an unstable adduct resulting from the [2+2] cycloaddition of $(CF_3)_2B{=}NMe_2$ to $PhN{=}C{=}NPh$ [9]. In the present work the syntheses, reactivities and molecular structures of a range of new boron-amidinate complexes are reported. In particular, their abilities to function as appropriate ligand supports for the isolation of reactive boron species, namely boron cations and terminal borylenes, will be explored.

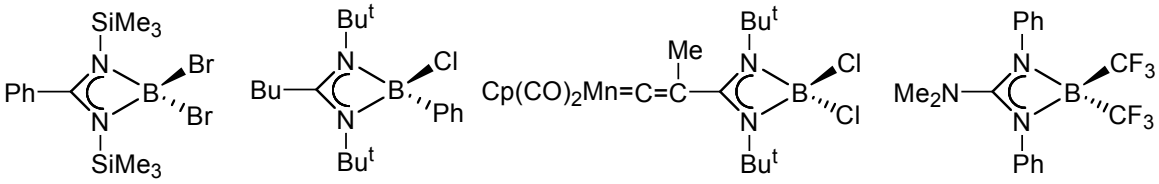

Figure 1-1. Examples of previously synthesized boron-amidinates.

Results and Discussion

Synthesis via trimethylsilyl-halide elimination

The elimination of halotrimethylsilane as the thermodynamic driving force in a metathesis reaction is an attractive synthetic option owing to the ease of removal of the volatile by-products. In terms of amidinate chemistry, this methodology provided a facile route to access the novel boron-substituted species, $[PhC\{N(SiMe_3)\}_2]BCl_2$ (**6**), and the known compound **1**, as outlined in Scheme 1.1.

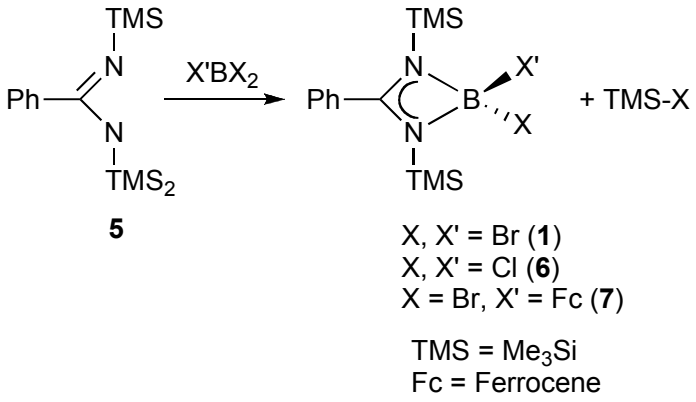

Scheme 1.1. Trimethylsilyl-halide elimination methodology.

Although **1** has been reported previously [6], the characterization of this compound was based solely on an infrared spectrum and micro-analytical data. Curiously, in the same report, it was mentioned that attempts to prepare **6** resulted in the isolation of an uncharacterized yellow oil [6]. However, it was found that crystalline **6** is indefinitely

stable under an inert atmosphere and shows no sign of reverting to an oil, even upon gentle heating.

In order to assess the structural and bonding features, single-crystal X-ray diffraction experiments were performed on **1** and **6**. Both compounds crystallize as monomers in the monoclinic space group *C*2/*c*, and have very similar unit cell dimensions. The molecular structure of **1** is illustrated in Fig. 1 along with the atom numbering scheme. An identical numbering scheme was employed for **6**.

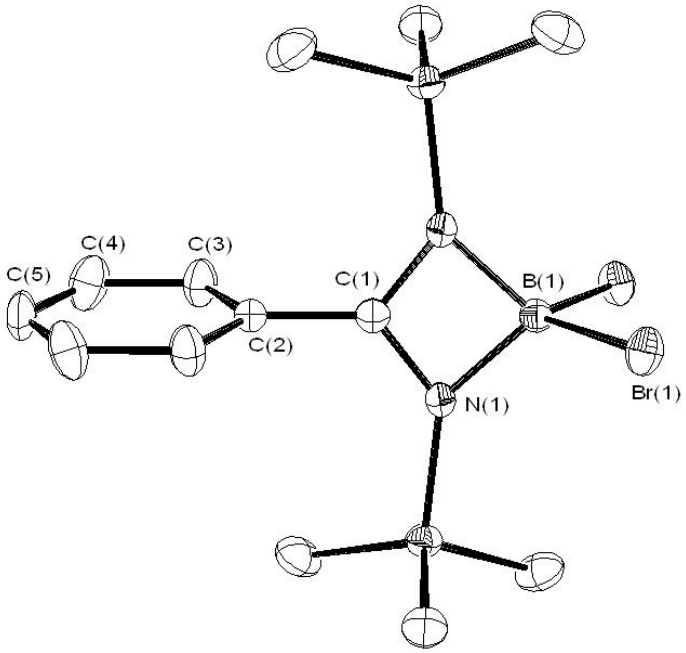

Fig. 1.2. ORTEP diagram of **1** with thermal ellipsoids at 40% probability and H-atoms omitted for clarity.

Individual molecules of **1** and **6**, which reside on a two-fold axis passing through atoms B(1)-C(1)-C(2)-C(5), feature a four-membered B-N-C-N chelate ring and a phenyl group which is orthogonal to the B(1)-N(1)-C(1)-N(1A) plane. The B-X, B-N, and C-N

bond distances in **1** and **6** are similar to those reported for **2**-**4**, and the related amido-pyridyl compounds **8** and **9** [10, 11]. The C(1)-N(1) bond distances for **1** and **6** are 1.339(3) and 1.332(4) Å, respectively. These values are approximately intermediate between typical C-N double bond and C-N single bond distances. Moreover, the B-N-C-

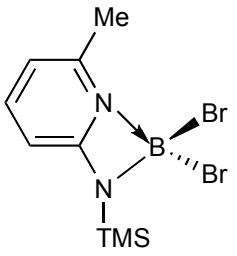

8

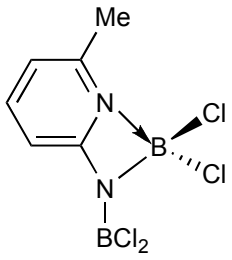

9

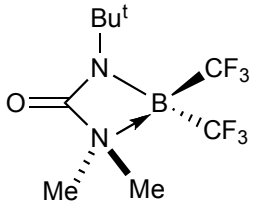

10

N torsion angles for both compounds are zero, indicating delocalization about the N-C-N junction. The B-N bond distances of 1.559(4) (**1**) and 1.580(5) Å (**6**) fall within the typical range of 1.55-1.61 Å for a B-N bond derived from a four-coordinate boron atom bound to a three-coordinate nitrogen atom [12]. In comparison, the B-N bond distances in **10**, an amido boron compound containing a base-stabilized, three-coordinate boron atom, are 1.535(8) and 1.635(8) Å [13]. The bite angles of the amidinate fragment (N(1)-B(1)-N(1A)) are 85.2(3) (**1**) and 86.1(3)^{o} (**6**), and thus *ca*. 4 ^{o} wider than the equivalent angle (81.6^{o}) in **2** [7], but closer to the mean bite angles of 84.0^{o} in **3** and 83.8^{o} in **4** (angles averaged for two crystallographically independent molecules in the asymmetric units of **3** and **4**) [8, 9]. By contrast, the N-Al-N bond angle in the congeneric complex [PhC{N(TMS)}$_2$]AlCl$_2$ is 72.9(2)^{o} and the Al-N bond distance is 1.882(3) Å [6]. The average N-B-X bond angle is 114.6^{o} in **1** and 114.8 ^{o} in **6**, hence the geometry about the boron atom is appreciably distorted from that of a regular tetrahedon.

The ^{1}H, $^{13}C\{^{1}H\}$, and ^{11}B NMR spectra of **1** and **6** confirm that the C_{2v}-symmetric structures observed in the solid-state are retained in solution. The ^{11}B NMR spectra exhibit intense singlet resonances at δ -3.8 (**1**) and 6.0 (**6**), values which are typical for a four-coordinate boron atom [14]. The ^{1}H and $^{13}C\{^{1}H\}$ spectra exhibit peaks due to the phenyl group and two equivalent trimethylsilyl groups. A low-intensity $^{13}C\{^{1}H\}$ peak attributable to the carbon atom of the NCN fragment was detected at δ 174.

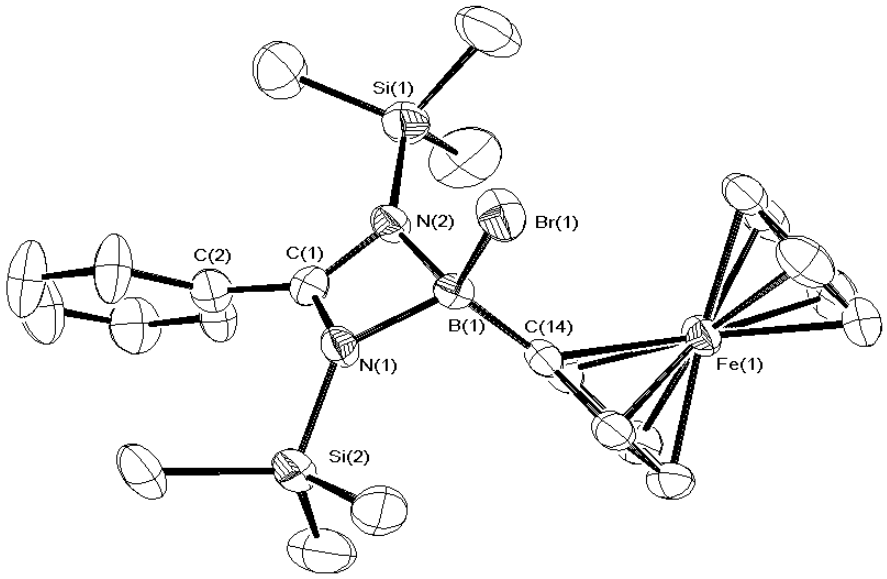

Fig. 1.3. ORTEP diagram of **7** with thermal ellipsoids at 40% probability and H-atoms omitted for clarity.

Treatment of a toluene solution of $FcBBr_2$, ferrocenyldibromoborane, with an equimolar toluene solution of **5** at ambient temperatures afforded, after work up, the ferrocenyl-substituted amidinate **7** as an orange powder. Recrystallisation from a saturated toluene solution gave orange block crystals suitable for X-ray diffraction

studies (Figure 2). As in the cases of **1** and **6**, the B-N-C-N heterocycle is planar and the boron atom possesses a distorted tetrahedral geometry (average bite angle 105.3°, and a mean N-B-Br bond angle of 112.0°. The other metrical parameters are very similar to those of the compounds previously discussed.

Synthesis via salt metathesis

Although the trimethylsilyl halide elimination method proved to be effective for the preparation of the $[RC(NR')_2]BX_2$ complexes described above, it was necessary to employ a different synthetic strategy to extend the range of these compounds. In this context, the salt metathesis reaction between BX_3 and a lithium amidinate $[RC(NR')_2]Li$ seemed like a more versatile approach for the introduction of a wide variety of R and R′ groups, thereby offering the possibility of tuning the steric environment of the BX_2 fragment. Indeed, the validity of this approach has already been demonstrated by the successful synthesis of mono- and bis(amidinate) complexes of aluminum and gallium [3, 4].

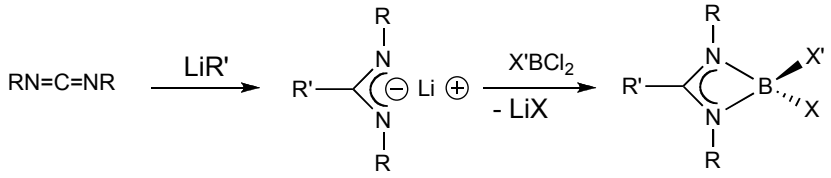

11: X, X' = Cl, R' = Me, R = Cy
12: X, X' = Cl, R' = Mes*, R = Cy
13: X, X' = Cl, R' = Me, R = ^{i}Pr
14: X = Cl, X' = Ph, R' = ^{t}Bu, R = Cy
15: X = Cl, X' = Ph, R' = ^{n}Bu, R = Cy

Scheme 1.2. Salt metathesis methodology.

The requisite lithium amidinates were prepared by addition of diethyl ether solutions of LiMe, ^{n}BuLi, ^{t}BuLi or LiMes* (Mes* = 2,4,6-tri(tert-butyl)phenyl) to cold (-78 ^{o}C) diethyl ether solutions of either 1,3-dicyclohexylcarbodiimide or 1,3-diisopropylcarbodiimide. Subsequent treatment with one equivalent of $X'BX_2$ and work-up of the reaction mixtures afforded good yields of the desired boron amidinate complexes **11-14** as colorless solids.

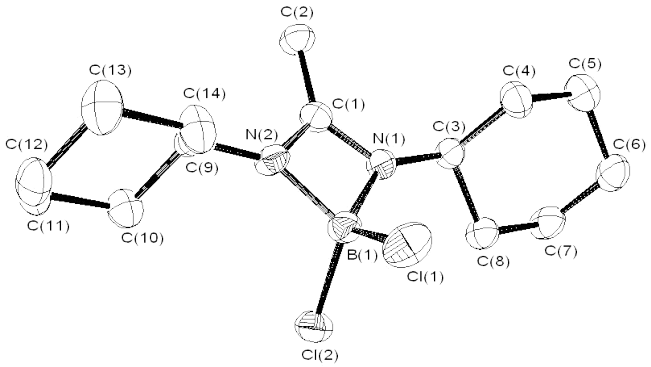

Fig. 1.4. ORTEP diagram of **11** with thermal ellipsoids at 40% probability and H-atoms omitted for clarity.

Single crystals of **11-15**, suitable for X-ray diffraction experiments, were obtained by recrystallization from toluene or pentane solution. The molecular structures of **11** (Fig. 3) and **12** (Fig. 4) are very similar to those of the boron amidinates discussed above, in the sense that the ligand is chelated to the BCl_2 fragment in a symmetrical bidentate fashion, resulting in a planar, four-membered B-N-C-N heterocycle with a delocalized N-C-N moiety. As expected, the bond distances and angles for **11** and **12** are also similar to

those for **1** and **6**. Likewise, the N(1)-B(1)-N(2) bite angles and average N-B-Cl bond angles of 82.17(2) and 115.23^{o} for **11**, and 82.1(4) and 115.4^{o} for **12**, indicate substantial distortion from the ideal tetrahedral value. However, the N(1)-C(1)-N(2) bond angles of 101.24(3)^{o} and 100.7(3)^{o} in **11** and **12**, respectively, are slightly more acute that those in **1** and **6** (av. 104^{o}).

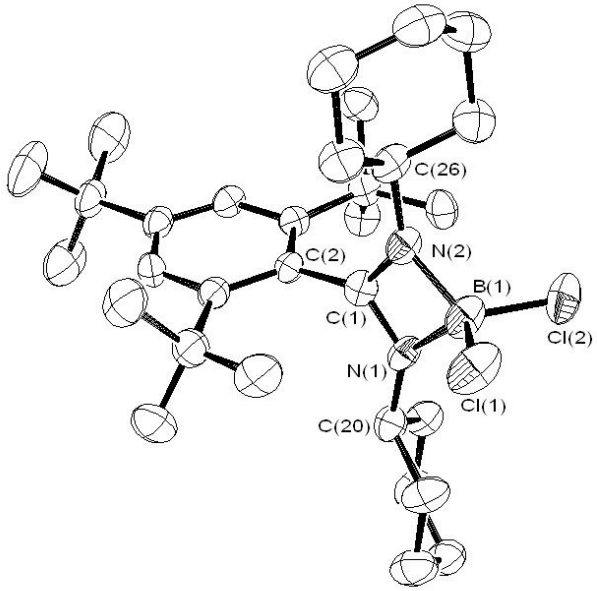

Fig. 1.5. ORTEP diagram of **12** with thermal ellipsoids at 40% probability and H-atoms omitted for clarity.

Single-crystal X-ray diffraction studies were also carried out on both **14** and **15** to assess their structural and bonding characteristics. Compounds **14** and **15** crystallize as monomers and there are no unusually short intermolecular contacts. The molecular structure of **14** is illustrated in Fig. 5. Both molecules feature an essentially planar B–N–C–N ring and an approximately tetrahedral geometry around the boron atom. The B–N–

C–N four-membered ring torsion angles are 3.35(10)° and 1.1(2)° for **14** and **15**, respectively.

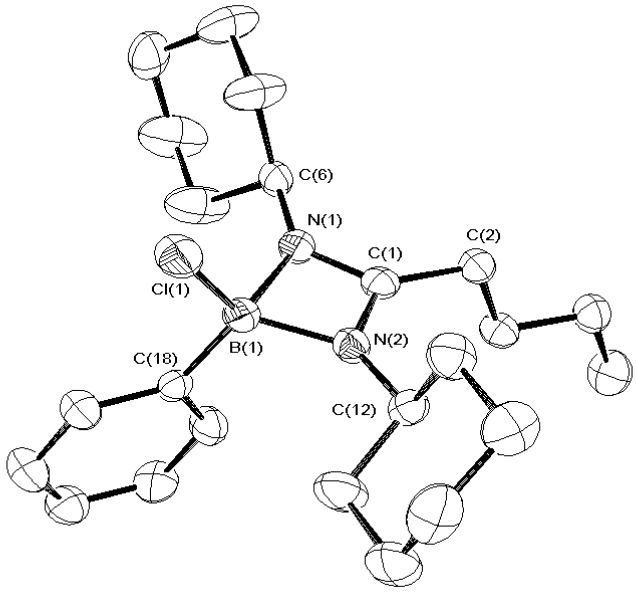

Fig. 1.6. ORTEP diagram of **14** with thermal ellipsoids at 40% probability and H-atoms omitted for clarity.

The B–N, B–Cl, and B–C(Ph) bond distances are similar to those reported previously for [nBuC{N(tBu)}$_2$]BCl(Ph) [15]. The C–N bond distances (averages 1.34035(19) Å for **14** and 1.3325(4) Å for **15**) are intermediate between those anticipated for single and double bonds and are indicative of delocalization at the NCN moiety. The B–N bonds in **14** and **15** are similar in length and once more fall in the range observed for B–N bonds in four-coordinate boron centers bound to three-coordinate nitrogen atoms [12].

The molecular structure of **13** was of interest to determine the effect, if any, of changing the steric bulk of the nitrogen and boron substituents (see Fig. 6) Overall, the

metrical parameters for **13** are very similar to those for **14** and **15** (Table 1.1). However, the B–N–C–N ring is less distorted from planarity (0.69(18)°) than those of the cyclohexyl-substituted amidinates, presumably due to the smaller size of the diisopropyl substituent.

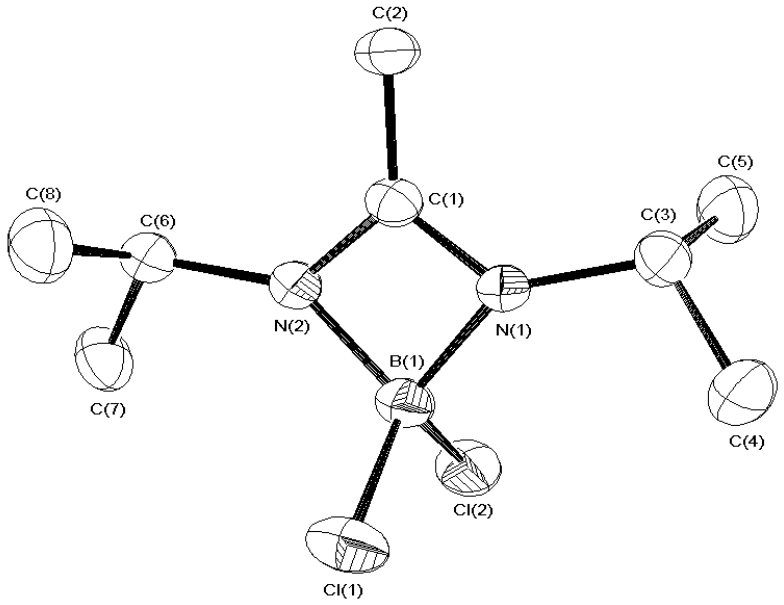

Fig. 1.7. ORTEP diagram of **13** with thermal ellipsoids at 40% probability and H-atoms omitted for clarity.

Table 1.1 Selected crystal data, data collection and refinement parameters for **1, 6, 7, 11, 12, 13, 14 and 15**

	1	**6**	**7**	**11**	**12**	**13**	**14**	**15**
Formula	$C_{13}H_{23}N_2BBr_2Si_2$	$C_{13}H_{23}N_2BCl_2Si_2$	$C_{23}H_{32}BBrFeN_2Si_2$	$C_{14}H_{25}N_2BCl_2$	$C_{37}H_{57}N_2BCl_2$	$C_8H_{17}N_2BCl_2$	$C_{23}H_{36}N_2BCl$	$C_{23}H_{36}N_2BCl$
Formula weight	434.14	345.22	539.26	303.07	611.56	222.95	386.80	386.80
Crystal system	Monoclinic	Monoclinic	Monoclinic	Monoclinic	Monoclinic	Triclinic	Monoclinic	Monoclinic
Space group	*C2/c*	*C2/c*	P2(1)/c	*P2(1)/n*	*P2(1)/n*	P-1	P2(1)/n	P2(1)/c
a/Å	15.329(5)	15.026(5)	31.462(5)	13.590(5)	13.338(5)	7.409(5)	8.893(5)	9.939(5)
b/Å	10.887(5)	10.799(5)	11.215(5)	7.324(5)	18.972(5)	8.127(5)	17.194(5)	20.598(5)
c/Å	13.019(5)	12.711(5)	29.771(5)	16.451(5)	15.336(5)	10.436(5)	14.511(5)	11.052(5)
α/°	90	90	90	90	90	94.529(5)	90	90
β/°	116.223(5)	114.477(5)	99.424(5)	94.622(5)	92.677(5)	92.529(5)	92.754(5)	93.204(5)
γ/°	90	90	90	90	90	104.188(5)	90	90
V/Å^3	1949.1(13)	1877.2(13)	10363(5)	1632.1(14)	3867(15)	606.0(6)	2216.3(16)	2259.1(16)
Z	4	4	4	4	4	2	4	4
P_{calcd}/g cm^{-3}	1.479	1.222	1.383	1.233	1.050	1.222	1.159	1.137
F(000)	872	728	4448	648	1328	236	840	840
Crystal size/mm	0.30 x 0.20 x 0.20	0.20 x 0.20 x 0.20	0.15 x 0.15 x 0.15	0.30 x 0.20 x 0.20	0.20 x 0.20 x 0.20	0.10 x 0.10 x 0.05	0.30 x 0.20 x 0.20	0.10 x 0.10 x 0.10
θ range/°	2.39 to 26.99	2.59 to 26.99	1.82 to 27.49	2.48 to 24.99	1.71 to 25.00	3.11–27.48	2.75–27.49	2.05–27.48
No. of reflns. collected	3207	3282	34696	5482	13301	2750	9399	8308
No. of indep reflns.	1718	2045	21180	2883	6811	1588	5028	5147
R1[$I > 2\sigma(I)$]	0.0259	0.0543	0.0634	0.0435	0.0653	0.0486	0.0432	0.0590
wR_2 (all data)	0.0636	0.1569	0.0986	0.1191	0.1990	0.1095	0.1019	0.1366
Peak and hole/e Å^{-2}	0.406 and 0.371	0.485 and -0.325	0.691 and -0.762	0.273 and -0.287	0.446 and -0.300	0.380 and -0.269	0.311 and -0.256	0.436 and -0.487

Synthesis via carbodiimide insertion

One of the potential routes, outlined in Scheme 1.3, to the desired compounds features the insertion of a carbodiimide into a boron–carbon or boron–heteroatom bond of a boron(III) derivative. In fact, insertion reactions of this type represent part of a broader tapestry of heterocumulene insertion processes that includes commercially and environmentally important CO_2. In an early mechanistic study of the insertion of a variety of heterocumulenes into Zr–carbon bonds, Gambarotta *et al*. [16] proposed that the prerequisite initial step involves coordination of one of the terminal heteroatoms to the Lewis acidic zirconium center. A similar conclusion has since been drawn by others [17]. Additional support for this proposal has also been forthcoming from theoretical studies of the insertion of CO2 into the Rh(III)–H bond [18] and of carbodiimide insertions into Al–Me and Al–NMe2 bonds [19]. Interestingly, and in contrast to $Al_2(NMe_2)_6$ and aluminium alkyls, all attempts to insert CyN=C=NCy (Cy = cyclohexyl) into $B(NMe_2)_3$ and BEt_3 were not successful. However, it did prove possible to isolate and structurally characterize an example of the putative initial Lewis acid–base complex (**16**) from the reaction of $PhBCl_2$ with CyN=C=NCy, subsequent heating of which in toluene solution furnishes the amidinate complex, $[PhC\{NCy\}_2]BCl_2$ (**17**).

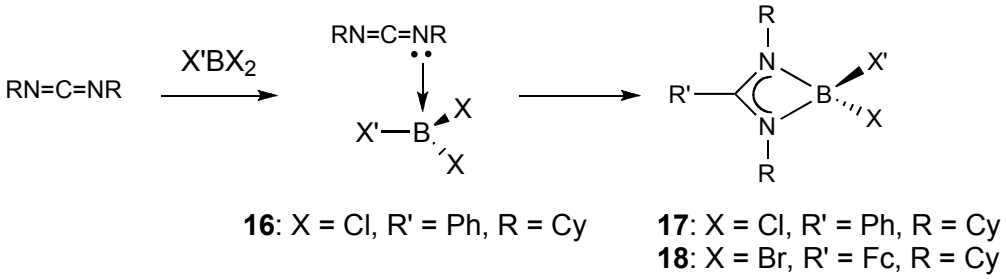

Scheme 1.3. Carbodiimide insertion methodology

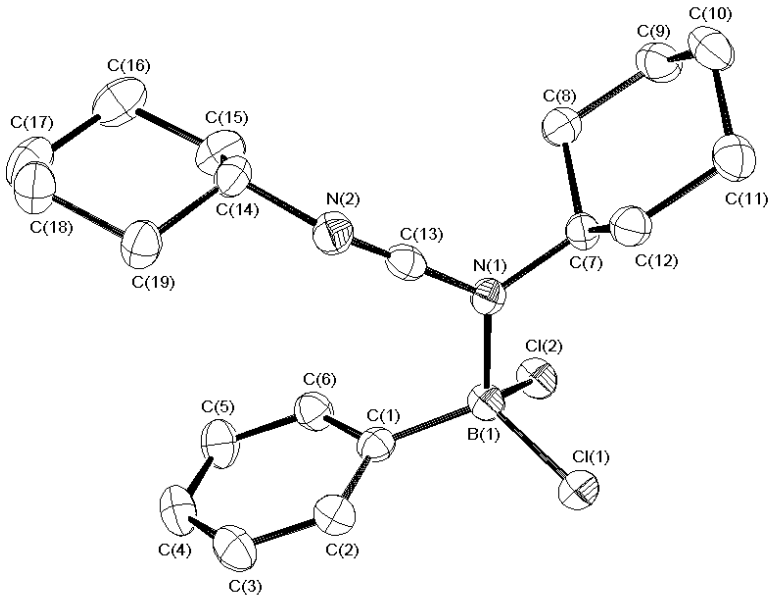

Fig. 1.8. ORTEP diagram of **16** with thermal ellipsoids at 40% probability and H-atoms omitted for clarity.

Treatment of $PhBCl_2$ with an equimolar quantity of CyN=C=NCy in hexane solution at ambient temperature results, after isolation and crystallization, in a 96% yield of **16**. The X-ray crystal structure of **16** (Fig. 7) reveals that one of the nitrogen atoms of the carbodiimide, N(1), forms a donor–acceptor bond of length 1.583(3) Å to the boron atom of $PhBCl_2$. As a consequence of the donor action on the part of the carbodiimide, the C(13)–N(1)–C(7) angle becomes more acute than the corresponding angle at N(2) and the C(13)–N(1) bond distance is ~ 0.12 Å longer than that of the C(13)–N(2) bond. Although there is some departure from the ideal angles, the geometry at N(1) is trigonal planar (sum of angles 359.9(2)°). The donor function is also evident from the fact that the sum of bond angles at B(1) is 334.0(2)°. In the case of $B(C_6F_5)_3$ as a reference Lewis acid, the departure of the sum of bond angles at boron from the ideal value of 360° has been taken as a measure of donor strength of the Lewis base [20]. Another significant

structural feature is the close proximity of the *ipso*-carbon of the phenyl ring to the carbodiimide carbon, a conformation that favors the migration of the phenyl group from B(1) to C(13) (the C(1)…C(13) distance is 2.796(7) Å and the C(1)–B(1)–N(1)–C(13) torsion angle is 7.5°). Upon migration of the phenyl group, formation of amidinate **17** is accomplished by means of a rotation of the N(1)–C(13) bond followed by ring closure. Despite making several attempts, it was not possible to isolate or detect the second intermediate by ^{11}B NMR. Compound **17** was prepared independently via the salt metathesis reaction of [Ph{NCy}$_2$Li] with BCl_3 and characterized by X-ray crystallography.

To gain additional mechanistic insights, the overall process was modeled by DFT calculations [21, 22]. In the interest of computational efficiency, the carbodiimide MeN=C=NMe was used instead of CyN=C=NCy. The profile for the reaction of MeN=C=NMe with $PhBCl_2$ features two intermediates (IM1 and IM2) and two transition states (TS1 and TS2) leading to product **17*** as depicted in Fig. 8. The overall reaction is exergic by 245.5 kcal mol^{-1}. The first intermediate, IM1, is a donor–acceptor complex between MeN=C=NMe and $PhBCl_2$. Comparison of the metrical parameters for **17** with those of the model complex, IM1, reveals that they are in good agreement (~2%) with the exception of the N-B bond distance which is overestimated by 3.7%. The first transition state, TS1, features a four-centre interaction between boron, nitrogen, the carbodiimide carbon and the ipso-carbon of the phenyl ring (C···C = 1.871 Å). The phenyl migration is completed by cleavage of the Ph–B bond in concert with mutation of the N→B dative bond into an N–B σ-bond. Transition state TS2, which is lower in energy than TS1, involves rotation around a C–N bond such that the two nitrogen atoms attain a

conformation that will permit chelation. Finally, chelation of both nitrogen atoms to the BCl_2 moiety completes the formation of the boron amidinate, $[PhC\{NMe\}_2]BCl_2$, (**17***). The ^{11}B chemical shifts for IM1, IM2, and **17*** were also calculated. The calculated (GAIO) values of δ 10.5 and 8.5 for IM1 and **17***, respectively, are in good agreement with those obtained experimentally for **16** and **17**, while the calculated value of δ 33.8 for IM2 falls within the range observed for similar three-coordinate boron compounds [14]. The general features of this mechanism are similar to those discussed for the insertion of heterocumulenes into Rh–H [18], Al–C [19] and Al–N [19] bonds.

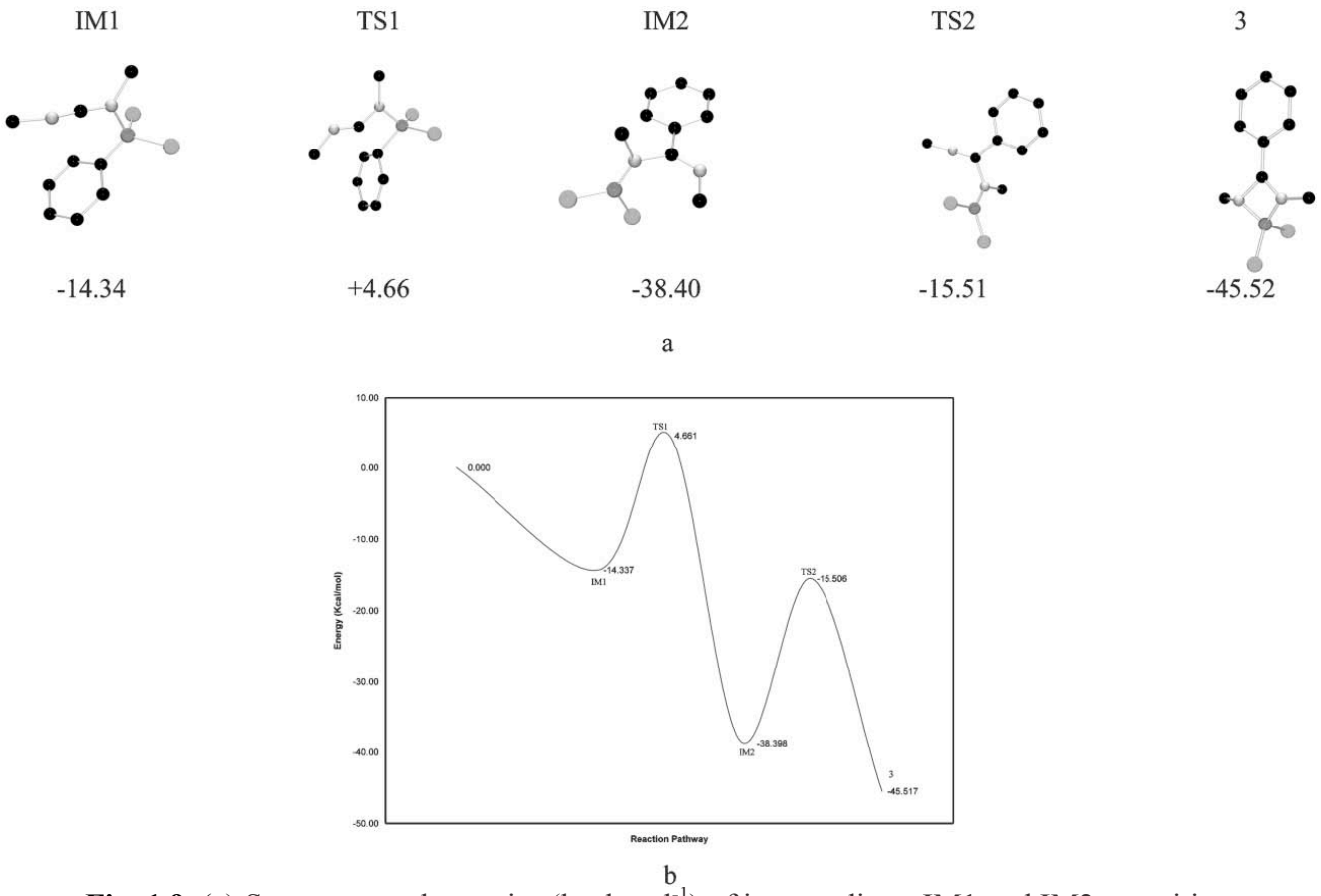

Fig. 1.9. (a) Structures and energies (kcal mol^{-1}) of intermediates IM1 and IM2, transition states TS1 and TS2, and amidinate **17*** as calculated by DFT. (b) Graphical representation of the calculated energy profile of the reaction between $PhBCl_2$ and MeN=C=NMe

The reaction of equimolar quantities of 1,3-dicyclohexylcarbodiimide and ferrocenyldibromoborane $FcBBr_2$ in hexane solution at room temperature afforded, upon work-up, orange crystalline **18** in good yield. The ^{11}B NMR spectrum of **18** revealed an intense resonance at δ -4.05, which falls in a similar region to that observed for **1**, thus suggesting that the desired insertion reaction had occurred. ^{1}H and $^{13}C\{^{1}H\}$ NMR data were also consistent with such a suggestion.

Recrystallization of **18** from toluene solution produced a crop of orange block crystals suitable for X-ray diffraction experiments. The X-ray crystal structure (Fig. 9) confirmed the structure proposed for **18**. As in the case of the boron amidinates discussed earlier, the B-N-C-N heterocycle is planar and the boron atom possesses a distorted tetrahedral geometry (bite angle 83.5(2)°, and a mean N-B-Br bond angle of 114.9°. The other metrical parameters are very similar to those of the compounds previously discussed.

The incorporation of a ferrocene unit into the framework of an amidinate ligand has precedent in the work of Arnold *et al.* [23, 24], who prepared a ferrocene-substituted amidine *via* the reaction of FcLi with 1,3-dicyclohexylcarbodiimide and subsequently explored its coordination chemistry with Fe(II), Co(II) and Rh(I) halides. To the best of my knowledge, **18** represented the first example of a p-block complex of the ferrocenylamidinate, and also constitutes the first report of the insertion of a carbodiimide ligand into a Cp-group 13 element bond.

The C_5H_5 plane of the Fc moiety is almost coplanar with the NCN plane of the amidinate ligand (torsion angles N(1)-C(1)-C(14)-C15) 10.0(5)°, N(2)-C(1)-C(14)-C(18) 15.1(6)°), which may indicate some degree of π-π interaction between the two fragments (C(1)-C(14) 1.450(4) Å) This arrangement contrasts with that of the uncomplexed

ferrocene-substitued amidine, in which the Fc group is approximately perpendicular to the NCN plane (corresponding torsion angles ~ 60°), and those of the Fe(II), Co(II) and Rh(I) complexes in which the torsion angle is ~ 45° [23, 24].

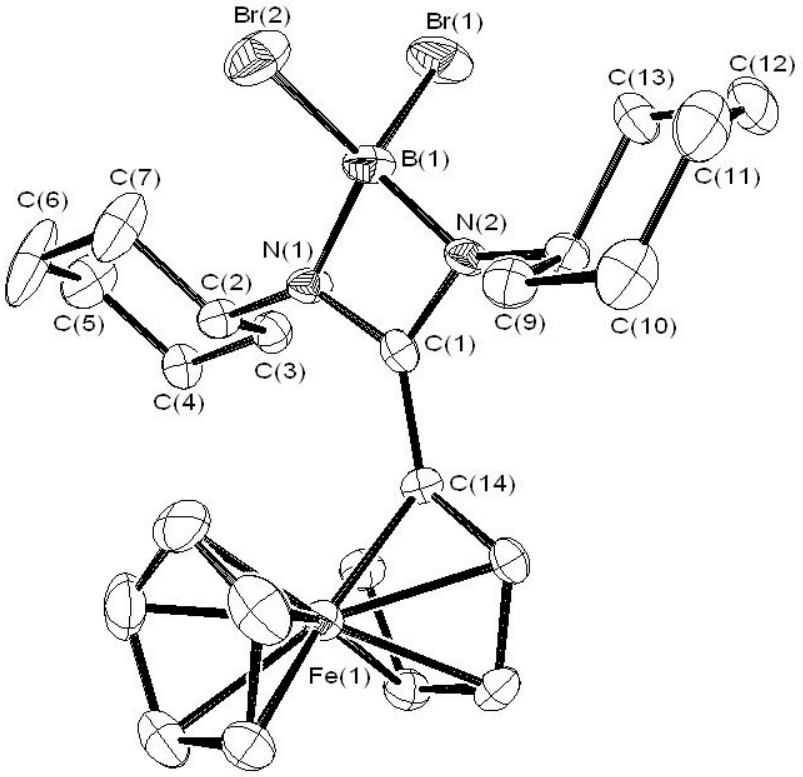

Fig. 1.10. ORTEP diagram of **18** with thermal ellipsoids at 40% probability and H-atoms omitted for clarity.

Reactive Boron Species Supported by Amidinate Fragments

Boron Cations

Perhaps the defining aspect of the group 13 element reactivity is their exceptional Lewis acidity, which is a result of their electron deficiency. The observed bonding and reactivity of these species derives mostly from their tendency to fill both their coordination sphere and their valence shell. This property is most notably employed in olefin polymerization, where three-coordinate boron species are used as Lewis acid co-catalysts due to their ability to readily abstract hydrides, halides etc. to produce anionic four-coordinate species [25]. Due to the increasing volume of research directed toward reactivity enhancement (increased Lewis acidity) while maintaining synthetic utility, recent work has focused on cationic members of the boron group [26].

Boron cations can be classified into three distinct groups, based upon the coordination number at the boron center. Borinium cations (**I**) are two-coordinate species and feature substituents which can donate lone-pair electron density *via* π-interactions. Borenium cations (**II**) are and feature σ-bonded substituents that are supplemented by a dative ligand interaction which both reduces some of the electron deficiency and helps to fill a vacant coordination site. The most common class of boron cation is the boronium cation (**III**), which possesses a four-coordinate tetrahedral geometry. These cations differ from borenium cations by addition of a second dative ligand interaction, thus further stabilizing the boron center by filling the coordination sphere and a concomitant 'relief' of the electron deficiency.

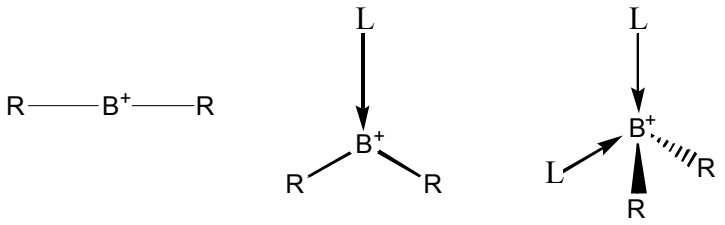

borinium (**I**) borenium (**II**) boronium (**III**)

Fig. 1.11. Classes of boron cation described in the literature

The donor ligands in both **II** and **III** serve to partially quench the positive charge at the boron center, however, the innate reactivity of these cations persists such that characterization can prove to be rather difficult. The ^{11}B chemical shifts observed for these cations in are diagnostic and are typically found significantly downfield of those for their neutral three-coordinate precursors or analogues. In general, more cationic charge density on the boron center and hence a lower degree of stabilization results in a more downfield shifted ^{11}B resonance. The presence of alkyl-substituents, for example, in **I** can render ^{11}B resonances in the δ = 60 ppm range [27]. Other characterization methods are of limited utility, mass spectrometry is usually confined to gas-phase studies, infrared spectroscopy suffers from less apparent stretching frequencies and crystal structures (whilst extremely useful) depend on the crystalline integrity and solid-state stability of such species. Indeed, only five examples of crystallographically characterized borinium and borenium ions had been reported prior to Nöth's review of the field in 1985 [28]. Previous reviews on the topic of boron cations focused largely on their synthesis and characterization. However, although there have been synthetic advances over the past 20 years, often involving unique routes to highly stabilized species, much of the interim work in the area has focused on the gas-phase reactivity of borinium ions. The

development of condensed-phase applications has, however, been initiated with promising results. Thus, advances in the syntheses of novel condensed-phase borocations as well as reactivity studies, both in the gas and condensed phases, prompted the recent excellent review by Piers *et al*. [29] and the reader is directed to their article for an in-depth discussion of boron cations.

Given the foregoing, it was decided to explore the use of amidinates as supporting ligands for the stabilization of boron cations. The objectives were two fold, namely: a) to study these highly interesting compounds in the solid state owing to the paucity of previous reports of structurally characterized cationic boron species, and b) to generate species which might prove to be useful as Lewis acid catalysts. In this regard, the mono-halo derivatives **14** and **15** seemed to be ideal choices as appropriate cationic precursors due to their ease of synthesis, the moderate steric-shielding imparted by their cyclohexyl-substituents and the related synthesis of a "PhB+" species stabilized by a bidentate chelating β-diketiminate ligand [30].

Synthesis via halide abstraction chemistry

Due to the inherent stability of the coordinatively saturated four-coordinate boron center in both **14** and **15** it was deemed appropriate to employ synthetic routes to cationic species which utilized an 'abstractive' approach (Scheme 1.4). This method avoids the implicit involvement of a five-coordinate transition state, which is strongly disfavored due to the steric constraints of the small, central, boron atom.

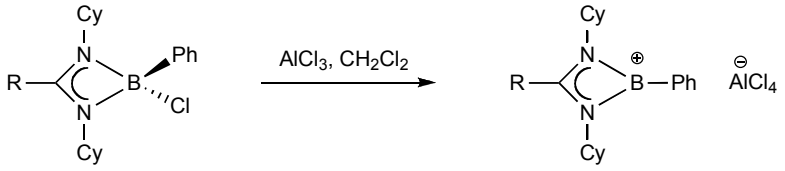

14: R = ^{t}Bu
15: R = ^{n}Bu

19: R = ^{t}Bu
20: R = ^{n}Bu

Scheme 1.4. Halide abstraction route to boron cations.

Treatment of a methylene chloride of either **14** or **15** with an equimolar amount of aluminum chloride, $AlCl_3$, resulted in the isolation of an off-white powder. This powder displayed a sharp peak in the ^{27}Al NMR (δ = 103.58 and 103.81 respectively) consistent with formation of the tetrachloroaluminate counterion, however, no discernible peak corresponding to the boron center was evident in the ^{11}B NMR. Repeated attempts at crystallization using a variety of solvents, solvent mixtures and crystallization techniques afforded no samples suitable for X-ray diffraction. Frustrated by the seeming lack of reactivity displayed by both **14** and **15** these compounds were treated with a variety of 'halide-abstractors' such as $NaBF_4$, TMS-OTf, $AgBF_4$ etc. all to no avail.

In one instance, it was possible to isolate a crystalline sample of a boron cation supported by an amidinate fragment *via* sequential *in-situ* treatment of **5** with $PhBCl_2$ followed by $AlCl_3$. The connectivity of **21** is shown in Figure 1.12. **21** crystallized in the monoclinic space group *P* 1 21/n 1 as two "half-cations" and an $AlCl_4$ anion. Unfortunately, the crystallographic symmetry of the compound meant that the identity of the boron and carbon atoms could not be determined unambiguously, thus a discussion of the metrical parameters at this junction would be somewhat misleading, although the data is sufficient to show the halide abstraction was successful.

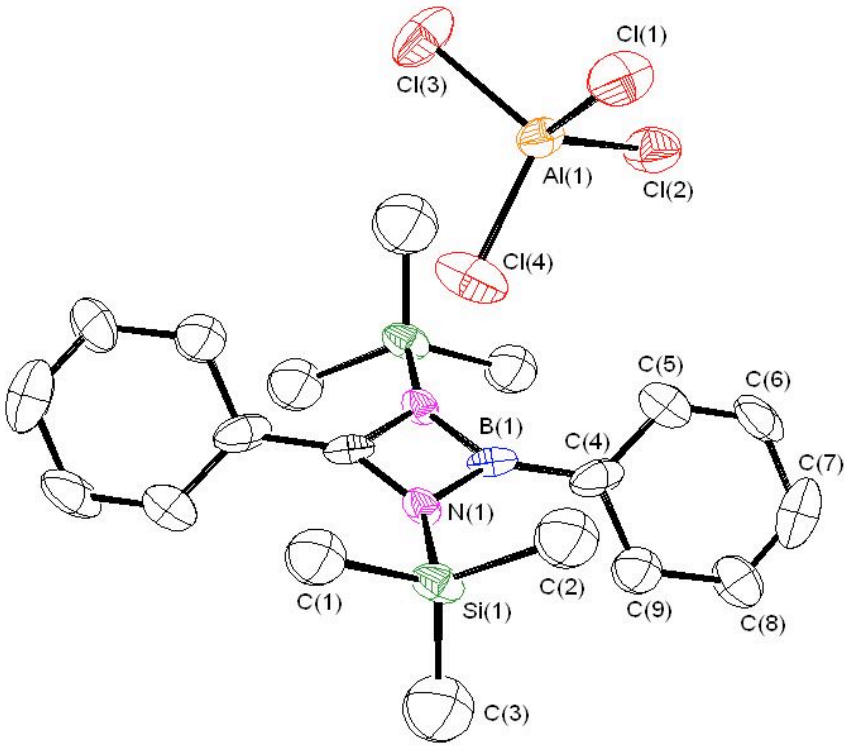

Fig. 1.12. ORTEP diagram of **21** with thermal ellipsoids at 40% probability and H-atoms omitted for clarity

Table 1.2 Selected crystal data, data collection and structure refinement parameters for **16, 17, and 18**

	16	**17**	**18**	**21**
Formula	$C_{19}H_{27}N_2BCl_2$	$C_{19}H_{27}N_2BCl_2$	$C_{23}H_{31}N_2BBr_2Fe$	$C_{37}H_{57}N_2BCl_2$
Formula weight	365.15	365.15	561.98	611.56
Crystal system	Monoclinic	Triclinic	Monoclinic	Monoclinic
Space group	*C2/c*	P-1	*P2(1)/n*	*P2(1)/n*
a/Å	37.418(5)	10.355(5)	13.953(5)	13.338(5)
b/Å	6.561(5)	11.914(5)	10.716(5)	18.972(5)
c/Å	15.964(5)	16.592(5)	15.723(5)	15.336(5)
α/°	90	73.933(5)	90	90
β/°	100.318(5)	83.657(5)	103.837	92.677(5)
γ/°	90	80.431(5)	90	90
V/Å^3	3856(3)	1935.1(14)	2282.7(15)	3867(15)
Z	4	2	4	4
P_{calcd}/g cm^{-3}	1.258	1.250	1.635	1.050
F(000)	1552	4448	1136	1328
Crystal size/mm	0.30 x 0.30 x 0.30	0.25 x 0.10 x 0.15	0.30 x 0.30 x 0.20	0.20 x 0.20 x 0.20
θ range/°	3.09 to 27.00	1.82 to 27.49	2.42 to 27.00	1.71 to 25.00
No. of reflns. collected	7446	34696	8684	13301
No. of indep reflns.	4204	21180	4966	6811
R1[$I > 2\sigma(I)$]	0.0480	0.0562	0.0431	0.0653
wR_2 (all data)	0.1209	0.1362	0.0849	0.1990
Peak and hole/e Å^{-2}	0.462 and -0.287	0.691 and -0.762	0.699 and -0.643	0.446 and -0.300

Reactive Boron Species Supported by Amidinate Fragments

Terminal Borylene

Transition metal complexes containing a conventional two-center, two-electron bond to a boron center have received much attention in recent years [31-39]. In part, this is due to the range of powerful and unusual organic transformations in which such complexes have been implicated. Noteworthy stoichiometric and catalytic processes include the selective functionalization of alkanes and arenes [40, 41] and the hydro- and diboration of carbon–carbon multiple bonds (see, for example [42]). Synthetic efforts have also targeted complexes with novel modes of coordination of the boron ligand, as part of a wider effort into an in-depth examination of the structure and bonding of mixed transition metal/group 13 complexes [43-50]. The breadth of recent studies encompassing synthetic, structural and reaction chemistry of these ligand systems is reflected in the publication of a number of reviews [33-39].

Inspired by Tilley's elegant synthesis of base-free silylenes via halide (or pseudo-halide) abstraction [51], Aldridge *et al.* examined the reaction of the arylhaloboryl complex **22** with several abstraction reagents. In the case of the reaction with $Na[BAr^f_4]$ ($Ar^f = C_6H_3(CF_3)_2$-3,5) or $Ag[CB_{11}H_6Br_6]$ complete consumption of the starting material and conversion to a cationic complex with a ^{11}B NMR chemical shift of δ = 145was observed. This ^{11}B chemical shift is some 30 ppm downfield from that of the starting material. This crystalline compound, which was isolated in yields of 50–60% was shown to be the cationic terminal borylene complex **22** on the basis of spectroscopic and X-ray crystallographic data (Figure 1.13) [50]. This compound represents the first example of a cationic borylene complex, and its synthesis opens up a new route to a range of related

highly unsaturated systems. Of particular interest from a structural viewpoint is the linear Fe–B–C unit (∠Fe(1)–B(1)–C(1) = 178.3(6)°) and the Fe–B distance (1.792(8) Å), which is significantly shorter than any transition metal to boron linkage previously reported.

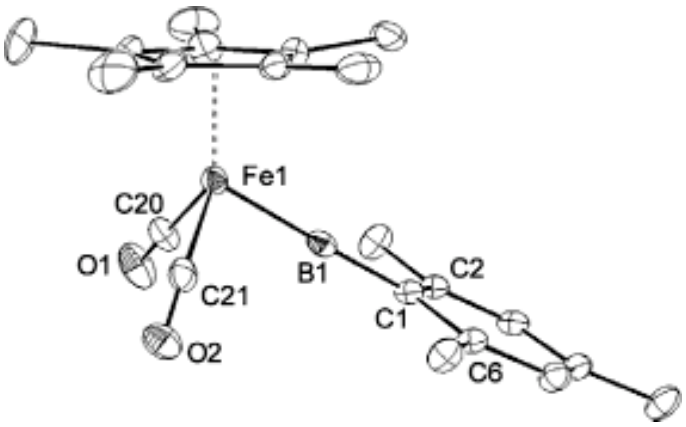

Fig. 1.13. Structure of one of two crystallographically independent cations in the asymmetric unit of **22**. Relevant bond lengths (Å) and angles (º): Fe(1)-B(1) 1.792(8), Fe(1)-C(20) 1.768(7), Fe(1)-Cp* centroid 1.733(7), B(1)-C(1) 1.491(10), Fe(1)-B(1)-C(1) 178.3(6), Cp* centroid-Fe(1)-C(1)-C(2) 91.3(6).

It was apparent that the reaction of amidinate metal (III) dihalides, [(amid)MX_2], (amid = general amidinate) with anionic transition metal fragments would afford complexes of the type [L_nM'M(X)(amid)], halide abstraction from which could yield cationic complexes of the type [L_nM'M(amid)]$^+$. As in the case of the Aldridge *et al.* work, it was anticipated that if complexes of the type [L_nM'M(amid)]$^+$ could be accessed, the probably vacant p-orbital at the Group 13 element center would act as a π-acceptor and result in significant metal-metal back bonding. Indeed, as initial efforts in this area were underway, a report appeared in which Jones *et al*. successfully prepared the

proposed complexes by reaction of $Na[CpFe(CO)_2]$ and $[MX_2(amid)]$, M = Al, Ga or In; X = Cl or Br; $amid^- = [(RN)_2C^tBu]^-$; R = ^{i}Pr or cyclohexyl [52]. However, efforts to convert these precursors to the corresponding group 13 diyl-complexes met with mixed results. Significantly, the lightest congener, boron, was conspicuous by its absence. It was therefore decided to develop a synthetic route to the heretofore neglected boron derivative.

Following a synthetic strategy analogous to that reported by Jones *et al.*, i.e. treatment of amidinate boron dihalides **1** or **6** with an appropriate organometallic anion resulted in no species that evidenced the presence of a boron-transition metal bond. In keeping with previous results, it seemed that once more the lack of reactivity was due to coordinative saturation at the boron center. Consequently, it was necessary to employ a more reactive three-coordinate species, namely $[(\eta^5\text{-}C_5H_5)Fe(CO)_2BCl_2]$ or Fp-BCl_2 [53]. Treatment of this boryl-complex with an equimolar quantity of **5** cleanly afforded the desired monohaloboryl complex **23** (Scheme 1.5). However, repeated attempts at crystallization of this product afforded no material that was appropriate for structural analysis *via* single crystal X-ray diffraction.

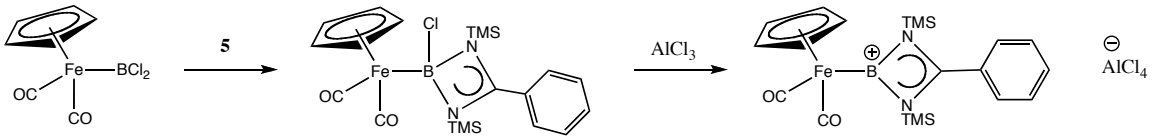

23 **24**

Scheme 1.5. Synthesis of amidinate-supported borylene **24**.

Subsequent treatment of **23** with a stoichiometric portion of $AlCl_3$ in methylene chloride solution resulted in an intensely colored (purple) solution, which once more defied repeated efforts at interrogation *via* single crystal X-ray diffraction techniques. Similarly, this synthesis resulted in no tractable materials, which could be characterized by either multinuclear NMR or mass spectrometry.

Conclusions

The utility of a range of complementary synthetic routes for the preparation of boron amidinate compounds has been. On the basis of NMR and X-ray structural data, the bonding in the four-membered B-N-C-N heterocycles may be described in terms of equal contributions from two diaza-allyl resonance forms, giving rise to delocalization about the N-C-N junction.

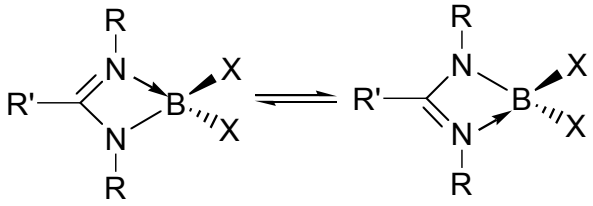

The inherent stability of the amidinate boron dihalides, whilst providing an ease of synthesis, affords products of decreased reactivity. However, circumstantial evidence [54] has pointed to an increased reactivity which may be accessed *via* substitution of the halide atoms with the triflate group by reaction of (amid)BX_2 with two equivalents of a suitable triflate source e.g. TMS-OTf, Ag-OTf etc. Future efforts in this area are expected to be directed towards the successful preparation of these more reactive derivatives.

Experimental

General procedures

All manipulations and reactions were performed under a dry, oxygen-free, catalyst-scrubbed argon atmosphere using a combination of standard Schlenk techniques or in an M-Braun or Vacuum Atmospheres drybox. All glassware was oven-dried and vacuum- and argon flow-degassed before use. All solvents were distilled over sodium benzophenone ketyl, except dichloromethane, which was distilled over CaH_2, and degassed prior to use. N,N,N′-tris(trimethylsilyl)benzamidine [55] ferrocenyldibromoborane ($FcBBr_2$) [56] and Fp-BCl_2 [53] were prepared according to the literature procedures. The compounds 1,3-dicyclohexylcarbodiimide, 1,3-diisopropylcarbodiimide, 1-bromo-2,4,6-tri(*tert*-butyl)benzene (Mes^*Br), boron halides, and alkyl lithium solutions were obtained commercially and used without further purification.

Physical measurements

Low-resolution CI mass spectra were obtained on a Finnigan MAT TSQ-700 mass spectrometer and high-resolution CI mass spectra recorded on a VG Analytical ZAB-VE sector instrument. All MS analyses were performed on samples that had been sealed in glass capillaries under an argon atmosphere. ^1H, $^{13}C\{^1H\}$, and ^{11}B NMR spectra were recorded at 295 K in C_6D_6 solutions on a GE EQ-300 instrument (^1H, 300 MHz; ^{13}C, 75 MHz, ^{11}B, 96 MHz) immediately following removal of the sample from the drybox. ^1H and $^{13}C\{^1H\}$ chemical shift values are reported in parts per million (ppm) relative to $SiMe_4$ (δ 0.00), using residual solvent resonances as internal standards. ^{11}B NMR data

are referenced to BF_3:OEt_2 (δ 0.00). Melting points (uncorrected) were obtained on a Fisher-Johns apparatus after flame-sealing the samples in glass capillaries under argon.

X-ray crystallography

For compounds **1**, **6**, **7**, **11**, **12**, **13**, **14**, **15**, **16**, **17** and **18**, a crystal of suitable quality was removed from a Schlenk flask under positive argon pressure, covered immediately with degassed hydrocarbon oil and mounted on a glass fiber. The X-ray diffraction data were collected at 153 K on a Nonius Kappa CCD diffractometer equipped with an Oxford Cryostream low-temperature device and a graphite-monochromated Mo Kα radiation source (λ = 0.71073 Å). Corrections were applied for Lorentz and polarization effects. All structures were solved by direct methods [56] and refined by full-matrix least-squares cycles on F^2. All non-hydrogen atoms were allowed anisotropic thermal motion, and hydrogen atoms were placed in fixed, calculated positions using a riding model (C-H 0.96 Å). Selected crystal data, and data collection and refinement parameters are listed in Table 1.

Preparation of [PhC{N(SiMe$_3$)}$_2$]BBr$_2$ (1). A solution of BBr_3 (10 mmol) in CH_2Br_2 (10 mL) was added to a stirred, equimolar solution of N,N,N'-tris(trimethylsilyl)benzamidine (3.4 g, 10 mmol) in CH_2Br_2 (30 mL) at room temperature. The reaction mixture was warmed to 45 ˚C for several minutes, then cooled to room temperature and stirred for 6 h. Concentration of the resulting solution (approx. ½ volume) under reduced pressure followed by storage at –30 ^{o}C resulted in a crop of colourless crystals which was isolated by filtration. A second crop of crystals formed upon cooling of the filtrate to –30 ^{o}C (3.9 g, 90 % yield, mp 127-128 ˚C).

^{1}H NMR (C_6D_6): δ 6.86 (m, 5H, Ph), 0.16 (s, 18H, $SiMe_3$); ^{13}C NMR (C_6D_6): δ 174.36 (N*C*N); 131.63; 128.88; 126.99 (Ph); 0.63 (Si*Me*$_3$); ^{11}B NMR (C_6D_6): δ -3.84 (s). MS (CI^+, CH_4): *m/z* 435 (M + H), 355 (M-Br). HRMS (CI, CH_4) calcd. for $C_{13}H_{24}N_2BBr_2$, 434.9917; found 434.9927.

Preparation of [PhC{N(SiMe$_3$)}$_2$]BCl$_2$ (6). Colorless crystalline **6** (mp 129 -131 ^{o}C) was prepared in 84% yield from BCl_3 (10 mmol, 10 mL 1.0 *M* solution in CH_2Cl_2) and N,N,N′-tris(trimethylsilyl)benzamidine (3.4 g, 10 mmol) using the procedure described for **1**. ^{1}H NMR (C_6D_6): δ 6.82 (m, 5H, Ph), 0.14 (s, 18H, $SiMe_3$); ^{13}C NMR (C_6D_6): δ 174.68 (N*C*N); 131.35; 129.02; 125.77 (Ph); 0.66 (Si*Me*$_3$); ^{11}B NMR (C_6D_6): δ 6.04 (s). MS (CI^+, CH_4): *m/z* 344 (M + H), 309 (M-Cl). HRMS (CI, CH_4) calcd. for $C_{13}H_{24}N_2BCl_2$, 344.0870; found 344.0871.

Preparation of [MeC{NCy}$_2$]BCl$_2$ (11). Methyllithium (3.1 mL of 1.6 *M* solution in diethyl ether, 4.85 mmol) was added to a cold (-78 ^{o}C) solution of 1,3-dicyclohexylcarbodiimide (1.00 g, 4.85 mmol) in 15 mL of diethyl ether. The stirred colorless reaction mixture was warmed to room temperature, then cooled to –78 ^{o}C following which BCl_3 (4.85 mL 1.0 M solution in hexane, 4.85 mmol) was added dropwise. After being stirred at room temperature for 2 h, the reaction mixture was filtered through Celite® and the solvent was stripped from the filtrate to afford a white powder. Recrystallization of this powder from toluene solution afforded a crop of pale yellow crystals of **10** (1.24 g, 85% yield, mp 82-84 ˚C).

^{1}H NMR (C_6D_6): δ 3.41 (m, 2H); 2.14 (s, 3H); 2.07 (m, 4H); 1.59–1.24 (br m, 10H); 1.18–1.03 (m, 6H); ^{13}C NMR (C_6D_6): δ 173.41 (N*C*N); 52.12 (Cy-C_1); 33.55 (Cy); 31.02 (Cy); 26.95; 25.97 (Cy); 10.82 (*Me*-C). ^{11}B NMR (C_6D_6): δ 6.01 (s). MS (CI^+, CH_4): *m/z* 302 (M + H), 267 (M-Cl). HRMS (CI, CH_4) calcd. for $C_{14}H_{25}N_2BCl_2$, 302.1488; found 302.1488.

Preparation of [Mes*C{NCy}$_2$]BCl$_2$ (12). A solution of ^{n}BuLi (10.2 mmol, 6.4 mL of 1.6 *M* solution in hexanes) was added to a solution of Mes*Br (10 mmol) in 25 mL of diethyl ether at -78 ^{o}C. The stirred reaction mixture was allowed to warm to ambient temperature over a 2 h period. The resulting Mes*Li solution (10 mmol) was chilled to -78 ^{o}C and an equimolar solution of 1,3-dicyclohexylcarbodiimide in 10 mL of diethyl ether was added dropwise. The reaction mixture was warmed to room temperature and stirred for 2 h, following which it was cooled to -78 ^{o}C. Boron trichloride (10 mL of 1.0 *M* solution in hexanes, 10 mmol) was added dropwise, and the stirred reaction mixture was allowed to warm to room temperature overnight. The resulting white slurry was filtered through Celite® and the solvent was removed from the filtrate under reduced pressure to give a pale yellow residue. Recrystallization of this residue from toluene solution afforded a crop of pale yellow crystals of **12** (3.2 g, 83% yield, mp 178-180 ˚C). ^{1}H NMR (C_6D_6): δ 7.45 (s, 2H); 3.28 (m, 2H); 2.01 (m, 4H); 1.65-1.54 (m, 10H); 1.48 (s, 27 H); 1.21-1.08 (m, 6H); ^{13}C NMR (C_6D_6): δ 176.43 (N*C*N), 152.13 (Ph); 148.86 (Ph); 126.73 (Ph); 120.03 (Ph); 55.84 (Cy-C_1), 39.44 (Cy), 35.47 (C(*C*H$_3$)$_3$), 33.14 (*C*(CH$_3$)$_3$), 31.36 (Cy); 26.76 (Cy); 25.53 (Cy); ^{11}B NMR (C_6D_6): δ 6.40 (s). MS (CI^+, CH_4): *m/z* 534

(M+H), 497 (M-Cl). HRMS (CI, CH_4) calcd. for $C_{31}H_{51}N_2BCl_2$, 532.3522; found 532.3516.

Preparation of [MeC{N^{i}Pr}$_2$]BCl$_2$ (13). Methyllithium (3.8 mL of 1.6 *M* solution in diethyl ether, 6.0 mmol) was added to a cold (-78 ^oC) solution of diisopropylcarbodiimide (0.75 g, 5.94 mmol) in 15 mL of diethyl ether. The stirred colorless reaction mixture was allowed to warm to room temperature, following which it was cooled to –78 ^oC and BCl_3 (6 mL of 1.0 *M* solution in hexane, 6 mmol) was added dropwise. After being stirred at room temperature for 2 h, the reaction mixture was filtered through Celite® and the solvent was stripped from the filtrate to afford a white powder, **13**. Yield 1.24 g, 94%, mp 38-40^{o}C. ^{1}H NMR (C_6D_6): 3.43 (sept, 2H); 2.17 (s, 3H); 1.19 (d, 12H); ^{13}C NMR (C_6D_6): 173.80 (N*C*N); 46.17 (*C*H-Me$_2$); 23.08 (CH-*Me*$_2$); 10.66 (*Me*-C); ^{11}B NMR (C_6D_6): 5.78 (s). MS (CI$^+$, CH_4): *m/z* 222 (M+H), 187 (M-Cl). HRMS (CI, CH_4) calcd. for $C_8H_{17}N_2BCl_2$, 222.0862; found 222.0863.

Synthesis of [tBuC{N(Cy)}$_2$]BCl(Ph) (14). tert-Butyllithium (2 mL of a 2.5 M solution in diethyl ether, 5.0 mmol) was added to a cold (-78 °C) solution of 1,3-dicyclohexylcarbodiimide (1.03 g, 5.0 mmol) in 15 mL of diethyl ether. The stirred colorless reaction mixture was warmed to room temperature, then cooled to -78 °C following which $PhBCl_2$ (0.794 g, 5.0 mmol) was added dropwise. After being stirred at room temperature for 2 h, the reaction mixture was filtered through Celite® and the solvent was stripped from the filtrate to afford a white powder. Recrystallization of this powder from hexane solution afforded a crop of colorless crystals of **14** (1.12 g, 58%

yield, mp 124–126 °C). ^{1}H NMR (C_6D_6): δ 8.02 (d, 2H, Ph); 7.35 (m, 2H, Ph); 7.26 (m, 1H, Ph); 3.53 (m, 2H, Cy); 2.07 (m, 4H, Cy); 1.62– 1.53 (br m, 10H, Cy); 1.28–1.15 (m, 6H, Cy); 1.08 (s, 9H, tBu). ^{13}C NMR (C_6D_6): δ 178.25 (NCN); 135.84; 135.62; 133.68; 127.83 (Ph); 56.39 (Cy–C1); 35.08 (Cy); 34.60 (Cy); 28.49 (C–Me_3); 26.45; 26.43 (Cy); 25.80 (C–Me_3). ^{11}B NMR (C_6D_6): δ 6.50 (s). MS (CI+, CH4): m/z 386 (M+H), 351 (M_Cl). HRMS (CI, CH4) calcd. for $C_{23}H_{36}N_2BCl$, 386.2660; found: 386.2655.

Synthesis of [^{n}BuC{N(Cy)}$_2$]BCl(Ph) (15). Colorless crystalline **15** (mp 99–101 °C) was prepared in 63% yield from n-butyllithium (2 mL of a 2.5 M solution in diethyl ether, 5.0 mmol), 1,3-dicyclohexylcarbodiimide (1.03 g, 5.0 mmol) in 15 mL of diethyl ether and $PhBCl_2$ (0.794 g, 5.0 mmol) using the procedure described above for **14**. ^{1}H NMR (C_6D_6): δ 8.08 (d, 2H, Ph); 7.39 (m, 2H, Ph); 7.26 (m, 1H, Ph); 3.19 (m, 2H); 1.98 (s, 4H); 1.83 (m, 2H); 1.57–1.28 (br m, 10H); 1.16 0.96 (br m, 10H); 0.74 (t, 3H, CH_3). ^{13}C NMR (C_6D_6): δ 166.93 (NCN); 133.54; 128.07; 127.99; 125.53 (Ph); 54.73 (Cy–C1); 46.71 ($CH_2CH_2CH_2$-CH_3); 34.50 (Cy); 29.10 (Cy); 26.55; 26.45 (Cy); 25.77 ($CH_2CH_2CH_2CH_3$); 24.95 ($CH_2CH_2CH_2CH_3$); 14.03 ($CH_2CH_2CH_2CH_3$). ^{11}B NMR (C_6D_6): δ 6.47 (s). MS (CI+, CH4): m/z 387 (M+H), 352 (M_Cl). HRMS (CI, CH4) calcd. for $C_{23}H_{36}N_2BCl$, 386.2660; found: 386.2660.

Preparation of Lewis acid: Base adduct of $PhBCl_2$ (16). Treatment of $PhBCl_2$ (0.794 g, 5.0 mmol) in 15 mL of hexane, with an equimolar quantity of dicyclohexylcarbodiimide (1.03 g, 5.0 mmol) as a hexane solution (10 mL) at ambient temperature afforded a near quantitative conversion to the adduct, **16** (1.71 g, 97% yield). ^{1}H NMR (C_6D_6): δ 7.39 -

7.19 (s, 5H); 3.13 (br s, 2H); 2.17 (br s, 4H); 1.68–0.95 (br m, 16H); ^{13}C NMR (C_6D_6): δ 154.34; 136.28; 133.93; 133.11; 58.52; 55.68; 33.95; 32.57; 31.26; 26.51; 26.37; 25.38; 25.04; 24.40; ^{11}B NMR (C_6D_6): δ 8.17 (s). MS (CI+, CH4): m/z 364 (M+), 207 (100%, CyN=C=NCy + H+); HRMS (CI, CH4) calcd for $C_{19}H_{27}N_2BCl_2$, 364.1644; found 364.1671.

Preparation of [PhC{NCy}$_2$]BCl$_2$ (17). Conversion to **17** was achieved by dissolution of **16** in 20 mL of toluene and subsequent reflux of this solution for 12 h (1.03 g, 88% yield). ^{1}H NMR (C_6D_6): δ 3.49 (s, 2H); 2.09 (s, 4H); 1.67–1.45 (m, 10H); 1.14–1.05 (m, 6H); ^{13}C{1H} NMR (C_6D_6): δ 176.17; 132.55; 129.79; 127.99; 54.95; 33.70; 27.23; 25.94; ^{11}B NMR (C_6D_6): δ 6.25 (s). MS (CI+, CH4): m/z 364 (M+), 329 (100%, M–Cl); HRMS (CI, CH4) calcd for $C_{19}H_{27}N_2BCl_2$, 364.1644; found 364.1642.

Preparation of [FcC{NCy}$_2$]BBr$_2$ (18). A solution of $FcBBr_2$ (0.89 g, 2.5 mmol) in 20 mL of hexane was added to a cold (- 78 ^{o}C) solution of 1,3-dicyclohexylcarbodiimide (0.52 g, 2.5 mmol) in 15 mL of hexane. The resulting yellow reaction mixture was stirred at room temperature for 2 h, following which the solvent and volatiles were removed under reduced pressure to give orange powder, **18**. Recrystallization of the crude product from toluene solution afforded orange-red block crystals of **18**. Yield 0.98 g, 71%, mp 177-179 ^{o}C. ^{1}H NMR (C_6D_6): δ 4.83-4.03 (br, 9H); 3.64 (m, 2H); 2.20-1.11 (m, 20H); ^{13}C{^{1}H} NMR (C_6D_6): δ 75.13; 72.90; 71.17; 70.54; 69.55; 68.63; 56.03; 33.89; 26.46; 25.95; ^{11}B NMR (C_6D_6): δ - 4.05 (s). MS (CI^+, CH_4): *m/z* 562 (M+H), 483 (M-Br). HRMS (CI, CH_4) calcd. for $C_{23}H_{31}N_2BBr_2Fe$, 560.0296; found 560.0295.

Preparation of [PhC{NSiMe$_3$}$_2$]BCl(Fp) (23). To a toluene (30 mL) solution of Fp-BCl_2 (0.258 g, 1 mmol) was added an equimolar amount of **5** (0.337 g, 1 mmol) also as a solution in toluene, 20 mL. The reaction mixture was stirred overnight and **23** was isolated as a brown powder after removal of the reaction solvent at reduced pressure. Yield 0.410 g, 84.4%. ^{1}H NMR ($CDCl_3$): δ 7.28-7.43 (br m, ArH, 5H), 4.77 (s, CpH, 5H), 0.04 (br s, 18H); ^{11}B NMR ($CDCl_3$): δ 18.0 (br s). MS (CI^+, CH_4): *m/z* 485 (M+H). HRMS (CI, CH_4) calcd. for $C_{20}H_{27}N_2BO_2Si_2ClFe$, 485.0742; found 485.0740.

References

1 (*a*) F. T. Edelmann, *Coord. Chem. Rev*., 1994, **137**, 403; (*b*) J. Barker and M. Kilner, *Coord. Chem. Rev*., 1994, **133**, 219.

2 A.R. Sanger, *Inorg. Nucl. Chem. Lett*. 1994, **9**, 351.

3 (*a*) M. L. Cole, C. Jones, P. C. Junk, M. Kloth and A. Stasch, *Chem. Eur. J*., DOI: 10.1002/chem.200500278; (*b*) V. Amo, R. Andres, E. de Jesus, F. J. de la Mata, J. C. Flores, R. Gomez, M. P. Gomez-Sal and J. F. C. Turner, *Organometallics*, 2005, **24**, 2331; (*c*) R. T. Boere, M. L. Cole and P. C. Junk, *New. J. Chem*., 2005, **29**, 128; (*d*) B. Clare, N. Sarker, R. Shoemaker and J. R. Hagadorn, *Inorg. Chem*., 2004, **43**, 1159; (*e*) H. A. Jenkins, D. Abeysekera, D. A. Dickie and J. A. C. Clyburne, *J. Chem. Soc., Dalton Trans.,* 2002, 3919; (*f*) D. Abeysekera, K. N. Robertson, T. S. Cameron and J. A. C. Clyburne, *Organometallics*, 2001, **20**, 5532; (*g*) K. Kincaid, C. P. Gerlach, G. R. Giesbrecht, J. R. Hagadorn, G. D. Wheeler, A. Shafir and J. Arnold, *Organometallics*, 1999, **18**, 5360; (*h*) C. C. Chang, C. S. Hsiung, H. L. Su, B. Srinivas, M. Y. Chiang, G. H. Lee and Y. Wang, *Organometallics*, 1998, **17**, 1595; (*i*) M. P. Coles, D. C. Swenson, R. F. Jordan and V. G. Young, *Organometallics*, 1998, **17**, 4042; (*j*) M. P Coles, D. C. Swenson, R. F. Jordan and V. G. Young, *Organometallics*, 1997, **16**, 5183.

4 (*a*) J. T. Patton, M. M. Bokota and K. A. Abboud, *Organometallics*, 2002, **21**, 2145; (*b*) S. Dagorne, R. F. Jordan and V. G. Young, *Organometallics*, 1999, **18**, 4619; (*c*) J. Barker, N. C. Blacker, P. R. Phillips, N. W. Alcock, W. Errington and M. G. H. Wallbridge, *J. Chem. Soc., Dalton Trans*., 1996, 431; (*d*) Y. Zhou and D. S.

Richeson, *Inorg. Chem*., 1996, **35**, 2448; (*e*) Y. Zhou and D. S. Richeson, *Inorg. Chem*., 1996, **35**, 1423.

5 (*a*) R. J. Meier, E. Koglin, *J. Phys. Chem. A*, 2001, **105**, 3867; (*b*) S. Dagorne, I. A. Guzei, M. P. Coles and R. F. Jordan, *J. Am. Chem. Soc*., 2000, **122**, 274; (*c*) M. P. Coles and R. F. Jordan, *J. Am. Chem. Soc*., 1997, **119**, 8125; (*d*) R. Duchateau, A. Meetsma and J. H. Teuben, *J. Chem. Soc., Chem. Commun*., 1996, 223.

6 C. Ergezinger, F. Weller and K. Dehnicke, *Z. Naturforsch.,*, 1988, **43b**, 1621.

7 P. Blais, T. Chivers, A. Downard and M. Parvez, *Can. J. Chem*., 2000, **78**, 10.

8 M. R. Terry, L. A. Mercando, C. Kelley, G. L. Geoffroy, P. Nombel, N. Lugen, R. Mathieu, R. L. Ostrander, B. E. Owens-Waltermire and A. L. Rheingold, *Organometallics*, 1994, **13**, 843.

9 D. J. Brauer, S. Buchheim-Spiegel, H. Burger, R. Gielen, G. Pawelke and J. Rothe, *Organometallics*, 1997, **16**, 5321.

10 S. Aldridge, R. J. Calder, D. L. Coombs, C. Jones, J. W. Steed, S. Coles and M. B. Hursthouse, *New. J. Chem*., 2002, **26**, 677.

11 L. M. Engelhardt, G. E. Jacobson, P. C. Junk, C. L. Raston and A. H. White, *J. Chem. Soc., Chem. Commun*., 1990, 89.

12 F. H. Allen, O. Kennard, D. G. Watson, L. Brammer, A. G. Orpen and R. Taylor, *J. Chem. Soc., Perkin Trans. 2*, 1987, S1-S19.

13 A. Ansorge, D. J. Brauer, H. Bürger, F. Dorrenbach, T. Hagen, G. Pawlke and W. Weuter, *J. Organomet. Chem*., 1991, **407**, 283.

14 H. Nöth and B. Wrackmeyer in Nuclear magnetic resonance spectroscopy of boron compounds. Springer Verlag, Berlin. 1978. Ch. 7. pp-74-101.

15 P. Blais, T. Chivers and M. Parvez, *Can. J. Chem.*, 2000, **78**, 10.

16 S. Gambarotta, S. Strologo, C. Floriani, A. Chiesi-Villa and C. Guastini, *Inorg. Chem.*, 1985, **24**, 654.

17 (a) P. Braunstein and D. Nobel, *Chem. Rev.*, 1989, **89**, 1927; (b) J. A. Tunge, C. J. Czerwinski, D. A. Gately and J. R. Norton, *Organometallics*, 2001, **20**, 254.

18 Y. Musashi and S. Sakaki, *J. Chem. Soc.*, *Dalton Trans.*, 1998, 577.

19 C. N. Rowley, G. N. Dilabio and S. T. Barry, *Inorg. Chem.*, 2005, **44**, 1983.

20 H. Jacobsen, H. Berke, S. Döring, G. Kehr, G. Erker, H. Fröhlich and O. Meyer, *Organometallics*, 1999, **18**, 1724.

21 Gaussian 03, Revision B.04, Frisch, M. J.; Trucks, G. W.; Schlegel, H. B.; Scuseria, G. E.; Robb, M. A.; Cheeseman, J. R.; Montgomery Jr., J. A.; Vreven, T.; Kudin, K. N.; Burant, J. C.; Millam, J. M.; Iyengar, S. S.; Tomasi, J.; Barone, V.; Mennucci, B.; Cossi, M.; Scalmani, G.; Rega, N.; Petersson, G. A.; Nakatsuji, H.; Hada, M.; Ehara, M.; Toyota, K.; Fukuda, R.; Hasegawa, J.; Ishida, M.; Nakajima, T.; Honda, Y.; Kitao, O.; Nakai, H.; Klene, M.; Li, X.; Knox, J. E.; Hratchian, H. P.; Cross, J. B.; Adamo, C.; Jaramillo, J.; Gomperts, R.; Stratmann, R. E.; Yazyev, O.; Austin, A. J.; Cammi, R.; Pomelli, C.; Ochterski, J. W.; Ayala, P. W.; Morokuma, K.; Voth, G. A.; Salvador, P.; Dannenberg, J. J.; Zakrzewski, V. G.; Dapprich, S.; Daniels, A. D.; Strain, M. C.; Farkas, O.; Malick, D. K.; Rabuck, A. D.; Raghavachari, K.; Foresman, J. B.; Ortiz, J. V.; Cui, Q.; Baboul, A. G.; Clifford, S.; Cioslowski, J.; Stefanov, B. B.; Liu, G.; Liashenko, A.; Piskorz, P.; Komaromi, I.; Martin, R. L.; Fox, D. J.; Keith, T.; Al-Laham, M. A.; Peng, C. Y.; Nanayakkara, A.;

Challacombe, M.; Gill, P. M. W.; Johnson, B.; Chen, W.; Wong, M. W.; Gonzalez, C.; Pople, J. A., Gaussian, Inc., Pittsburgh PA, **2003**.

22 All calculations were performed at the R3BLYP level of theory and 6-311++G(d,p) basis set using the Gaussian 03 suite of programs. Points on the potential energy surface were confirmed by the calculation of the vibrational frequencies. There were no imaginary frequencies for IM1, IM2 and **17*** and one imaginary frequency was found for TS1 and TS2.

23 J. R. Hagadorn and J. Arnold, *Inorg. Chem*., 1997, **36**, 132.

24 J. R. Hagadorn and J. Arnold, *J. Organomet. Chem*., 2001, **637-639**, 521.

25 (a) E. Y.-X. Chen and T. J. Marks, *Chem. Rev.*, 2000, **100**, 1391, and references therein; (b) W. E. Piers, *Adv. Organomet. Chem.*, 2005, **52**, 1.

26 A. D. Dilman and S. L. Ioffe, *Chem. Rev.*, 2003, **103**, 733.

27 H. Nöth, R. Staudigl and H.-U. Wagner, *Inorg. Chem.*, 1982, **21**, 706.

28 P. Kölle and H. Nöth, *Chem. Rev.*, 1985, **85**, 399.

29 W. E. Piers, S. C. Bourke and K. D. Conroy, *Angew. Chem. Int. Ed.*, 2005, **44**, 5016.

30 A. H. Cowley, Z. Lu, J. N. Jones and J. A. Moore, *J. Organomet. Chem.*, 2004, **689**, 2562.

31 G. Schmid, *Angew. Chem. Int. Ed. Engl.*, 1970, **9**, 819.

32 H. Wadepohl, *Angew. Chem. Int. Ed. Engl.*, 1997, **36**, 2441.

33 G. J. Irvine, M. J. G. Lesley, T. B. Marder, N. C. Norman, C. R. Rice, E. G. Robins, W. R. Roper, G. R. Whittell and L. J. Wright, *Chem. Rev.*, 1998, **98**, 2685.

34 H. Braunschweig, *Angew. Chem. Int. Ed. Engl.*, 1998, **37**, 1786.

35 M. R. Smith III, *Prog. Inorg. Chem.*, 1999, **48**, 505.

36 B. Wrackmeyer, *Angew. Chem. Int. Ed. Engl.*, 1999, **38**, 771.

37 H. Braunschweig and M. Colling, *J. Organomet. Chem.*, 2000, **614-615**, 18.

38 H. Braunschweig and M. Colling, *Coord. Chem. Rev.*, 2001, **223**, 1.

39 H. Braunschweig and M. Colling, *Eur. J. Inorg. Chem.*, 2003, 393.

40 (a) K. M. Waltz, X. He, C. Muhoro and J. F. Hartwig, *J. Am. Chem. Soc.*, 1995, **117**, 11357; (b) K. M. Waltz and J. F. Hartwig, *Science*, 1997, **277**, 211; (c) K. M. Waltz, C. Muhoro and J. F. Hartwig, *Organometallics*, 1999, **18**, 3383; (d) K. M. Waltz and J. F. Hartwig, *J. Am. Chem. Soc.*, 2001, **122**, 11358; (e) K. Kawamura and J. F. Hartwig, *J. Am. Chem. Soc.*, 2001, **123**, 8422; (f) T. Ishiyama, J. Tagaki, K. Ishida, N. Miyaura, N. R. Anastasi, and J. F. Hartwig, *J. Am. Chem. Soc.*, 2002, **124**, 390; (g) T. Ishiyama, and N. Miyaura, *J. Organomet. Chem.*, 2003, **680**, 3, and references therein.

41 (a) C. N. Iverson and M. R. Smith III, *J. Am. Chem. Soc.*, 1999, **121**, 7696; (b) H. Chen and J. F. Hartwig, *Angew. Chem. Int. Ed. Engl.*, 1999, **38**, 3391; (c) H. Chen, S. Schlecht, T. C. Semple and J. F. Hartwig, *Science*, 2000, **287**, 1995; (d) J.-Y. Cho, C. N. Iverson and M. R. Smith III, *J. Am. Chem. Soc.*, 2000, **122**, 12868; (e) S. Shimada, A. S. Batsanov, J. A. K. Howard and T. B. Marder, *Angew. Chem. Int. Ed. Engl.*, 2001, **40**, 2168; (f) J.-Y. Cho, M. K. Tse, D. Holmes, R. E. Maleckza Jr. and M. R. Smith III, *Science*, 2002, **295**, 305; (g) Y. Kondo, D. Garcia-Cuadrado, J. F. Hartwig, N. K. Boaen, N. L. Wagner and M. A. Hillmeyer, *J. Am. Chem. Soc.*, 2002, **124**, 1164; (h) R. E. Maleczka Jr., F. Shi, D. Holmes and M. R. Smith III, *J. Am. Chem. Soc.*, 2003, **125**, 7792.

42 (a) H. C. Brown and B. Singaram, *Pure Appl. Chem.*, 1987, **59**, 879; (b) K. Burgess and M. J. Ohlmeyer, *Chem. Rev.*, 1991, **91**, 1179; (c) I. Beletskaya and A. Pelter, *Tetrahedron*, 1997, **53**, 4957; (d) T. B. Marder and N. C. Norman, *Top. Catal.*, 1998, **5**, 63; (e) T. Ishiyama and N. Miyaura, *J. Organomet. Chem.*, 2000, **611**, 392.

43 A. H. Cowley, V. Lomeli and A. Voight, *J. Am. Chem. Soc.*, 1998, **120**, 6401.

44 H. Braunschweig, C. Kollann and U. Englert, *Angew. Chem. Int. Ed. Engl*, 1998, **37**, 3179.

45 G. J. Irvine, C. E. F. Rickard, W. R. Roper, A. Williamson and L. J. Wright, *Angew. Chem. Int. Ed. Engl*, 2000, **39**, 948.

46 H. Braunschweig, M. Colling, C. Kollann, H. G. Stammler and B. Neumann, *Angew. Chem. Int. Ed. Engl*, 2001, **40**, 2298.

47 H. Braunschweig, M. Colling, C. Kollann, K. Merz and K. Radacki, *Angew. Chem. Int. Ed. Engl*, 2001, **40**, 4198.

48 C. E. F. Rickard, W. R. Roper, A. Williamson and L. J. Wright, *Organometallics*, 2002, **21**, 4862.

49 H. Braunschweig, M. Colling, C. Hu and K. Radacki, *Angew. Chem. Int. Ed. Engl*, 2003, **42**, 205.

50 D. L. Coombs, S. Aldridge, C. Jones and D. J. Willock, *J. Am. Chem. Soc.*, 2003, **125**, 6356.

51 S. K. Grumbine, T. D. Tilley, F. P. Arnold and A. L. Rheingold, *J. Am. Chem. Soc.*, 1994, **116**, 5495.

52 C. Jones, S. Aldridge, T. Gans-Eichler and A. Stasch, *Dalton Trans.*, 2006, 5357.

53 H. Braunschweig, K. Radacki, F. Seeler and G. R. Whittell, *Organometallics*, 2004, **23**, 4178.

54 D. Vidovic, G. Reeske, M. Findlater and A. H. Cowley, *Dalton Trans.*, 2008, manuscript accepted for publication.

55 R. T. Boere, R. G. Hicks and R. T. Oakley, *Inorg. Synth.*, 1997, **31**, 94.

56 T. Renk, W. Ruf and W. Siebert, *J. Organomet. Chem,* 1976, **120**, 1.

57 G. M. Sheldrick, SHELL-PC Version 5;03, Siemens Analytical X-ray Instruments, Inc., Madison, WI, USA, 1994.

Tables of Crystallographic Data

Table 1.3. Crystal data and structure refinement for **1**.

Identification code	**1**	
Empirical formula	C13 H23 B Br2 N2 Si2	
Formula weight	434.14	
Temperature	153(2) K	
Wavelength	0.71069 Å	
Crystal system	Monoclinic	
Space group	C2/c	
Unit cell dimensions	a = 15.329(5) Å	α= 90.000(5)°.
	b = 10.887(5) Å	β= 116.223(5)°.
	c = 13.019(5) Å	γ = 90.000(5)°.
Volume	1949.1(13) $Å^3$	
Z	4	
Density (calculated)	1.479 Mg/m^3	
Absorption coefficient	4.275 mm^{-1}	
F(000)	872	
Crystal size	0.24 x 0.20 x 0.20 mm^3	
Theta range for data collection	2.39 to 24.99°.	
Index ranges	-18<=h<=18, -12<=k<=12, -15<=l<=15	
Reflections collected	3208	
Independent reflections	1719 [R(int) = 0.0216]	
Completeness to theta = 24.99°	99.7 %	
Absorption correction	None	
Max. and min. transmission	0.4819 and 0.4269	
Refinement method	Full-matrix least-squares on F^2	
Data / restraints / parameters	1719 / 0 / 91	
Goodness-of-fit on F^2	0.945	
Final R indices [I>2sigma(I)]	R1 = 0.0262, wR2 = 0.0709	
R indices (all data)	R1 = 0.0328, wR2 = 0.0750	
Extinction coefficient	0.0013(3)	
Largest diff. peak and hole	0.416 and -0.389 $e.Å^{-3}$	

Table 1.4. Selected bond lengths [Å] and angles [°] for **1**.

Br(1)-B(1)	2.000(3)
Si(2)-N(1)	1.768(2)
N(1)-C(1)	1.338(3)
N(1)-B(1)	1.559(4)
B(1)-N(1)#1	1.559(4)
B(1)-C(1)	1.972(6)
B(1)-Br(1)#1	2.000(3)
C(1)-N(1)#1	1.338(3)
C(1)-C(2)	1.479(6)
C(5)-C(4)-C(3)	120.7(3)
C(1)-N(1)-B(1)	85.4(2)
C(1)-N(1)-Si(2)	135.5(2)
B(1)-N(1)-Si(2)	138.70(18)
N(1)-B(1)-N(1)#1	85.1(3)
N(1)-B(1)-C(1)	42.57(14)
N(1)#1-B(1)-C(1)	42.57(14)
N(1)-B(1)-Br(1)#1	115.10(9)
N(1)#1-B(1)-Br(1)#1	114.23(9)
C(1)-B(1)-Br(1)#1	124.51(11)
N(1)-B(1)-Br(1)	114.23(9)
N(1)#1-B(1)-Br(1)	115.10(9)
C(1)-B(1)-Br(1)	124.51(11)
Br(1)#1-B(1)-Br(1)	111.0(2)
N(1)#1-C(1)-N(1)	104.0(3)
N(1)#1-C(1)-B(1)	51.99(16)
N(1)-C(1)-B(1)	51.99(16)
C(2)-C(1)-B(1)	180.000(1)

Symmetry transformations used to generate equivalent atoms:

#1 -x+1,y,-z+1/2

Table 1.5. Torsion angles [°] for **1**.

C(1)-N(1)-B(1)-N(1)#1	0.0
C(1)-N(1)-B(1)-Br(1)#1	-114.51(16)
C(1)-N(1)-B(1)-Br(1)	115.38(15)
B(1)-N(1)-C(1)-N(1)#1	0.0
B(1)-N(1)-C(1)-C(2)	180.0
N(1)-B(1)-C(1)-N(1)#1	180.0
Br(1)#1-B(1)-C(1)-N(1)#1	-89.28(12)
Br(1)-B(1)-C(1)-N(1)#1	90.72(12)
N(1)#1-B(1)-C(1)-N(1)	180.0
Br(1)#1-B(1)-C(1)-N(1)	90.72(12)
Br(1)-B(1)-C(1)-N(1)	-89.28(12)

Symmetry transformations used to generate equivalent atoms:

#1 -x+1,y,-z+1/2

Table 1.6. Crystal data and structure refinement for **6**.

Identification code	**6**	
Empirical formula	C13 H23 B Cl2 N2 Si2	
Formula weight	345.22	
Temperature	153(2) K	
Wavelength	0.71069 Å	
Crystal system	Monoclinic	
Space group	C2/c	
Unit cell dimensions	a = 15.026(5) Å	α= 90.000(5)°.
	b = 10.799(5) Å	β= 114.477(5)°.
	c = 12.711(5) Å	γ = 90.000(5)°.
Volume	1877.2(13) $Å^3$	
Z	4	
Density (calculated)	1.222 Mg/m^3	
Absorption coefficient	0.466 mm^{-1}	
F(000)	728	
Crystal size	0.20 x 0.20 x 0.20 mm^3	
Theta range for data collection	2.59 to 27.47°.	
Index ranges	-19<=h<=19, -14<=k<=12, -16<=l<=16	
Reflections collected	3390	
Independent reflections	2140 [R(int) = 0.0505]	
Completeness to theta = 27.47°	99.4 %	
Absorption correction	None	
Max. and min. transmission	0.9126 and 0.9126	
Refinement method	Full-matrix least-squares on F^2	
Data / restraints / parameters	2140 / 0 / 93	
Goodness-of-fit on F^2	0.929	
Final R indices [I>2sigma(I)]	R1 = 0.0544, wR2 = 0.1181	
R indices (all data)	R1 = 0.1621, wR2 = 0.1546	
Largest diff. peak and hole	0.462 and -0.325 $e.Å^{-3}$	

Table 1.7. Selected bond lengths [Å] and angles [°] for **6**.

C(1)-N(1)#1	1.331(4)
C(1)-N(1)	1.331(4)
C(1)-C(2)	1.483(7)
B(1)-N(1)	1.580(5)
B(1)-N(1)#1	1.580(5)
B(1)-Cl(1)#1	1.828(3)
B(1)-Cl(1)	1.828(3)
N(1)#1-C(1)-N(1)	104.4(4)
N(1)#1-C(1)-C(2)	127.8(2)
N(1)-C(1)-C(2)	127.8(2)
N(1)-B(1)-N(1)#1	83.5(3)
N(1)-B(1)-Cl(1)#1	114.11(11)
N(1)#1-B(1)-Cl(1)#1	115.52(11)
N(1)-B(1)-Cl(1)	115.52(11)
N(1)#1-B(1)-Cl(1)	114.11(11)
Cl(1)#1-B(1)-Cl(1)	111.6(3)
C(1)-N(1)-B(1)	86.1(3)
C(1)-N(1)-Si(1)	135.7(3)
B(1)-N(1)-Si(1)	138.0(2)
N(1)-Si(1)-C(6)	109.10(16)
N(1)-Si(1)-C(8)	104.86(15)
C(6)-Si(1)-C(8)	111.34(17)
N(1)-Si(1)-C(7)	108.15(15)
C(6)-Si(1)-C(7)	111.50(17)
C(8)-Si(1)-C(7)	111.60(17)

Symmetry transformations used to generate equivalent atoms:

#1 -x,y,-z+1/2

Table 1.8. Torsion angles [°] for **6**.

N(1)#1-C(1)-N(1)-B(1)	0.0
C(2)-C(1)-N(1)-B(1)	180.0
N(1)#1-B(1)-N(1)-C(1)	0.0
Cl(1)#1-B(1)-N(1)-C(1)	115.1(2)
Cl(1)-B(1)-N(1)-C(1)	-113.6(2)
N(1)#1-B(1)-N(1)-Si(1)	-174.9(3)
Cl(1)#1-B(1)-N(1)-Si(1)	-59.8(3)
Cl(1)-B(1)-N(1)-Si(1)	71.5(3)
C(1)-N(1)-Si(1)-C(6)	34.7(3)
B(1)-N(1)-Si(1)-C(6)	-152.6(2)
C(1)-N(1)-Si(1)-C(8)	154.1(2)
B(1)-N(1)-Si(1)-C(8)	-33.3(3)
C(1)-N(1)-Si(1)-C(7)	-86.7(3)
B(1)-N(1)-Si(1)-C(7)	85.9(3)

Symmetry transformations used to generate equivalent atoms:

#1 -x,y,-z+1/2

Table 1.9 Crystal data and structure refinement for **7**.

Identification code	**7**	
Empirical formula	C92 H128 B4 Br4 Fe4 N8 Si8	
Formula weight	2157.02	
Temperature	153(2) K	
Wavelength	0.71069 Å	
Crystal system	Monoclinic	
Space group	P2(1)/c	
Unit cell dimensions	a = 31.462(5) Å	α= 90.000(5)°.
	b = 11.215(5) Å	β= 99.424(5)°.
	c = 29.771(5) Å	γ = 90.000(5)°.
Volume	10363(5) $Å^3$	
Z	4	
Density (calculated)	1.383 Mg/m^3	
Absorption coefficient	2.230 mm^{-1}	
F(000)	4448	
Crystal size	0.15 x 0.15 x 0.15 mm^3	
Theta range for data collection	1.63 to 27.49°.	
Index ranges	-40<=h<=40, -14<=k<=12, -38<=l<=38	
Reflections collected	34704	
Independent reflections	21186 [R(int) = 0.1085]	
Completeness to theta = 27.49°	88.9 %	
Absorption correction	None	
Max. and min. transmission	0.7309 and 0.7309	
Refinement method	Full-matrix least-squares on F^2	
Data / restraints / parameters	21186 / 0 / 1081	
Goodness-of-fit on F^2	0.957	
Final R indices [I>2sigma(I)]	R1 = 0.0649, wR2 = 0.1055	
R indices (all data)	R1 = 0.2138, wR2 = 0.1488	
Largest diff. peak and hole	0.872 and -0.750 $e.Å^{-3}$	

Table 1.10. Bond lengths [Å] and angles [°] for **7**.

C(1)-N(1)	1.318(7)
C(1)-N(2)	1.352(7)
C(1)-C(2)	1.495(8)
C(14)-B(1)	1.581(9)
C(24)-N(3)	1.325(7)
C(24)-N(4)	1.349(7)
C(37)-B(2)	1.568(10)
C(47)-N(6)	1.316(7)
C(47)-N(5)	1.333(7)
C(60)-B(3)	1.558(9)
C(70)-N(8)	1.320(7)
C(70)-N(7)	1.344(7)
C(83)-B(4)	1.589(10)
B(1)-N(2)	1.581(9)
B(1)-N(1)	1.586(8)
B(1)-Br(1)	2.050(7)
B(2)-N(4)	1.584(9)
B(2)-N(3)	1.596(8)
B(2)-Br(2)	2.030(8)
B(3)-N(5)	1.586(9)
B(3)-N(6)	1.603(8)
B(3)-Br(3)	2.054(7)
B(4)-N(7)	1.579(9)
B(4)-N(8)	1.596(8)
B(4)-Br(4)	2.041(8)
N(1)-C(1)-N(2)	104.9(5)
N(1)-C(1)-C(2)	127.9(6)
N(2)-C(1)-C(2)	127.1(6)
N(3)-C(24)-N(4)	105.0(5)
N(3)-C(24)-C(25)	127.4(5)
N(4)-C(24)-C(25)	127.4(6)
N(6)-C(47)-N(5)	105.4(5)
N(6)-C(47)-C(48)	125.9(6)

N(5)-C(47)-C(48)	128.7(6)
N(8)-C(70)-N(7)	105.6(5)
N(8)-C(70)-C(71)	128.2(5)
N(7)-C(70)-C(71)	126.0(6)
N(2)-B(1)-N(1)	83.9(4)
N(2)-B(1)-C(14)	117.4(6)
N(1)-B(1)-C(14)	114.2(5)
N(2)-B(1)-Br(1)	113.1(4)
N(1)-B(1)-Br(1)	111.1(5)
C(14)-B(1)-Br(1)	113.6(5)
C(37)-B(2)-N(4)	116.5(6)
C(37)-B(2)-N(3)	112.8(6)
N(4)-B(2)-N(3)	83.7(4)
C(37)-B(2)-Br(2)	114.1(5)
N(4)-B(2)-Br(2)	114.4(5)
N(3)-B(2)-Br(2)	111.7(5)
C(60)-B(3)-N(5)	119.9(6)
C(60)-B(3)-N(6)	115.7(5)
N(5)-B(3)-N(6)	82.7(4)
C(60)-B(3)-Br(3)	112.5(5)
N(5)-B(3)-Br(3)	112.1(4)
N(6)-B(3)-Br(3)	110.5(4)
N(7)-B(4)-C(83)	117.4(6)
N(7)-B(4)-N(8)	83.9(4)
C(83)-B(4)-N(8)	113.8(5)
N(7)-B(4)-Br(4)	112.8(5)
C(83)-B(4)-Br(4)	114.7(5)
N(8)-B(4)-Br(4)	110.3(5)
C(1)-N(1)-B(1)	85.7(5)
C(1)-N(2)-B(1)	84.8(5)
C(24)-N(3)-B(2)	85.5(5)
C(24)-N(4)-B(2)	85.3(5)
C(47)-N(5)-B(3)	85.9(5)
C(47)-N(6)-B(3)	85.8(5)
C(70)-N(7)-B(4)	85.0(5)

C(70)-N(8)-B(4)	85.1(5)

Symmetry transformations used to generate equivalent atoms:

Table 1.11. Torsion angles [°] for **7**.

N(2)-C(1)-N(1)-B(1)	-6.7(5)
N(2)-B(1)-N(1)-C(1)	5.6(4)
Br(1)-B(1)-N(1)-C(1)	118.0(5)
N(1)-C(1)-N(2)-B(1)	6.7(5)
N(1)-B(1)-N(2)-C(1)	-5.4(4)
N(4)-C(24)-N(3)-B(2)	5.6(6)
N(4)-B(2)-N(3)-C(24)	-4.6(5)
Br(2)-B(2)-N(3)-C(24)	-118.4(5)
N(3)-C(24)-N(4)-B(2)	-5.6(6)
N(3)-B(2)-N(4)-C(24)	4.5(5)
Br(2)-B(2)-N(4)-C(24)	115.5(5)
N(6)-C(47)-N(5)-B(3)	4.5(5)
N(6)-B(3)-N(5)-C(47)	-3.6(4)
Br(3)-B(3)-N(5)-C(47)	-112.8(4)
N(5)-C(47)-N(6)-B(3)	-4.4(5)
N(5)-B(3)-N(6)-C(47)	3.6(4)
Br(3)-B(3)-N(6)-C(47)	114.6(5)
N(8)-C(70)-N(7)-B(4)	-4.0(6)
N(8)-B(4)-N(7)-C(70)	3.2(5)
Br(4)-B(4)-N(7)-C(70)	112.7(5)
N(7)-C(70)-N(8)-B(4)	3.9(6)
N(7)-B(4)-N(8)-C(70)	-3.3(5)
Br(4)-B(4)-N(8)-C(70)	-115.3(5)

Symmetry transformations used to generate equivalent atoms:

Table 1.12. Crystal data and structure refinement for **11**.

Identification code	**11**	
Empirical formula	C14 H25 B Cl2 N2	
Formula weight	303.07	
Temperature	153(2) K	
Wavelength	0.71069 Å	
Crystal system	Monoclinic	
Space group	P2(1)/n	
Unit cell dimensions	a = 13.590(5) Å	α= 90.000(5)°.
	b = 7.324(5) Å	β= 94.622(5)°.
	c = 16.451(5) Å	γ = 90.000(5)°.
Volume	1632.1(14) $Å^3$	
Z	4	
Density (calculated)	1.233 Mg/m^3	
Absorption coefficient	0.387 mm^{-1}	
F(000)	648	
Crystal size	0.26 x 0.20 x 0.18 mm^3	
Theta range for data collection	2.48 to 27.49°.	
Index ranges	-17<=h<=17, -9<=k<=9, -21<=l<=21	
Reflections collected	6930	
Independent reflections	3739 [R(int) = 0.0584]	
Completeness to theta = 27.49°	99.6 %	
Absorption correction	None	
Max. and min. transmission	0.9336 and 0.9061	
Refinement method	Full-matrix least-squares on F^2	
Data / restraints / parameters	3739 / 0 / 172	
Goodness-of-fit on F^2	0.973	
Final R indices [I>2sigma(I)]	R1 = 0.0484, wR2 = 0.1045	
R indices (all data)	R1 = 0.1284, wR2 = 0.1309	
Largest diff. peak and hole	0.286 and -0.305 $e.Å^{-3}$	

Table 1.13. Bond lengths [Å] and angles [°] for **11**.

C(1)-N(2)	1.329(3)
C(1)-N(1)	1.330(3)
B(1)-N(1)	1.559(3)
B(1)-N(2)	1.569(3)
B(1)-Cl(1)	1.820(3)
B(1)-Cl(2)	1.846(3)
N(2)-C(1)-N(1)	101.21(18)
N(1)-B(1)-N(2)	82.14(16)
N(1)-B(1)-Cl(1)	115.89(18)
N(2)-B(1)-Cl(1)	116.20(17)
N(1)-B(1)-Cl(2)	114.51(17)
N(2)-B(1)-Cl(2)	114.32(17)
Cl(1)-B(1)-Cl(2)	111.13(14)
C(1)-N(1)-B(1)	88.52(17)
C(3)-N(1)-B(1)	141.09(19)
C(1)-N(2)-B(1)	88.13(17)
C(9)-N(2)-B(1)	141.18(19)

Symmetry transformations used to generate equivalent atoms:

Table 1.14. Torsion angles [°] for **11**.

N(2)-C(1)-N(1)-B(1)	-0.12(19)
C(2)-C(1)-N(1)-B(1)	179.6(2)
N(2)-B(1)-N(1)-C(1)	0.10(16)
N(1)-C(1)-N(2)-B(1)	0.12(19)
C(2)-C(1)-N(2)-B(1)	-179.6(2)
N(1)-B(1)-N(2)-C(1)	-0.10(16)

Symmetry transformations used to generate equivalent atoms:

Table 1.15. Crystal data and structure refinement for **12**.

Identification code	**12**	
Empirical formula	C40 H60 B Cl2 N2	
Formula weight	650.61	
Temperature	153(2) K	
Wavelength	0.71069 Å	
Crystal system	Monoclinic	
Space group	C2/c	
Unit cell dimensions	a = 13.338(5) Å	α= 90°.
	b = 18.927(5) Å	β= 92.677(5)°.
	c = 15.336(5) Å	γ = 90°.
Volume	3867(2) $Å^3$	
Z	4	
Density (calculated)	1.117 Mg/m^3	
Absorption coefficient	0.196 mm^{-1}	
F(000)	1412	
Crystal size	0.20 x 0.16 x 0.14 mm^3	
Theta range for data collection	2.87 to 27.00°.	
Index ranges	-17<=h<=17, -24<=k<=23, -19<=l<=19	
Reflections collected	15927	
Independent reflections	8407 [R(int) = 0.0821]	
Completeness to theta = 27.00°	99.7 %	
Absorption correction	None	
Max. and min. transmission	0.9730 and 0.9618	
Refinement method	Full-matrix least-squares on F^2	
Data / restraints / parameters	8407 / 0 / 406	
Goodness-of-fit on F^2	0.916	
Final R indices [I>2sigma(I)]	R1 = 0.0604, wR2 = 0.1287	
R indices (all data)	R1 = 0.1775, wR2 = 0.1712	
Largest diff. peak and hole	0.266 and -0.288 $e.Å^{-3}$	

Table 1.16. Bond lengths [Å] and angles [°] for **12**.

C(1)-N(2)	1.333(3)
C(1)-N(1)	1.338(3)
B(1)-N(2)	1.564(4)
B(1)-N(1)	1.565(4)
B(1)-Cl(2)	1.832(4)
B(1)-Cl(1)	1.832(4)
N(2)-C(1)-N(1)	100.6(2)
N(2)-C(1)-C(2)	129.3(3)
N(2)-B(1)-N(1)	82.1(2)
N(2)-B(1)-Cl(2)	117.0(2)
N(1)-B(1)-Cl(2)	114.5(2)
N(2)-B(1)-Cl(1)	113.7(2)
N(1)-B(1)-Cl(1)	116.5(2)
Cl(2)-B(1)-Cl(1)	110.62(19)
C(1)-N(1)-C(20)	130.6(2)
C(1)-N(1)-B(1)	88.5(2)
C(1)-N(2)-C(26)	130.7(2)
C(1)-N(2)-B(1)	88.8(2)

Symmetry transformations used to generate equivalent atoms:

#1 -x+1,-y+1,-z+1

Table 1.17. Torsion angles [°] for **12**.

N(2)-C(1)-N(1)-B(1)	0.2(2)
C(2)-C(1)-N(1)-B(1)	179.4(3)
C(21)-C(20)-N(1)-C(1)	91.9(3)
C(25)-C(20)-N(1)-C(1)	-146.6(3)
C(21)-C(20)-N(1)-B(1)	-94.6(4)
C(25)-C(20)-N(1)-B(1)	26.9(4)
N(2)-B(1)-N(1)-C(1)	-0.16(19)
Cl(2)-B(1)-N(1)-C(1)	-116.3(2)
Cl(1)-B(1)-N(1)-C(1)	112.4(2)
N(2)-B(1)-N(1)-C(20)	-175.3(3)
Cl(2)-B(1)-N(1)-C(20)	68.6(4)
Cl(1)-B(1)-N(1)-C(20)	-62.7(4)
N(1)-C(1)-N(2)-C(26)	178.8(2)
C(2)-C(1)-N(2)-C(26)	-0.4(4)
N(1)-C(1)-N(2)-B(1)	-0.2(2)
C(2)-C(1)-N(2)-B(1)	-179.4(3)
C(27)-C(26)-N(2)-C(1)	92.0(3)
C(31)-C(26)-N(2)-C(1)	-145.3(3)
C(27)-C(26)-N(2)-B(1)	-89.6(4)
C(31)-C(26)-N(2)-B(1)	33.0(4)
N(1)-B(1)-N(2)-C(1)	0.16(19)
Cl(2)-B(1)-N(2)-C(1)	113.7(2)
Cl(1)-B(1)-N(2)-C(1)	-115.4(2)
N(1)-B(1)-N(2)-C(26)	-178.6(3)
Cl(2)-B(1)-N(2)-C(26)	-65.1(4)
Cl(1)-B(1)-N(2)-C(26)	65.9(4)

Symmetry transformations used to generate equivalent atoms:

#1 -x+1,-y+1,-z+1

Table 1.18. Crystal data and structure refinement for **13**.

Identification code	**13**	
Empirical formula	C8 H17 B Cl2 N2	
Formula weight	222.95	
Temperature	153(2) K	
Wavelength	0.71069 Å	
Crystal system	triclinic	
Space group	P-1	
Unit cell dimensions	a = 7.409(5) Å	α= 94.529(5)°.
	b = 8.127(5) Å	β= 92.529(5)°.
	c = 10.436(5) Å	γ = 104.188(5)°.
Volume	606.0(6) $Å^3$	
Z	2	
Density (calculated)	1.222 Mg/m^3	
Absorption coefficient	0.497 mm^{-1}	
F(000)	236	
Crystal size	0.10 x 0.10 x 0.10 mm^3	
Theta range for data collection	3.11 to 27.48°.	
Index ranges	-9<=h<=9, -10<=k<=10, -13<=l<=13	
Reflections collected	4848	
Independent reflections	2750 [R(int) = 0.0432]	
Completeness to theta = 27.48°	98.7 %	
Absorption correction	None	
Max. and min. transmission	0.9520 and 0.9520	
Refinement method	Full-matrix least-squares on F^2	
Data / restraints / parameters	2750 / 0 / 123	
Goodness-of-fit on F^2	0.989	
Final R indices [I>2sigma(I)]	R1 = 0.0486, wR2 = 0.1095	
R indices (all data)	R1 = 0.1109, wR2 = 0.1336	
Largest diff. peak and hole	0.379 and -0.269 $e.Å^{-3}$	

Table 1.19. Bond lengths [Å] and angles [°] for **13**.

C(1)-N(1)	1.325(3)
C(1)-N(2)	1.334(3)
B(1)-N(1)	1.561(4)
B(1)-N(2)	1.567(4)
B(1)-Cl(1)	1.835(3)
B(1)-Cl(2)	1.842(3)
N(1)-C(1)-N(2)	101.2(2)
N(1)-B(1)-N(2)	82.15(18)
N(1)-B(1)-Cl(1)	115.25(19)
N(2)-B(1)-Cl(1)	115.36(18)
N(1)-B(1)-Cl(2)	115.62(18)
N(2)-B(1)-Cl(2)	115.5(2)
Cl(1)-B(1)-Cl(2)	110.52(16)
C(1)-N(1)-B(1)	88.59(19)
C(1)-N(2)-B(1)	88.05(19)

Symmetry transformations used to generate equivalent atoms:

Table 1.20. Torsion angles [°] for **12**.

N(2)-C(1)-N(1)-B(1)	0.8(2)
N(2)-B(1)-N(1)-C(1)	-0.69(18)
Cl(1)-B(1)-N(1)-C(1)	-115.1(2)
Cl(2)-B(1)-N(1)-C(1)	113.9(2)
N(1)-C(1)-N(2)-B(1)	-0.8(2)
N(1)-B(1)-N(2)-C(1)	0.69(18)
Cl(1)-B(1)-N(2)-C(1)	115.0(2)
Cl(2)-B(1)-N(2)-C(1)	-114.0(2)

Symmetry transformations used to generate equivalent atoms:

Table 1.21. Crystal data and structure refinement for **14**.

Identification code	**14**	
Empirical formula	C23 H36 B Cl N2	
Formula weight	386.80	
Temperature	153(2) K	
Wavelength	0.71069 Å	
Crystal system	Monoclinic	
Space group	P2(1)/n	
Unit cell dimensions	a = 8.893(5) Å	α= 90°.
	b = 17.194(5) Å	β= 92.754(5)°.
	c = 14.511(5) Å	γ = 90°.
Volume	2216.3(16) $Å^3$	
Z	4	
Density (calculated)	1.159 Mg/m^3	
Absorption coefficient	0.182 mm^{-1}	
F(000)	840	
Crystal size	0.30 x 0.20 x 0.20 mm^3	
Theta range for data collection	2.75 to 27.49°.	
Index ranges	-11<=h<=11, -22<=k<=22, -18<=l<=18	
Reflections collected	9399	
Independent reflections	5028 [R(int) = 0.0329]	
Completeness to theta = 27.49°	98.8 %	
Absorption correction	None	
Max. and min. transmission	0.9644 and 0.9473	
Refinement method	Full-matrix least-squares on F^2	
Data / restraints / parameters	5028 / 0 / 244	
Goodness-of-fit on F^2	1.028	
Final R indices [I>2sigma(I)]	R1 = 0.0432, wR2 = 0.1019	
R indices (all data)	R1 = 0.0817, wR2 = 0.1172	
Largest diff. peak and hole	0.311 and -0.256 $e.Å^{-3}$	

Table 1.22. Bond lengths [Å] and angles [°] for **14**.

C(1)-N(2)	1.3361(19)
C(1)-N(1)	1.3446(19)
C(18)-B(1)	1.595(2)
B(1)-N(2)	1.572(2)
B(1)-N(1)	1.583(2)
B(1)-Cl(1)	1.8658(18)
N(2)-C(1)-N(1)	100.20(12)
N(2)-C(1)-C(2)	128.01(13)
N(2)-B(1)-N(1)	81.36(10)
N(2)-B(1)-C(18)	115.75(13)
N(1)-B(1)-C(18)	115.89(13)
N(2)-B(1)-Cl(1)	112.81(11)
N(1)-B(1)-Cl(1)	113.41(11)
C(18)-B(1)-Cl(1)	113.77(11)
C(1)-N(1)-C(6)	134.57(12)
C(1)-N(1)-B(1)	88.70(11)
C(6)-N(1)-B(1)	134.33(11)
C(1)-N(2)-C(12)	134.87(12)
C(1)-N(2)-B(1)	89.50(11)
C(12)-N(2)-B(1)	135.57(12)

Symmetry transformations used to generate equivalent atoms:

Table 1.23. Torsion angles [°] for **14**.

N(2)-C(1)-N(1)-B(1)	-3.94(12)
C(2)-C(1)-N(1)-B(1)	172.56(16)
N(2)-B(1)-N(1)-C(1)	3.33(10)
C(18)-B(1)-N(1)-C(1)	-111.17(14)
Cl(1)-B(1)-N(1)-C(1)	114.53(12)
N(2)-B(1)-N(1)-C(6)	166.90(15)
C(18)-B(1)-N(1)-C(6)	52.4(2)
Cl(1)-B(1)-N(1)-C(6)	-81.90(18)
N(1)-C(1)-N(2)-C(12)	-173.35(15)
C(2)-C(1)-N(2)-C(12)	10.0(3)
N(1)-C(1)-N(2)-B(1)	3.97(12)
C(2)-C(1)-N(2)-B(1)	-172.71(15)
C(17)-C(12)-N(2)-C(1)	88.14(19)
C(13)-C(12)-N(2)-C(1)	-149.89(16)
C(17)-C(12)-N(2)-B(1)	-88.03(19)
C(13)-C(12)-N(2)-B(1)	33.9(2)
N(1)-B(1)-N(2)-C(1)	-3.35(10)
C(18)-B(1)-N(2)-C(1)	111.30(14)
Cl(1)-B(1)-N(2)-C(1)	-115.20(12)
N(1)-B(1)-N(2)-C(12)	173.94(15)
C(18)-B(1)-N(2)-C(12)	-71.4(2)
Cl(1)-B(1)-N(2)-C(12)	62.1(2)

Symmetry transformations used to generate equivalent atoms:

Table 1.24. Crystal data and structure refinement for **15**.

Identification code	**15**	
Empirical formula	C23 H36 B Cl N2	
Formula weight	386.80	
Temperature	153(2) K	
Wavelength	0.71069 Å	
Crystal system	monoclinic	
Space group	P2(1)/c	
Unit cell dimensions	a = 9.939(5) Å	α= 90°.
	b = 20.598(5) Å	β= 93.204(5)°.
	c = 11.052(5) Å	γ = 90°.
Volume	2259.1(16) $Å^3$	
Z	4	
Density (calculated)	1.137 Mg/m^3	
Absorption coefficient	0.179 mm^{-1}	
F(000)	840	
Crystal size	0.10 x 0.10 x 0.10 mm^3	
Theta range for data collection	2.05 to 27.48°.	
Index ranges	-12<=h<=12, -26<=k<=21, -14<=l<=14	
Reflections collected	8308	
Independent reflections	5147 [R(int) = 0.0543]	
Completeness to theta = 27.48°	99.4 %	
Absorption correction	None	
Max. and min. transmission	0.9823 and 0.9823	
Refinement method	Full-matrix least-squares on F^2	
Data / restraints / parameters	5147 / 0 / 244	
Goodness-of-fit on F^2	1.009	
Final R indices [I>2sigma(I)]	R1 = 0.0590, wR2 = 0.1366	
R indices (all data)	R1 = 0.1729, wR2 = 0.2026	
Largest diff. peak and hole	0.436 and -0.487 $e.Å^{-3}$	

Table 1.25. Bond lengths [Å] and angles [°] for **15**.

C(1)-N(2)	1.332(4)
C(1)-N(1)	1.333(4)
C(1)-C(2)	1.485(4)
C(18)-B(1)	1.591(5)
B(1)-N(2)	1.580(4)
B(1)-N(1)	1.590(4)
B(1)-Cl(1)	1.862(4)
N(2)-C(1)-N(1)	101.1(2)
N(2)-B(1)-C(18)	116.6(2)
N(2)-B(1)-N(1)	80.90(19)
C(18)-B(1)-N(1)	116.5(3)
N(2)-B(1)-Cl(1)	112.5(2)
C(18)-B(1)-Cl(1)	113.7(2)
N(1)-B(1)-Cl(1)	112.6(2)
C(1)-N(1)-B(1)	88.8(2)
C(1)-N(2)-B(1)	89.2(2)

Symmetry transformations used to generate equivalent atoms:

Table 1.26. Torsion angles [°] for **15**.

N(2)-C(1)-N(1)-B(1)	-1.3(2)
N(2)-B(1)-N(1)-C(1)	1.1(2)
Cl(1)-B(1)-N(1)-C(1)	111.8(2)
N(1)-C(1)-N(2)-B(1)	1.4(2)
N(1)-B(1)-N(2)-C(1)	-1.1(2)
Cl(1)-B(1)-N(2)-C(1)	-111.9(2)
C(18)-B(1)-N(2)-C(12)	-74.0(4)
N(1)-B(1)-N(2)-C(12)	170.7(3)
Cl(1)-B(1)-N(2)-C(12)	60.0(4)

Symmetry transformations used to generate equivalent atoms:

Table 1.27 Crystal data and structure refinement for **16**.

Identification code	**16**	
Empirical formula	$C_{19}H_{27}BCl_2N_2$	
Formula weight	365.15	
Temperature	153(2) K	
Wavelength	0.71069 Å	
Crystal system	monoclinic	
Space group	C2/c	
Unit cell dimensions	a = 37.418(5) Å	α= 90°
	b = 6.561(5) Å	β= 100.318(5)°
	c = 15.964(5) Å	γ = 90°
Volume	3856(3) $Å^3$	
Z	4	
Density (calculated)	1.258 Mg/m^3	
Absorption coefficient	0.340 mm^{-1}	
F(000)	1552	
Crystal size	0.30 x 0.30 x 0.30 mm^3	
Theta range for data collection	3.09 to 27.00°.	
Index ranges	-47<=h<=47, -8<=k<=7, -20<=l<=20	
Reflections collected	7446	
Independent reflections	4204 [R(int) = 0.0518]	
Completeness to theta = 27.00°	99.6 %	
Absorption correction	None	
Max. and min. transmission	0.9050 and 0.9050	
Refinement method	Full-matrix least-squares on F^2	
Data / restraints / parameters	4204 / 0 / 217	
Goodness-of-fit on F^2	1.031	
Final R indices [I>2sigma(I)]	R1 = 0.0480, wR2 = 0.1018	
R indices (all data)	R1 = 0.1029, wR2 = 0.1209	
Largest diff. peak and hole	0.462 and -0.287 $e.Å^{-3}$	

Table 1.28. Bond lengths [Å] and angles [°] for **16**.

C(1)-B(1)	1.589(3)
C(7)-N(1)	1.501(3)
C(13)-N(2)	1.166(3)
C(13)-N(1)	1.282(3)
B(1)-N(1)	1.583(3)
B(1)-Cl(2)	1.874(3)
B(1)-Cl(1)	1.887(3)
N(2)-C(13)-N(1)	172.7(3)
N(1)-B(1)-C(1)	110.15(18)
N(1)-B(1)-Cl(2)	106.16(16)
C(1)-B(1)-Cl(2)	113.21(17)
N(1)-B(1)-Cl(1)	106.08(16)
C(1)-B(1)-Cl(1)	112.99(17)
Cl(2)-B(1)-Cl(1)	107.78(13)
C(13)-N(1)-C(7)	116.91(17)
C(13)-N(1)-B(1)	119.68(18)
C(7)-N(1)-B(1)	123.34(17)

Symmetry transformations used to generate equivalent atoms:

Table 1.29. Torsion angles [°] for **16**.

N(2)-C(13)-N(1)-C(7)	-75.6(19)
N(2)-C(13)-N(1)-B(1)	101.5(19)
C(8)-C(7)-N(1)-B(1)	126.9(2)
C(1)-B(1)-N(1)-C(13)	7.5(3)
Cl(2)-B(1)-N(1)-C(13)	130.4(2)
Cl(1)-B(1)-N(1)-C(13)	-115.1(2)
C(1)-B(1)-N(1)-C(7)	-175.60(19)

Symmetry transformations used to generate equivalent atoms:

Table 1.30. Crystal data and structure refinement for **18**.

Identification code	**18**	
Empirical formula	C23 H31 B Br2 Fe N2	
Formula weight	561.98	
Temperature	153(2) K	
Wavelength	0.71069 Å	
Crystal system	monoclinic	
Space group	P2(1)/n	
Unit cell dimensions	a = 13.953(5) Å	α= 90.000(5)°.
	b = 10.716(5) Å	β= 103.837(5)°.
	c = 15.723(5) Å	γ = 90.000(5)°.
Volume	2282.7(15) $Å^3$	
Z	4	
Density (calculated)	1.635 Mg/m^3	
Absorption coefficient	4.174 mm^{-1}	
F(000)	1136	
Crystal size	0.30 x 0.30 x 0.30 mm^3	
Theta range for data collection	2.42 to 27.00°.	
Index ranges	-17<=h<=17, -13<=k<=13, -20<=l<=20	
Reflections collected	8684	
Independent reflections	4966 [R(int) = 0.0459]	
Completeness to theta = 27.00°	99.5 %	
Absorption correction	None	
Max. and min. transmission	0.3674 and 0.3674	
Refinement method	Full-matrix least-squares on F^2	
Data / restraints / parameters	4966 / 0 / 298	
Goodness-of-fit on F^2	0.995	
Final R indices [I>2sigma(I)]	R1 = 0.0431, wR2 = 0.0736	
R indices (all data)	R1 = 0.0927, wR2 = 0.0849	
Largest diff. peak and hole	0.699 and -0.643 $e.Å^{-3}$	

Table 1.31. Bond lengths [Å] and angles [°] for **18**.

C(1)-N(2)	1.337(4)
C(1)-N(1)	1.345(4)
C(1)-B(1)	2.013(5)
B(1)-N(1)	1.545(5)
B(1)-N(2)	1.545(5)
B(1)-Br(2)	2.009(4)
B(1)-Br(1)	2.009(4)
N(2)-C(1)-N(1)	100.2(3)
N(2)-C(1)-B(1)	50.09(19)
N(1)-C(1)-B(1)	50.10(19)
C(14)-C(1)-B(1)	178.1(3)
N(1)-B(1)-N(2)	83.5(2)
N(1)-B(1)-Br(2)	115.3(2)
N(2)-B(1)-Br(2)	116.1(3)
N(1)-B(1)-Br(1)	114.3(3)
N(2)-B(1)-Br(1)	114.1(2)
Br(2)-B(1)-Br(1)	111.09(19)
N(1)-B(1)-C(1)	41.89(16)
N(2)-B(1)-C(1)	41.61(16)
Br(2)-B(1)-C(1)	125.6(2)
Br(1)-B(1)-C(1)	123.3(2)
C(1)-N(1)-C(2)	132.7(3)
C(1)-N(1)-B(1)	88.0(2)

Symmetry transformations used to generate equivalent atoms:

Table 1.32. Torsion angles [°] for **18**.

N(1)-C(2)-C(3)-C(4)	178.4(3)
N(1)-C(2)-C(7)-C(6)	-179.4(3)
N(2)-C(8)-C(9)-C(10)	-177.4(3)
N(2)-C(8)-C(13)-C(12)	179.2(3)
N(2)-C(1)-B(1)-N(1)	-179.9(4)
C(14)-C(1)-B(1)-N(1)	56(8)
N(1)-C(1)-B(1)-N(2)	179.9(4)
C(14)-C(1)-B(1)-N(2)	-124(8)
N(2)-C(1)-B(1)-Br(2)	-90.5(3)
N(1)-C(1)-B(1)-Br(2)	89.4(3)
C(14)-C(1)-B(1)-Br(2)	145(8)
N(2)-C(1)-B(1)-Br(1)	89.9(3)
N(1)-C(1)-B(1)-Br(1)	-90.3(3)
C(14)-C(1)-B(1)-Br(1)	-34(8)
N(2)-C(1)-N(1)-C(2)	170.8(3)
B(1)-C(1)-N(1)-C(2)	170.7(4)
N(2)-C(1)-N(1)-B(1)	0.1(3)
C(3)-C(2)-N(1)-B(1)	89.2(5)
C(7)-C(2)-N(1)-B(1)	-34.5(5)
N(2)-B(1)-N(1)-C(1)	-0.1(2)
Br(2)-B(1)-N(1)-C(1)	-116.0(3)
Br(1)-B(1)-N(1)-C(1)	113.5(3)
Br(2)-B(1)-N(1)-C(2)	74.4(5)
Br(1)-B(1)-N(1)-C(2)	-56.1(5)
N(1)-C(1)-N(2)-B(1)	-0.1(3)
N(1)-B(1)-N(2)-C(1)	0.1(2)

Symmetry transformations used to generate equivalent atoms:

Table 1.33 Crystal data and structure refinement for **21**.

Identification code	**21**	
Empirical formula	C19 H28 Al B Cl4 N2 Si2	
Formula weight	520.20	
Temperature	153(2) K	
Wavelength	0.71069 Å	
Crystal system	Monoclinic	
Space group		
Unit cell dimensions	a = 10.270(5) Å	α= 90.000(5)°.
	b = 17.940(5) Å	β= 96.673(5)°.
	c = 16.896(5) Å	γ = 90.000(5)°.
Volume	3092(2) $Å^3$	
Z	4	
Density (calculated)	1.118 Mg/m^3	
Absorption coefficient	0.497 mm^{-1}	
F(000)	1080	
Crystal size	0.20 x 0.15 x 0.10 mm^3	
Theta range for data collection	1.66 to 27.50°.	
Index ranges	-13<=h<=13, -23<=k<=17, -21<=l<=21	
Reflections collected	11603	
Independent reflections	7066 [R(int) = 0.0403]	
Completeness to theta = 27.50°	99.4 %	
Absorption correction	None	
Refinement method	Full-matrix least-squares on F^2	
Data / restraints / parameters	7066 / 0 / 268	
Goodness-of-fit on F^2	2.356	
Final R indices [I>2sigma(I)]	R1 = 0.2248, wR2 = 0.5817	
R indices (all data)	R1 = 0.3054, wR2 = 0.6198	
Largest diff. peak and hole	9.742 and -0.954 e.$Å^{-3}$	

CHAPTER 2: Towards Boron(I): Rational Ligand Design *Via* A Combined Theoretical and Experimental Approach

Introduction

One of the vibrant themes of current main group chemistry is focused on the preparation, structural characterization and ligative behaviour of group 13 carbene analogues. An early development in this respect was the isolation of the gallyl anions $[Ga\{N(R)CH\}_2]^-$ (**25**: R= ^{t}Bu; **26**: R = 2,6-^{i}Pr$_2$C$_6$H$_3$) [1,2], which represent the first examples of anionic NHC analogues (**A**, Scheme 2.1). Gallyl anion **26** exhibits a rich coordination chemistry [3]. More recently, the boryl anion $[B\{N(R)CH\}_2]^-$ (R = 2,6-^{i}Pr$_2$C$_6$H$_3$) (**27**) has been isolated as its lithium salt [4] as has the saturated Wanzlick carbene analogue, $[B\{N(R)CH_2\}_2]^-$ (**28**)[5] (**B**, Scheme 2.1). The latter undergoes reactions with group 11 metal chlorides to afford the corresponding boryl complexes [5] and the former reacts with $MgBr_2{\cdot}OEt_2$ to form boryl-magnesium derivatives [6]. In terms of neutral carbene-analogous systems, the guanidinate ligand $[Cy_2NC\{NR\}_2]^-$ has proved to be effective for the support of Ga (**29**) [7] and In (**30**) [7] in the +1 oxidation state (**C**, Scheme 2.1). Moreover, compounds **29** and **30** are interesting analogues of a recently reported four-membered NHC [8]. The use of the β-diketiminate supporting ligand $[HC(CMe)_2(NR)_2]^-$ (R = 2,6-^{i}Pr$_2$C$_6$H$_3$) has permitted the isolation of the widest range of group 13 metal (I) entities reported thus far, namely M = Al [9], Ga [10], In [11], and Tl [12]. However, a structurally authenticated example of a boron (I) carbenoid species of this type is conspicuos by

its absence. On the basis of theoretical studies [13,14], this absence has been attributed to the small energy gap between the singlet and triplet ground states of boron(I)-β-diketiminates. For example, B3LYP/LANL2DZ calculations by Chen *et al.* [13] on [{HC(CMe)$_2$(NPh)$_2$}B] revealed the triplet state to be more stable than the singlet state by 3.5 kcal/mol, while for the Al, Ga, In, and Tl analogues the singlet-triplet gap exceeds 45 kcal/mol. The triplet state of such β-diketiminate-supported boron (I) compounds can be visualized as featuring a single electron at the B atom and a second electron that is delocalized over the five remaining ring atoms [14]. In turn, this unpaired electron density on the ring periphery is capable of promoting facile reactions of boron(I)-β-diketiminates with e.g. solvents and residual reactants.

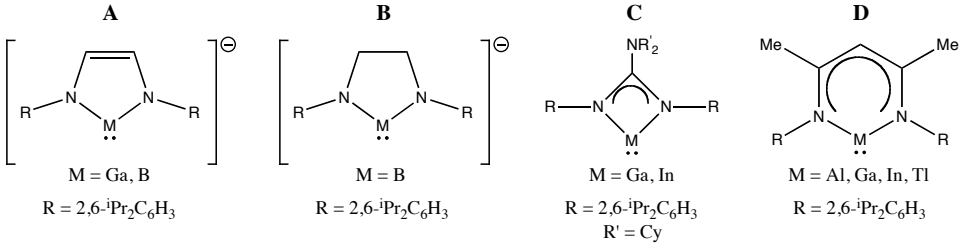

Scheme 2.1 Carbene analogous group 13 compounds.

The recent discovery that sterically encumbered guanidinate ligands are able to support N,N-chelated Ga(I) and In(I), compounds **29** [7] and **30** [7], prompted curiosity regarding the potential use of this ligand class for the stabilization and isolation of analogous B(I) derivatives. As the first step in this direction, a theoretical investigation of the singlet-triplet splitting of a model compound, [Me$_2$NC{N(Ph)}$_2$]B (**31**) was undertaken.

Results and Discussion

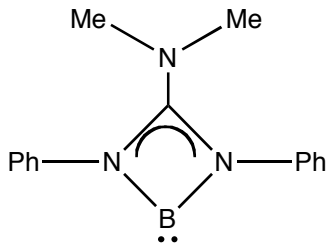

31

It has been pointed out that DFT calculations inherently favor spin states of high multiplicities due to the explicit consideration of Fermi correlation through exact exchange admixture [14,15]. Accordingly, it was considered appropriate to carry out both DFT and MP2 calculations on the model compound **31**. The results are summarized in Table 2.1. The largest differences in the two sets of metrical parameters are found for the B-N bond length and the N-C-N angle. As expected on the basis of the overemphasis of triplet state stability in the DFT calculation, the singlet-triplet gap is computed to be smaller by this method than by the MP2 method. The salient point however, is that according to either method the singlet ground state is preferred by between 6 and 10 kcal/mol. While the singlet-triplet splitting for **31** is less than that computed for e.g. $[Cy_2NC(NDipp)_2]Al$ by the DFT method (61.8 kcal/mol) [7], these calculations suggest that an appropriately substituted (guanidinate)boron(I) derivative might be viable.The HOMO and LUMO of **31** are depicted in Fig. 2.1.

Table 2.1. Computed bond lengths (Å), bond angles (°) and singlet-triplet splitting (kcal/mol) for **31**

	B3LYP	MP2
B-N	1.553	1.589
C-N_{ring}	1.365	1.351
C-N_{exo}	1.348	1.343
N-B-N	83.59	82.41
C-N-B	86.42	87.97
N-C-N	98.62	101.66
Singlet-triplet gap	6.0	10.1

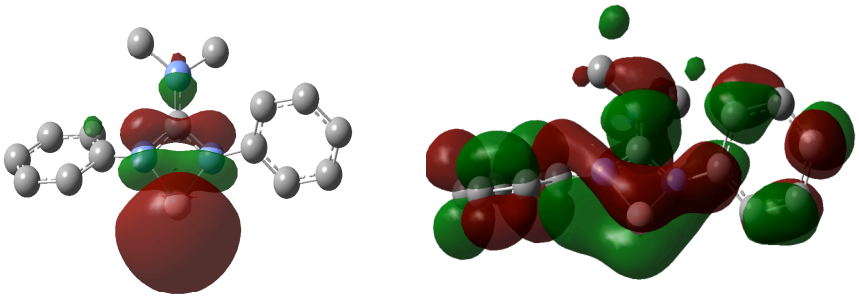

Figure 2.1. HOMO and LUMO of **31**. Calculations performed at the MP2/6-31G* level of theory

(Guanidinate)boron dihalides represented an obvious first choice as precursors to the desired boron (I) derivatives. However, as pointed out by Aldridge *et al.* [16], until recently there were no structurally authenticated examples of this type of compound and, at the time of writing, $[Cy_2NC(NCy)_2BCl_2]$ (**32**) and $[^{i}Pr_2NC(NCy)_2BCl_2]$ (**33**) represent the only such examples [16]. The syntheses and X-ray crystal structures of two new examples of this rare class of compound have now been accomplished, namely $[Ph_2NC(NMes)_2BCl_2]$ (Mes = 2,4,6-trimethylphenyl) and $[Ph_2NC(NDipp)_2BCl_2]$ (Dipp = 2,6-$^{i}Pr_2C_6H_3$). Previously, it has been shown [17] that $[(Me_3Si)_2NC\{NCy\}_2BCl_2]$ can be prepared either by the metathetical reaction of $(Me_3Si)_2NLi$ with the carbodiimide CyN=C=NCy or by the insertion of this carbodiimide into $(Me_3Si)_2NBCl_2$. Unfortunately, neither method resulted in crystals suitable for X-ray diffraction experiments. For the syntheses of the new (guanidinate)boron dichlorides the metathetical route summarized in Scheme 2.2, was selected.

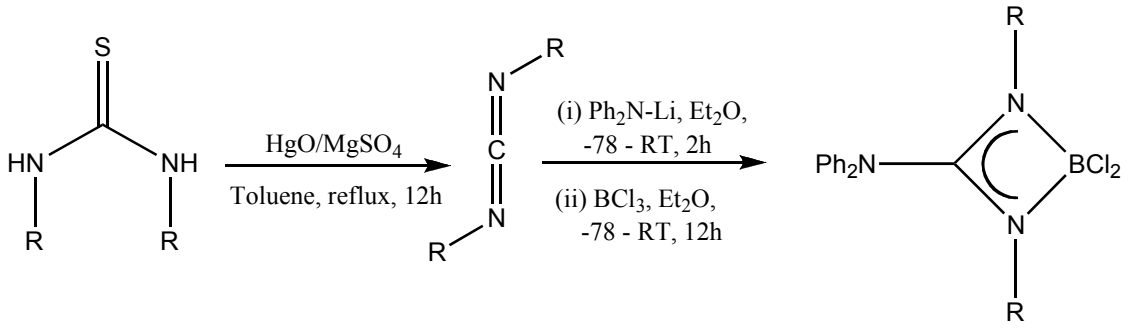

R = Mes (**34**) and Dipp (**35**)

R = Mes (**36**) and Dipp (**37**)

R = Mes (**38**) and Dipp (**39**)

Scheme 2.2. Synthesis of (guanidinate)boron dichlorides.

The thioureas **34** and **35** were isolated as colorless microcrystalline solids from the reaction of CS_2 with a solution of the appropriate aniline, trimethylamine and water. Although both compounds were claimed in a Japanese patent [18], we considered it useful to provide full details of the synthetic method as well as the X-ray crystal structure of **35** (*vide infra*). Treatment of thioureas **34** and **35** with mercuric oxide and magnesium sulfate in refluxing toluene solution afforded the corresponding carbodiimides **36** and **37** in yields of 85% and 87% respectively [19]. The initial step in the synthesis of the guanidinate(boron) dichlorides **38** and **39** involved the insertion of one equivalent of the appropriate carbodiimide into the lithium-nitrogen bond of $LiNPh_2$. Subsequent treatment of these reaction mixtures with boron trichloride in diethyl ether solution at low temperature readily afforded these compounds in yields of 90% and 88%, respectively. Attempts were made to reduce **38** and **39** to the corrresponding boron (I) derivatives using a variety of alkali metals and other reducing agents. However, **38** and **39** failed to react.

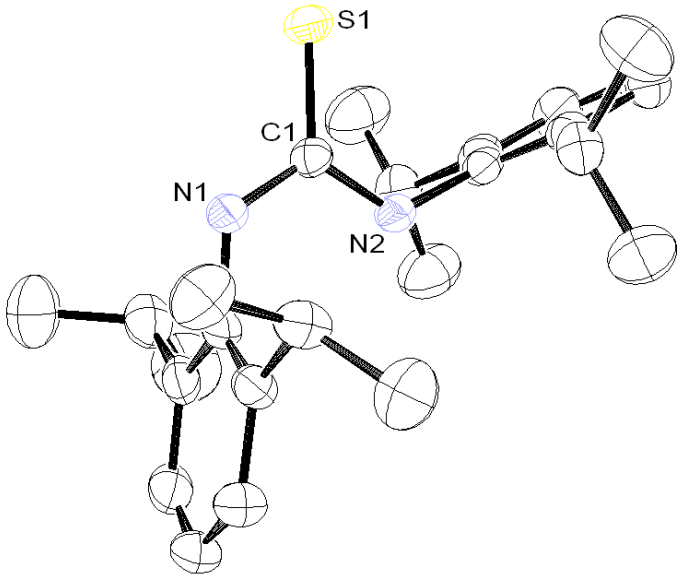

Fig 2.2. ORTEP diagram of **35**, with thermal ellipsoids at 40 % probability. All hydrogen atoms have been omitted for clarity. Selected bond lengths (Å) and angles (°): N(1)-C(1) 1.346(3), N(2)-C(1) 1.353(3), C(1)-S(1) 1.682(2), N(1)-C(1)-N(2) 116.61(19), N(1)-C(1)-S(1) 121.38(17), N(2)-C(1)-S(1) 122.00(17).

Crystals of **35** suitable for study by X-ray diffraction were grown from toluene solution at -40°C. Thiourea **35** crystallizes in the monoclinic space group *C*2/c and the solid state consists of arrays of individual molecules with no unusually short intermolecular contacts. The molecular structure is depicted in Fig. 2.2 and data collection/refinement details are listed in Table 2.2. Interestingly, despite the presence of the bulky Dipp substituents, the N-C-N bond angle (116.61(19)°) is less than the ideal trigonal planar value. Note, however, that the Dipp substituents are arranged in a transoid fashion to minimize steric interactions. Compound **36** crystallizes from toluene solution in the triclinic space group *P*-1. The solid state comprises monomers

of **36** (Fig. 2.3) and there are no short intermolecular contacts. The N-C-N bond angle of 167.82(15)° deviates substantially from the ideal value of 180° and the bulky Mes substituents are arranged in a mutually orthogonal fashion. The average N-C bond distance of 1.213(2) Å is consistent with those reported previously for carbodiimides with less bulky substituents [20].

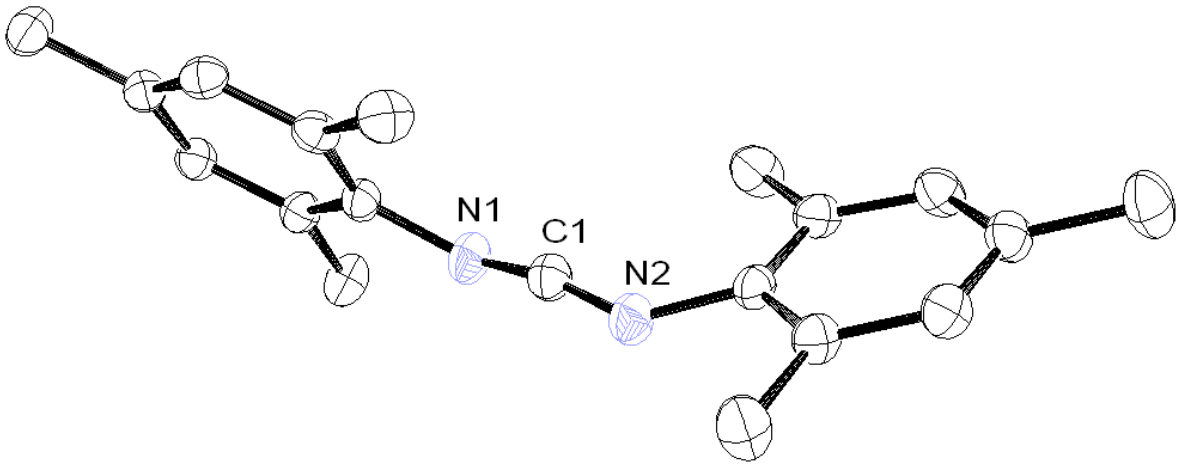

Fig 2.3. ORTEP diagram of **36**, with thermal ellipsoids at 40% probability. All hydrogen atoms have been omitted for clarity. Selected bond lengths (Å) and angles (°): N(1)-C(1) 1.2107(18), N(2)-C(1) 1.2179(18), N(1)-C(2) 1.4072(19), N(2)-C(11) 1.4077(18), N(1)-C(1)-N(2) 167.82(15), C(1)-N(1)-C(2) 137.62(13), C(1)-N(2)-C(11) 135.75(13).

The Dipp-substituted analogue **37** crystallizes in the monoclinic space group $P2_1/c$ as an ensemble of monomers. While the N-C-N bond angle of **37** (169.3(2)°) is

marginally less distorted than that of **36**, the most striking structural feature is the near co-planarity of the aryl rings – in marked contrast to the orthogonal relationship observed in the case of **36**. Examination of the packing diagram for **37** shows that this confirmation is influenced by the existence of weak intermolecular interactions between the carbon atoms of one monomer with the methyl-hydrogens of another.

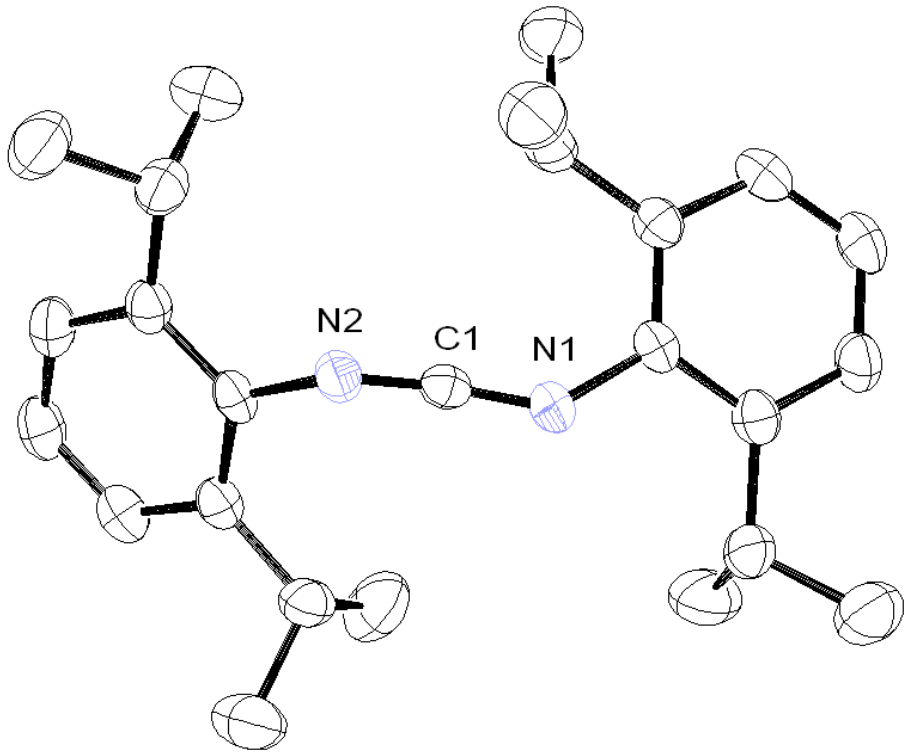

Fig 2.4. ORTEP diagram of **37**, with thermal ellipsoids at 40% probability. All hydrogen atoms have been omitted for clarity. Selected bond lengths (Å) and angles (°): N(1)-C(1) 1.213(2), N(2)-C(1) 1.221(2), N(1)-C(2) 1.415(2), N(2)-C(14) 1.425(2), N(1)-C(1)-N(2) 169.3(2), C(1)-N(1)-C(2) 138.73(17), C(1)-N(2)-C(14) 131.51(17).

Crystals of **38** and **39** suitable for X-ray diffraction studies were grown from toluene solution at -40°C. Compounds **38** and **39** crystallize in the monoclinic space groups $P2_1/c$ and Pc, respectively. Neither solid state structure exhibits any unusually short intermolecular contacts. The molecular structures of **38** and **39** are illustrated in Fig. 2.4 and 2.55, respectively. Both compounds feature a four-membered B-N-C-N chelate ring, the average C-N bond distances for which are 1.350(3) (**38**) and 1.351(6) Å (**39**). These values are approximately intermediate between those of typical C=N double and C-N single bonds. Moreover, the B-N-C-N torsion angles for both compounds are zero (within experimental error), which is indicative of π-electron delocalization about the N-C-N junction. The average B-N distances of 1.564(3) (**14**) and 1.574(2) Å (**15**) fall within the typical range of 1.55-1.61 Å that has been observed for a four coordinate boron atom bound to a three coordinate nitrogen atom [21]. The N-B-N bite angles for the guanidinate rings are 83.69(14) and 83.4(3)° for **38** and **39**, respectively and are more acute than those reported by Aldridge *et al*. [16]. By contrast, the bite angles in closely related amidinate rings fall within the range of approximately 85-86° [17,22]. The average N-B-Cl bond angles are 114.90(16)° and 117.6(3)° for **38** and **39**, respectively, hence the geometry about the boron atom is appreciably distorted form that of a regular tetrahedron. Finally, it is worth noting that the C(1)-N(3) distances of 1.342(3) (**38**) and 1.353(6) Å (**39**) are remarkably short and therefore consistent with the idea of a substantial contribution from the iminium/diamide resonance form to the bonding descriptions of both compounds.

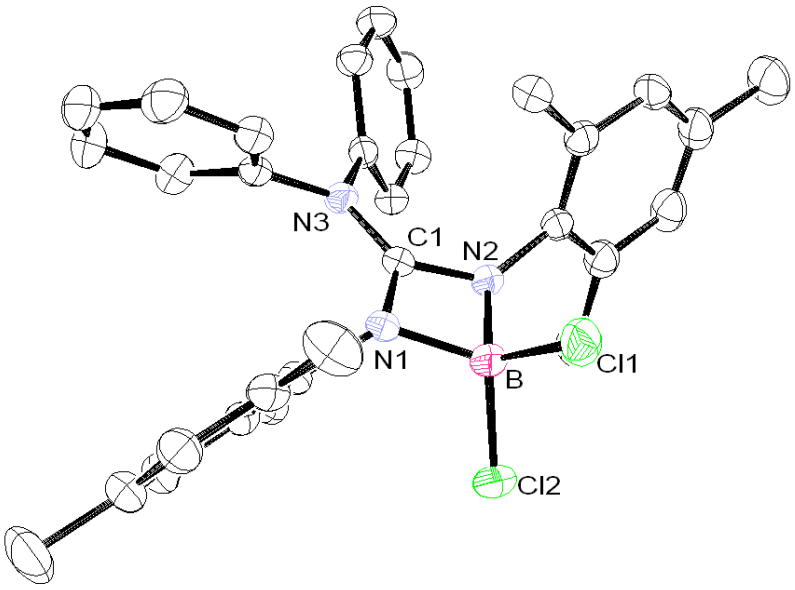

Fig 2.5. ORTEP diagram of **38**, with thermal ellipsoids at 40% probability. All hydrogen atoms have been omitted for clarity. Selected bond lengths (Å) and angles (°): N(1)-C(1) 1.346(3), N(2)-C(1) 1.353(2), N(3)-C(1) 1.342(2), N(1)-B(1) 1.559(3), N(2)-B(1) 1.566(3), B(1)-Cl(1) 1.833(3), B(1)-Cl(2) 1.837(3), N(1)-C(1)-N(2) 101.15(16), N(1)-C(1)-N(3) 129.00(17), N(2)-C(1)-N(3) 129.84(18), N(1)-B(1)-N(2) 83.69(14), N(1)-B(1)-Cl(1) 117.56(16), N(1)-B(1)-Cl(2) 112.95(15), N(2)-B(1)-Cl(1) 113.36(16), N(2)-B(1)-Cl(2) 116.84(17), N(1)-C(1)-N(2)-B(1) 0.15(0.17).

The ^{1}H, $^{13}C\{^{1}H\}$ and ^{11}B NMR spectra of both **38** and **39** indicate that the solid state structure is retained in solution. The ^{11}B NMR spectra exhibit intense singlet resonances at δ 6.8 (**38**) and 9.2 (**39**), values which are typical of those reported for four-coordinate boron atoms [23] and are in good agreement with values reported for closely related (guanidinate)boron dihalides [17]. Moreover, due to the inherent difficulty in detecting low intensity quaternary carbon centers, the carbon atom of the N-C-N fragment could not be detected.

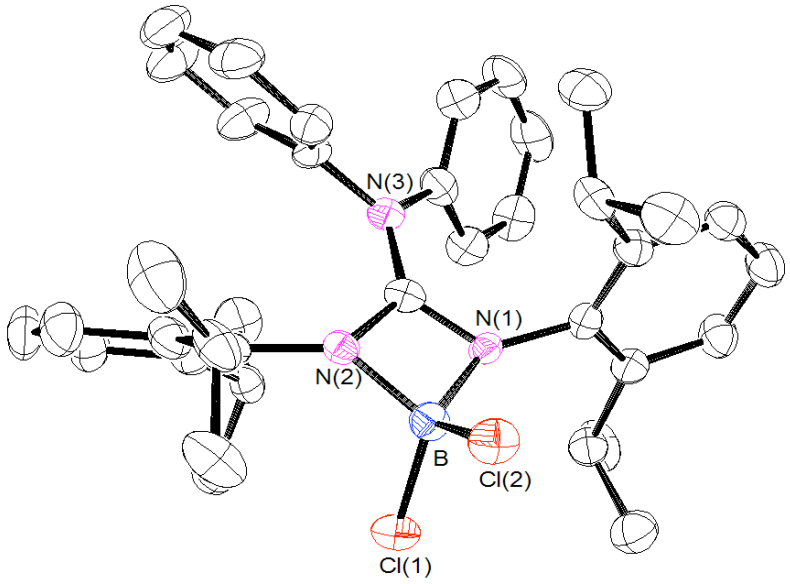

Fig 2.6. ORTEP diagram of **39**, with thermal ellipsoids at 40% probability. All hydrogen atoms have been omitted for clarity. Selected bond lengths (Å) and angles (°): N(1)-C(1) 1.341(6), N(2)-C(1) 1.360(5), N(3)-C(1) 1.353(6), N(1)-B(1) 1.578(6), N(2)-B(1) 1.570(7), B(1)-Cl(1) 1.833(6), B(1)-Cl(2) 1.833(5), N(1)-C(1)-N(2) 101.6(4), N(1)-C(1)-N(3) 131.6(4), N(2)-C(1)-N(3) 126.8(4), N(1)-B(1)-N(2) 83.4(3), N(1)-B(1)-Cl(1) 118.1(3), N(1)-B(1)-Cl(2) 112.4(3), N(2)-B(1)-Cl(1) 112.4(3), N(2)-B(1)-Cl(2) 117.1(3), N(1)-C(1)-N(2)-B(1) 0.9(0.3).

Conclusions

In summary, the possibility of synthesizing guanidinate-supported boron(I) derivatives by reduction of two new (guanidinate)boron dichlorides has been explored. Although the desired compounds were not obtained, DFT and MP2 calculations on a model system revealed the ground state is a singlet and that the HOMO-LUMO gap may be sufficiently large to permit the future isolation of the desired boron(I) species. Ongoing computational work is aimed at addressing the specific tailoring of substituents to maximize this energy splitting to determine the most desirable ligand scaffold.

Experimental section

(a) General procedures

All manipulations and reactions were performed under a dry, oxygen-free, catalysts scrubbed argon atmosphere using a combination of standard Schlenk techniques or in an M-Braun or Vacuum Atmospheres drybox. All glassware was oven dried and vacuum- and argon-flow degassed before use. All solvents were distilled over sodium benzophenone ketyl, except dichloromethane, which was distilled over CaH_2, and degassed prior to use. All reagents were purchased from commercial sources and used without further purification.

(b) Physical measurements

Low-resolution mass spectra were obtained on a Finnigan MAT TSQ-700 mass spectrometer and high-resolution CI mass spectra recorded on a VG analytical ZAB-VE sector instrument. All MS analyses were performed on samples that had been sealed in glass capillaries under an argon atmosphere. ^{1}H, $^{13}C\{^{1}H\}$ and ^{11}B NMR spectra were recorded at 295 K on a GE EQ-300 instrument (^{1}H, 300 MHz ^{13}C, 75 MHz, ^{11}B, 96 MHz) immediately following removal of the sample from the drybox. ^{1}H and $^{13}C\{^{1}H\}$ chemical shift values are reported in parts per million (ppm) relative to $SiMe_4$ (δ 0.00), using residual solvent resonances as internal standards. ^{11}B NMR data are referenced to $BF_3{\cdot}OEt_2$ (δ 0.00).

(c) X-ray crystallography

For compounds **35**, **36**, **37**, **38** and **39**, a crystal of suitable quality was removed from a Schlenk flask under positive argon pressure, covered immediately with degassed

hydrocarbon oil and mounted on a glass fiber. The X-ray diffraction data were collected at 153 K on a Nonius Kappa CCD diffractometer equipped with an Oxford Cryostream low-temperature device and a graphite-monochromated Mo Kα radiation source (λ = 0.71073 Å). Corrections were applied for Lorentz and polarization effects. All structures were solved by direct methods [24] and refined for full-matrix least-squares cycles on F^2. All non-hydrogen atoms were allowed anisotropic thermal motion, and all hydrogen atoms were placed in fixed, calculated positions using the riding model (C-H 0.96 Å). Selected crystal data, and data collection and refinement parameters are listed in Table 2.2.

(d) Syntheses

Synthesis of MesN(H)C(S)N(H)Mes (34). Carbon disulfide (9.53 g, 125 mmol) was added dropwise to a stirred mixture of $MesNH_2$ (33.8 g, 250 mmol) and NEt_3 (25.5 g, 250 mmol) in 100 mL of water at room temperature. The reaction mixture was stirred for 1 h at room temperature and then heated to 90ºC for 14 h. After re-cooling the reaction mixture to room temperature, it was poured into 100 mL of CH_2Cl_2, following which the organic layer was separated and dried over $MgSO_4$. After filtration, the filtrate was concentrated and stored at -40ºC to afford a 90% yield of white powder **34**. ^{1}H NMR ($CDCl_3$): δ 7.66 (s, 1H, NH), 7.01 (s, 2H, Ar-H), 6.87 (s, 2H, Ar-H), 6.51 (s, 1H, NH), 2.41 (s, 6H, Ar-CH_3), 2.35 (s, 3H, Ar-CH_3), 2.25 (s, 3H, Ar-CH_3), 2.18 (s, 6H, Ar-CH_3); ^{13}C NMR ($CDCl_3$): δ 181.7 (C=S), 138.0 (Ar), 137.6 (Ar), 136.3 (Ar), 130.1 (Ar), 129.3 (Ar), 21.3 (Ar-CH_3), 18.8 (Ar-CH_3), 18.4 (Ar-CH_3). MS (CI^+, CH_4): *m/z* 313 (M+H). HRMS (CI, CH_4) calcd. For $C_{19}H_{25}N_2S$ 313.1738; found 313.1735.

Synthesis of DippN(H)C(S)N(H)Dipp (35). Colorless crystals of **35** were prepared in 93% yield from $DippNH_2$ (94 g, 530 mmol), CS_2 (20.20 g, 260 mmol) and NEt_3 (54.0 g, 530 mmol) using the procedure described above for **34**. ^1H NMR ($CDCl_3$): δ 8.93 (s, 1H, NH), 7.29 (dd, 2H, Ar-H), 7.20 (d, 4H, Ar-H), 6.41 (s, 1H, NH), 3.42 (sept, 2H, Ar-C(H)Me_2), 3.05 (sept, 2H, Ar-C(H)Me_2), 1.38 (m, 18H, Ar-CH$(Me)_2$), 1.08 (d, 6H, Ar-CH$(Me)_2$); ^{13}C NMR ($CDCl_3$): δ 182.6 (C=S), 148.4 (Ar), 146.9 (Ar), 133.4 (Ar), 131.1 (Ar), 130.4 (Ar), 128.9 (Ar), 124.6 (Ar), 123.9 (Ar), 29.3 (Ar-C(H)Me_2), 28.9 (Ar-C(H)Me_2), 26.2 (Ar-CH$(Me)_2$), 24.5 (Ar-C(H)Me_2), 24.0 (Ar-C(H)Me_2), 22.1 (Ar-CH$(Me)_2$ MS (CI^+, CH_4): *m/z* 397 (M+H). HRMS (CI, CH_4) calcd. for $C_{25}H_{37}N_2S$ 397.2677; found 397.2671.

Synthesis of MesN=C=NMes (36). A mixture of **34** (624 mg, 2 mmol), HgO (870 mg, 4 mmol) and anhydrous $MgSO_4$ (580 mg, 4.8 mmol) in 50 mL of toluene was refluxed overnight. After cooling to room temperature, the reaction mixture was filtered over Celite ® and the filtrate concentrated to dryness to afford an 85% yield of the title compound as a colorless microcrystalline solid. ^1H NMR (CD_2Cl_2): δ 6.89 (s, 4H, Ar-H), 2.40 (s, 12H, Ar-CH_3), 2.30 (s, 6H, Ar-CH_3); ^{13}C NMR (CD_2Cl_2): δ 134.5 (Ar), 132.9 (Ar), 129.5 (Ar), 129.4 (Ar), 21.1 (Ar-CH_3), 19.2 (Ar-CH_3). MS (CI^+, CH_4): *m/z* 278 (M+H). HRMS (CI, CH_4) calcd. for $C_{19}H_{23}N_2$, 279.1861; found 279.1860.

Synthesis of DippN=C=NDipp (37). Colorless crystals of **37** were prepared in 87% yield from **35** using the procedure described above for **36**. ^1H NMR ($CDCl_3$): δ 7.39

(dd, 2H, Ar-H), 7.31 (d, 4H, Ar-H), 3.62 (sept, 4H, Ar-C(H)Me_2), 1.41 (d, 24H, Ar-CH$(Me)_2$); ^{13}C NMR ($CDCl_3$): δ 143.2 (Ar), 129.1 (Ar), 125.3 (Ar), 123.7 (Ar), 29.6 (Ar-C(H)Me_2), 23.6 (Ar-CH$(Me)_2$). MS (CI^+, CH_4): *m/z* 363 (M+H). HRMS (CI, CH_4) calcd. for $C_{25}H_{35}N_2$ 363.2800; found 363.2789.

Synthesis of $[Ph_2NC\{NMes\}_2]BCl_2$ (38). A stirred solution of diphenylamine (339 mg, 2 mmol) in diethyl ether (20 mL) was cooled to -78ºC and ^{n}BuLi (1 eq.) added *via* syringe. The reaction mixture was allowed to warm to room temperature and stirred for a further hour, at which point it was re-cooled to -78ºC and an ethereal solution (10 mL) of **36** (558 mg, 2 mmol) was added. The reaction mixture was once more allowed to warm to room temperature following which it was stirred for 1 h. For a third time the solution was cooled to -78ºC and BCl_3 (2 mL, 1.0 M solution in hexane, 1 eq.) was added *via* syringe. The reaction mixture was then allowed to warm slowly to room temperature amd was stirred overnight. After filtration and solvent stripping, **38** was isolated as a white solid in 90% yield. ^{1}H NMR (CD_2Cl_2): δ 6.93 (dd, 2H, Ar-H), 6.66 (m, 4H, Ar-H), 6.57 (m, 4H, Ar-H), 6.46 (s, 4H, Ar-H), 2.43 (s, 12H, Ar-CH_3), 2.21 (s, 6H, Ar-CH_3); ^{13}C NMR (CD_2Cl_2): δ 140.3 (Ar), 136.0 (Ar), 135.73 (Ar), 129.65 (Ar), 129.52 (Ar), 127.50 (Ar), 125.43 (Ar), 21.06 (Ar-Me), 20.26 (Ar-Me); ^{11}B NMR (CD_2Cl_2): δ 6.79. MS (CI^+, CH_4): *m/z* minor 528 (M+H), major 491 (M-Cl).

Synthesis of $[Ph_2NC\{NDipp\}_2]BCl_2$ (39). Colorless needle-like, crystals of **39** were prepared in 88% yield from **37** using the same procedure that was described for

38. ^{1}H NMR ($CDCl_3$): δ 7.24 (m, 8H, Ar-H), 7.10 (m, 8H, Ar-H), 3.78 (sept, 2H, Ar-C(H)Me_2), 3.61 (sept, 2H, Ar-C(H)Me_2), 1.41 (m, 24H, Ar-CH$(Me)_2$); ^{13}C NMR ($CDCl_3$): δ 147.32 (Ar), 146.80 (Ar), 142.96 (Ar), 128.79 (Ar), 127.60 (Ar), 125.1 (Ar), 124.89 (Ar), 124.63 (Ar), 123.48 (Ar), 29.35 (Ar-(C)HMe_2), 23.45 (Ar-CH$(Me)_2$); ^{11}B NMR ($CDCl_3$): δ 9.17. MS (CI^+, CH_4): *m/z* 612 (M+H). HRMS (CI, CH_4) calcd. for $C_{37}H_{44}BCl_2N_3$ 611.3131; found 611.3123.

References

1 E. S. Schmidt, A. Jockish and H. Schmidbaur, *J. Am. Chem. Soc.*, 1999, **121**, 9758.

2 R. J. Baker, R. D. Farley, C. Jones, M. Kloth and D. M. Murphy, *J. Chem. Soc., Dalton Trans.*, 2002, 3844.

3 R. J. Baker and C. Jones, *Coord. Chem. Rev.*, 2005, **249**, 1857.

4 Y. Segawa, M. Yamashita and K. Nozaki, *Science*, 2006, **314**, 5796.

5 Y. Segawa, M. Yamashita and K. Nozaki, *Angew. Chem., Int. Ed.*, 2007, **46**, 6710.

6 M. Yamashita, Y. Suzuki, Y. Segawa and K. Nozaki, *J. Am. Chem. Soc.*, 2007, **129**, 9570.

7 C. Jones, P. C. Junk, J. A. Platts and A. Stasch, *J. Am. Chem. Soc.*, 2006, **128**, 2206.

8 E. Despagnet-Ayoub and R. H. Grubbs, *J. Am. Chem. Soc.*, 2004, **126**, 10198.

9 C. Cui, H. W. Roesky, H.-G. Schmidt, M. Noltemeyer, H. Hao and F. Cimpoesu, *Angew. Chem., Int. Ed.*, 2000, **39**, 4274.

10 N. J. Hardman, B. E. Eichler and P. P. Power, *Chem. Commun.*, 2000, 1991.

11 M. S. Hill and P. B. Hitchcock, *Chem Commun.*, 2004, 1818

12 M. S. Hill, P. B. Hitchcock and R. Pongtavornpinyo, *Dalton Trans.*, 2005, 273.

13 C.-H. Chen, M.-L. Tsai and M.-D. Su, *Organometallics*, 2006, **25**, 2766.

14 M. Reiher and A. Sundermann, *Eur. J. Inorg. Chem.*, 2002, 1854.

15 M. Reiher, O. Salomon and B. A. Hess, *Theo. Chim. Acta*, 2001, **107**, 48.

16 G. A. Pierce, N. D. Coombs, D. J. Willock, J. K. Day, A. Stasch and S. Aldridge, *Dalton Trans.*, 2007, 4405.

17 M. Findlater, N. J. Hill and A. H. Cowley, *Polyhedron*, 2006, **25**, 983.

18 K. Ogawa and M. Akazawa, Japanese Patent JP 04312568, 1992.

19 W. Weith, *Chem. Ber.*, 1873, **6**, 1389.

20 V. H. Irngartinger and H.-U. Jäger, *Acta. Cryst.*, 1978, B**34**, 3262; A. T. Vincent and P. J. Wheatley, *J. Chem. Soc, Perkin Trans. 2*, 1972, 1567

21 A. Ansorge, D. J. Braner, H. Burger, F. Dorrenbach, T. Hagen, G. Pawlke and W. Wenter, *J. Organomet. Chem.*, 1991, **407**, 283.

22 N. J. Hill, M. Findlater and A. H. Cowley, *Dalton Trans.*, 2005, 3229; N. J. Hill, J. A. Moore, M. Findlater and A. H. Cowley, *Chem. Commun.*, 2005, 5462.

23 H. Nöth and B. Wrackmeyer, *Nuclear Magnetic Resonance of Boron Compounds*, Springer Verlag, Berlin, 1978.

24 G. M. Sheldrick, SHELL-PC, Version 5.03, Siemens Analytical Instruments Inc., Madison, WI, USA, 1994.

Table 2.2. Selected crystal data, data collection and refinement parameters for **35**, **36**, **37**, **38** and **39**

	35	**36**	**37**	**38**	**39**
Formula	$C_{25}H_{34}N_2S$	$C_{19}H_{22}N_2$	$C_{25}H_{34}N_2$	$C_{31}H_{32}N_3BCl_2$	$C_{37}H_{44}N_3BCl_2$
Formula weight	394.6	278.39	362.54	528.31	612.46
Crystal system	Monoclinic	Triclinic	Monoclinic	Monoclinic	Monoclinic
Space group	*C2/c*	*P-1*	P2(1)/c	*P2(1)/c*	Pc
a/Å	25.444(5)	8.400(5)	9.0454(18)	16.925(5)	12.258(5)
b/*Å*	14.858(5)	8.612(5)	13.424(3)	12.612(5)	10.481(5)
c/Å	18.332(5)	11.692(5)	18.684(4)	16.354(5)	16.149(5)
α /°	90	76.709(5)	90	90	90
β /°	122.823(5)	75.502(5)	102.93(3)	104.074(5)	124.90(2)
γ/°	90	82.349	90	90	90
V/Å^3	5824(5)	794.4(7)	2211.1(9)	3386(2)	1701.5(12)
Z	8	2	4	4	2
P_{calcd}/g cm^{-3}	0.900	1.164	1.089	1.036	1.195
F(000)	1712	300	792	1112	652
Crystal size/mm	0.30 x 0.30 x 0.25	0.40 x 0.40 x 0.30	0.30 x 0.25 x 0.20	0.35 x 0.35 x 0.25	0.10 x 0.06 x 0.06
θ range/°	2.39 to 26.99	2.75 to 27.52	2.70 to 27.43	2.56 to 27.50	1.94 to 27.49
No. of reflns. collected	11537	5357	4989	13089	6945
No. of indep reflns.	6670	3594	2375	7728	6936
R1[$I > 2\sigma(I)$]	0.0716	0.0488	0.0566	0.0562	0.0581
wR$_2$ (all data)	0.2144	0.1294	0.1250	0.1426	0.1242
Peak and hole/e.Å^{-3}	0.426 and -0.296	0.210 and -0.241	0.181 and -0.182	0.378 and -0.295	0.433 and -0.743

Tables of Crystallographic Data

Table 2.3. Crystal data and structure refinement for **35.**

Identification code	**35**	
Empirical formula	C50 H72 N4 S2	
Formula weight	793.24	
Temperature	153(2) K	
Wavelength	0.71069 Å	
Crystal system	Monoclinic	
Space group	C2/c	
Unit cell dimensions	a = 25.444(5) Å	α= 90.000(5)°.
	b = 14.858(5) Å	β= 122.823(5)°.
	c = 18.332(5) Å	γ = 90.000(5)°.
Volume	5824(3) $Å^3$	
Z	4	
Density (calculated)	0.905 Mg/m^3	
Absorption coefficient	0.121 mm^{-1}	
F(000)	1728	
Crystal size	0.30 x 0.30 x 0.25 mm^3	
Theta range for data collection	1.67 to 27.49°.	
Index ranges	-33<=h<=33, -19<=k<=16, -23<=l<=23	
Reflections collected	11537	
Independent reflections	6670 [R(int) = 0.0352]	
Completeness to theta = 27.49°	99.7 %	
Absorption correction	None	
Max. and min. transmission	0.9704 and 0.9646	
Refinement method	Full-matrix least-squares on F^2	
Data / restraints / parameters	6670 / 0 / 269	
Goodness-of-fit on F^2	1.032	
Final R indices [I>2sigma(I)]	R1 = 0.0716, wR2 = 0.2144	
R indices (all data)	R1 = 0.1043, wR2 = 0.2328	
Largest diff. peak and hole	0.426 and -0.296 $e.Å^{-3}$	

Table 2.4. Bond lengths [Å] and angles [°] for **35**.

C(1)-N(1)	1.346(3)
C(1)-N(2)	1.353(3)
C(1)-S(1)	1.682(2)
C(2)-C(3)	1.393(3)
C(2)-C(7)	1.417(4)
C(2)-N(1)	1.439(3)
C(3)-C(4)	1.396(4)
C(3)-C(8)	1.518(4)
C(4)-C(5)	1.370(5)
C(5)-C(6)	1.408(4)
C(6)-C(7)	1.405(3)
C(7)-C(11)	1.503(3)
C(8)-C(10)	1.532(5)
C(8)-C(9)	1.545(4)
C(11)-C(12)	1.517(4)
C(11)-C(13)	1.536(4)
C(14)-C(15)	1.383(3)
C(14)-C(19)	1.404(3)
C(14)-N(2)	1.442(3)
C(15)-C(16)	1.392(4)
C(15)-C(20)	1.518(4)
C(16)-C(17)	1.401(4)
C(17)-C(18)	1.382(4)
C(18)-C(19)	1.391(3)
C(19)-C(23)	1.525(3)
C(20)-C(21)	1.511(4)
C(20)-C(22)	1.521(5)
C(23)-C(24)	1.498(4)
C(23)-C(25)	1.522(4)
N(1)-H(1)	0.94(4)
N(2)-H(2)	0.91(3)
N(1)-C(1)-N(2)	116.61(19)
N(1)-C(1)-S(1)	121.38(17)

N(2)-C(1)-S(1)	122.00(17)
C(3)-C(2)-C(7)	122.6(2)
C(3)-C(2)-N(1)	119.5(2)
C(7)-C(2)-N(1)	117.7(2)
C(2)-C(3)-C(4)	117.4(3)
C(2)-C(3)-C(8)	121.3(2)
C(4)-C(3)-C(8)	121.2(2)
C(5)-C(4)-C(3)	121.9(3)
C(4)-C(5)-C(6)	120.6(2)
C(7)-C(6)-C(5)	119.6(3)
C(6)-C(7)-C(2)	117.9(2)
C(6)-C(7)-C(11)	120.4(2)
C(2)-C(7)-C(11)	121.6(2)
C(3)-C(8)-C(10)	109.1(3)
C(3)-C(8)-C(9)	112.3(3)
C(10)-C(8)-C(9)	111.9(3)
C(7)-C(11)-C(12)	110.2(2)
C(7)-C(11)-C(13)	112.1(2)
C(12)-C(11)-C(13)	110.9(2)
C(15)-C(14)-C(19)	122.3(2)
C(15)-C(14)-N(2)	119.3(2)
C(19)-C(14)-N(2)	118.5(2)
C(14)-C(15)-C(16)	118.9(2)
C(14)-C(15)-C(20)	123.0(2)
C(16)-C(15)-C(20)	118.1(2)
C(15)-C(16)-C(17)	120.0(3)
C(18)-C(17)-C(16)	120.0(2)
C(17)-C(18)-C(19)	121.3(2)
C(18)-C(19)-C(14)	117.6(2)
C(18)-C(19)-C(23)	119.5(2)
C(14)-C(19)-C(23)	122.8(2)
C(21)-C(20)-C(15)	112.5(3)
C(21)-C(20)-C(22)	110.8(3)
C(15)-C(20)-C(22)	112.1(3)
C(24)-C(23)-C(25)	110.2(2)
C(24)-C(23)-C(19)	110.8(2)

C(25)-C(23)-C(19)	113.8(2)
C(1)-N(1)-C(2)	125.56(19)
C(1)-N(1)-H(1)	122(2)
C(2)-N(1)-H(1)	112(2)
C(1)-N(2)-C(14)	123.11(19)
C(1)-N(2)-H(2)	122(2)
C(14)-N(2)-H(2)	115(2)

Symmetry transformations used to generate equivalent atoms:

Table 2.5. Torsion angles [°] for **35**.

C(7)-C(2)-C(3)-C(4)	0.3(4)
N(1)-C(2)-C(3)-C(4)	-175.7(2)
C(7)-C(2)-C(3)-C(8)	177.4(2)
N(1)-C(2)-C(3)-C(8)	1.3(4)
C(2)-C(3)-C(4)-C(5)	1.1(4)
C(8)-C(3)-C(4)-C(5)	-175.9(3)
C(3)-C(4)-C(5)-C(6)	-1.6(4)
C(4)-C(5)-C(6)-C(7)	0.7(4)
C(5)-C(6)-C(7)-C(2)	0.7(4)
C(5)-C(6)-C(7)-C(11)	178.1(3)
C(3)-C(2)-C(7)-C(6)	-1.2(4)
N(1)-C(2)-C(7)-C(6)	174.9(2)
C(3)-C(2)-C(7)-C(11)	-178.6(2)
N(1)-C(2)-C(7)-C(11)	-2.4(3)
C(2)-C(3)-C(8)-C(10)	-100.0(3)
C(4)-C(3)-C(8)-C(10)	76.9(3)
C(2)-C(3)-C(8)-C(9)	135.3(3)
C(4)-C(3)-C(8)-C(9)	-47.8(4)
C(6)-C(7)-C(11)-C(12)	-84.1(3)
C(2)-C(7)-C(11)-C(12)	93.2(3)
C(6)-C(7)-C(11)-C(13)	40.0(3)
C(2)-C(7)-C(11)-C(13)	-142.8(3)
C(19)-C(14)-C(15)-C(16)	-0.9(4)
N(2)-C(14)-C(15)-C(16)	178.5(2)
C(19)-C(14)-C(15)-C(20)	178.8(2)
N(2)-C(14)-C(15)-C(20)	-1.8(4)
C(14)-C(15)-C(16)-C(17)	-0.2(4)
C(20)-C(15)-C(16)-C(17)	-179.9(3)
C(15)-C(16)-C(17)-C(18)	1.0(4)
C(16)-C(17)-C(18)-C(19)	-0.8(4)
C(17)-C(18)-C(19)-C(14)	-0.3(4)
C(17)-C(18)-C(19)-C(23)	176.8(2)
C(15)-C(14)-C(19)-C(18)	1.1(3)
N(2)-C(14)-C(19)-C(18)	-178.2(2)

C(15)-C(14)-C(19)-C(23)	-175.8(2)
N(2)-C(14)-C(19)-C(23)	4.8(3)
C(14)-C(15)-C(20)-C(21)	121.7(3)
C(16)-C(15)-C(20)-C(21)	-58.6(4)
C(14)-C(15)-C(20)-C(22)	-112.6(3)
C(16)-C(15)-C(20)-C(22)	67.1(4)
C(18)-C(19)-C(23)-C(24)	-84.7(3)
C(14)-C(19)-C(23)-C(24)	92.2(3)
C(18)-C(19)-C(23)-C(25)	40.3(3)
C(14)-C(19)-C(23)-C(25)	-142.8(3)
N(2)-C(1)-N(1)-C(2)	-1.2(3)
S(1)-C(1)-N(1)-C(2)	179.05(17)
C(3)-C(2)-N(1)-C(1)	-92.7(3)
C(7)-C(2)-N(1)-C(1)	91.0(3)
N(1)-C(1)-N(2)-C(14)	177.4(2)
S(1)-C(1)-N(2)-C(14)	-2.8(3)
C(15)-C(14)-N(2)-C(1)	-91.4(3)
C(19)-C(14)-N(2)-C(1)	88.0(3)

Symmetry transformations used to generate equivalent atoms:

Table 2.6. Crystal data and structure refinement for **36**

Identification code	**36**	
Empirical formula	C19 H22 N2	
Formula weight	278.39	
Temperature	153(2) K	
Wavelength	0.71069 Å	
Crystal system	Triclinic	
Space group	P-1	
Unit cell dimensions	a = 8.400(5) Å	α= 76.709(5)°.
	b = 8.612(5) Å	β= 75.502(5)°.
	c = 11.692(5) Å	γ = 82.349(5)°.
Volume	794.4(7) $Å^3$	
Z	2	
Density (calculated)	1.164 Mg/m^3	
Absorption coefficient	0.068 mm^{-1}	
F(000)	300	
Crystal size	0.40 x 0.40 x 0.30 mm^3	
Theta range for data collection	2.75 to 27.50°.	
Index ranges	-10<=h<=8, -11<=k<=11, -15<=l<=14	
Reflections collected	5353	
Independent reflections	3591 [R(int) = 0.0219]	
Completeness to theta = 27.50°	98.4 %	
Absorption correction	None	
Max. and min. transmission	0.9798 and 0.9732	
Refinement method	Full-matrix least-squares on F^2	
Data / restraints / parameters	3591 / 0 / 196	
Goodness-of-fit on F^2	1.038	
Final R indices [I>2sigma(I)]	R1 = 0.0488, wR2 = 0.1294	
R indices (all data)	R1 = 0.0689, wR2 = 0.1446	
Largest diff. peak and hole	0.210 and -0.241 $e.Å^{-3}$	

Table 2.7. Bond lengths [Å] and angles [°] for **36**.

C(1)-N(1)	1.2107(18)
C(1)-N(2)	1.2179(18)
C(2)-C(7)	1.3985(19)
C(2)-C(3)	1.4037(19)
C(2)-N(1)	1.4073(19)
C(3)-C(4)	1.388(2)
C(3)-C(8)	1.5034(19)
C(4)-C(5)	1.3915(19)
C(5)-C(6)	1.3926(19)
C(5)-C(9)	1.500(2)
C(6)-C(7)	1.389(2)
C(7)-C(10)	1.5049(19)
C(11)-C(12)	1.4012(19)
C(11)-C(16)	1.404(2)
C(11)-N(2)	1.4077(18)
C(12)-C(13)	1.389(2)
C(12)-C(17)	1.509(2)
C(13)-C(14)	1.386(2)
C(14)-C(15)	1.389(2)
C(14)-C(18)	1.507(2)
C(15)-C(16)	1.389(2)
C(16)-C(19)	1.508(2)
N(1)-C(1)-N(2)	167.82(15)
C(7)-C(2)-C(3)	121.18(12)
C(7)-C(2)-N(1)	116.39(12)
C(3)-C(2)-N(1)	122.42(12)
C(4)-C(3)-C(2)	118.08(12)
C(4)-C(3)-C(8)	120.34(12)
C(2)-C(3)-C(8)	121.57(13)
C(3)-C(4)-C(5)	122.38(12)
C(4)-C(5)-C(6)	117.84(13)
C(4)-C(5)-C(9)	120.93(12)
C(6)-C(5)-C(9)	121.23(13)

C(7)-C(6)-C(5)	122.12(12)
C(6)-C(7)-C(2)	118.40(12)
C(6)-C(7)-C(10)	121.05(12)
C(2)-C(7)-C(10)	120.53(12)
C(12)-C(11)-C(16)	120.92(13)
C(12)-C(11)-N(2)	116.84(12)
C(16)-C(11)-N(2)	122.15(12)
C(13)-C(12)-C(11)	118.33(13)
C(13)-C(12)-C(17)	121.01(12)
C(11)-C(12)-C(17)	120.65(13)
C(14)-C(13)-C(12)	122.27(12)
C(13)-C(14)-C(15)	117.94(13)
C(13)-C(14)-C(18)	121.39(13)
C(15)-C(14)-C(18)	120.65(13)
C(16)-C(15)-C(14)	122.35(13)
C(15)-C(16)-C(11)	118.16(12)
C(15)-C(16)-C(19)	120.57(13)
C(11)-C(16)-C(19)	121.25(13)
C(1)-N(1)-C(2)	137.62(13)
C(1)-N(2)-C(11)	135.75(13)

Symmetry transformations used to generate equivalent atoms:

Table 2.8. Torsion angles [°] for **36**.

C(7)-C(2)-C(3)-C(4)	-0.35(19)
N(1)-C(2)-C(3)-C(4)	-179.19(12)
C(7)-C(2)-C(3)-C(8)	178.84(12)
N(1)-C(2)-C(3)-C(8)	0.0(2)
C(2)-C(3)-C(4)-C(5)	0.0(2)
C(8)-C(3)-C(4)-C(5)	-179.23(12)
C(3)-C(4)-C(5)-C(6)	0.4(2)
C(3)-C(4)-C(5)-C(9)	-178.73(12)
C(4)-C(5)-C(6)-C(7)	-0.50(19)
C(9)-C(5)-C(6)-C(7)	178.66(12)
C(5)-C(6)-C(7)-C(2)	0.14(19)
C(5)-C(6)-C(7)-C(10)	178.98(13)
C(3)-C(2)-C(7)-C(6)	0.30(19)
N(1)-C(2)-C(7)-C(6)	179.20(11)
C(3)-C(2)-C(7)-C(10)	-178.55(12)
N(1)-C(2)-C(7)-C(10)	0.36(19)
C(16)-C(11)-C(12)-C(13)	1.5(2)
N(2)-C(11)-C(12)-C(13)	177.91(12)
C(16)-C(11)-C(12)-C(17)	-178.30(13)
N(2)-C(11)-C(12)-C(17)	-1.87(19)
C(11)-C(12)-C(13)-C(14)	-0.8(2)
C(17)-C(12)-C(13)-C(14)	178.93(13)
C(12)-C(13)-C(14)-C(15)	-0.2(2)
C(12)-C(13)-C(14)-C(18)	178.65(14)
C(13)-C(14)-C(15)-C(16)	0.8(2)
C(18)-C(14)-C(15)-C(16)	-178.15(14)
C(14)-C(15)-C(16)-C(11)	-0.1(2)
C(14)-C(15)-C(16)-C(19)	-178.78(13)
C(12)-C(11)-C(16)-C(15)	-1.0(2)
N(2)-C(11)-C(16)-C(15)	-177.24(12)
C(12)-C(11)-C(16)-C(19)	177.63(13)
N(2)-C(11)-C(16)-C(19)	1.4(2)
N(2)-C(1)-N(1)-C(2)	131.6(7)
C(7)-C(2)-N(1)-C(1)	-175.19(16)

C(3)-C(2)-N(1)-C(1)	3.7(3)
N(1)-C(1)-N(2)-C(11)	133.0(7)
C(12)-C(11)-N(2)-C(1)	159.41(16)
C(16)-C(11)-N(2)-C(1)	-24.2(3)

Symmetry transformations used to generate equivalent atoms:

Table 2.9. Crystal data and structure refinement for **37**.

Identification code	**37**	
Empirical formula	C_{25} H_{34} N_2	
Formula weight	362.54 $gmol^{-1}$	
Temperature	153(2) K	
Wavelength	0.71073 Å	
Crystal system	monoclinic	
Space group	P21/c	
Unit cell dimensions	a = 9.0454(18) Å	α= 90°.
	b = 13.424(3) Å	β= 102.93(3)°.
	c = 18.684(4) Å	γ = 90°.
Volume	2211.1(8) $Å^3$	
Z	2	
Density (calculated)	1.089 Mg/m^3	
Absorption coefficient	0.063 mm^{-1}	
F(000)	792	
Crystal size	0.30 x 0.25 x 0.20 mm^3	
Theta range for data collection	2.70 to 27.43°.	
Index ranges	-11<=h<=11, -16<=k<=17, -24<=l<=24	
Reflections collected	8257	
Independent reflections	4989 [R(int) = 0.0592]	
Completeness to theta = 27.43°	99.1 %	
Absorption correction	None	
Max. and min. transmission	0.9875 and 0.9814	
Refinement method	Full-matrix least-squares on F^2	
Data / restraints / parameters	4989 / 0 / 253	
Goodness-of-fit on F^2	0.934	
Final R indices [I>2sigma(I)]	R1 = 0.0566, wR2 = 0.1250	
R indices (all data)	R1 = 0.1488, wR2 = 0.1615	
Extinction coefficient	0.009(2)	
Largest diff. peak and hole	0.181 and -0.182 $e.Å^{-3}$	

Table 2.10. Bond lengths [Å] and angles [°] for **37**.

C(1)-N(1)	1.213(2)
C(1)-N(2)	1.221(2)
C(2)-C(7)	1.400(3)
C(2)-C(3)	1.408(3)
C(2)-N(1)	1.415(2)
C(3)-C(4)	1.392(3)
C(3)-C(8)	1.510(3)
C(4)-C(5)	1.381(3)
C(5)-C(6)	1.376(3)
C(6)-C(7)	1.390(3)
C(7)-C(11)	1.519(3)
C(8)-C(10)	1.525(3)
C(8)-C(9)	1.527(3)
C(11)-C(12)	1.520(3)
C(11)-C(13)	1.522(3)
C(14)-C(15)	1.401(3)
C(14)-C(19)	1.405(3)
C(14)-N(2)	1.425(2)
C(15)-C(16)	1.398(3)
C(15)-C(20)	1.519(3)
C(16)-C(17)	1.375(3)
C(17)-C(18)	1.385(3)
C(18)-C(19)	1.380(3)
C(19)-C(23)	1.522(3)
C(20)-C(22)	1.527(3)
C(20)-C(21)	1.530(3)
C(23)-C(25)	1.520(3)
C(23)-C(24)	1.526(3)

N(1)-C(1)-N(2)	169.3(2)
C(7)-C(2)-C(3)	122.68(17)
C(7)-C(2)-N(1)	115.66(17)
C(3)-C(2)-N(1)	121.64(18)
C(4)-C(3)-C(2)	116.71(19)

C(4)-C(3)-C(8)	121.55(17)
C(2)-C(3)-C(8)	121.72(17)
C(5)-C(4)-C(3)	121.51(19)
C(6)-C(5)-C(4)	120.46(19)
C(5)-C(6)-C(7)	120.9(2)
C(6)-C(7)-C(2)	117.68(18)
C(6)-C(7)-C(11)	121.46(19)
C(2)-C(7)-C(11)	120.82(17)
C(3)-C(8)-C(10)	110.69(17)
C(3)-C(8)-C(9)	114.03(17)
C(10)-C(8)-C(9)	110.17(18)
C(7)-C(11)-C(12)	109.91(18)
C(7)-C(11)-C(13)	113.93(17)
C(12)-C(11)-C(13)	110.32(18)
C(15)-C(14)-C(19)	121.97(17)
C(15)-C(14)-N(2)	117.05(16)
C(19)-C(14)-N(2)	120.86(17)
C(16)-C(15)-C(14)	117.53(18)
C(16)-C(15)-C(20)	120.77(18)
C(14)-C(15)-C(20)	121.70(17)
C(17)-C(16)-C(15)	121.1(2)
C(16)-C(17)-C(18)	120.06(19)
C(19)-C(18)-C(17)	121.40(18)
C(18)-C(19)-C(14)	117.80(18)
C(18)-C(19)-C(23)	120.18(17)
C(14)-C(19)-C(23)	122.02(17)
C(15)-C(20)-C(22)	111.08(17)
C(15)-C(20)-C(21)	111.86(17)
C(22)-C(20)-C(21)	111.02(18)
C(25)-C(23)-C(19)	112.54(19)
C(25)-C(23)-C(24)	111.2(2)
C(19)-C(23)-C(24)	111.66(18)
C(1)-N(1)-C(2)	138.73(17)
C(1)-N(2)-C(14)	131.51(17)

Symmetry transformations used to generate equivalent atoms:

Table 2.11. Torsion angles [°] for **37**.

C(7)-C(2)-C(3)-C(4)	0.4(3)
N(1)-C(2)-C(3)-C(4)	178.53(18)
C(7)-C(2)-C(3)-C(8)	-177.92(17)
N(1)-C(2)-C(3)-C(8)	0.2(3)
C(2)-C(3)-C(4)-C(5)	-0.1(3)
C(8)-C(3)-C(4)-C(5)	178.20(18)
C(3)-C(4)-C(5)-C(6)	-0.2(3)
C(4)-C(5)-C(6)-C(7)	0.3(3)
C(5)-C(6)-C(7)-C(2)	0.0(3)
C(5)-C(6)-C(7)-C(11)	177.82(19)
C(3)-C(2)-C(7)-C(6)	-0.3(3)
N(1)-C(2)-C(7)-C(6)	-178.56(17)
C(3)-C(2)-C(7)-C(11)	-178.18(18)
N(1)-C(2)-C(7)-C(11)	3.6(3)
C(4)-C(3)-C(8)-C(10)	-99.0(2)
C(2)-C(3)-C(8)-C(10)	79.2(2)
C(4)-C(3)-C(8)-C(9)	25.9(3)
C(2)-C(3)-C(8)-C(9)	-155.91(19)
C(6)-C(7)-C(11)-C(12)	-91.1(2)
C(2)-C(7)-C(11)-C(12)	86.6(2)
C(6)-C(7)-C(11)-C(13)	33.2(3)
C(2)-C(7)-C(11)-C(13)	-149.0(2)
C(19)-C(14)-C(15)-C(16)	-3.7(3)
N(2)-C(14)-C(15)-C(16)	-179.63(16)
C(19)-C(14)-C(15)-C(20)	177.28(18)
N(2)-C(14)-C(15)-C(20)	1.3(3)
C(14)-C(15)-C(16)-C(17)	1.2(3)
C(20)-C(15)-C(16)-C(17)	-179.75(18)
C(15)-C(16)-C(17)-C(18)	1.3(3)
C(16)-C(17)-C(18)-C(19)	-1.5(3)
C(17)-C(18)-C(19)-C(14)	-0.9(3)
C(17)-C(18)-C(19)-C(23)	178.12(19)
C(15)-C(14)-C(19)-C(18)	3.6(3)
N(2)-C(14)-C(19)-C(18)	179.35(17)

C(15)-C(14)-C(19)-C(23)	-175.48(18)
N(2)-C(14)-C(19)-C(23)	0.3(3)
C(16)-C(15)-C(20)-C(22)	-78.1(2)
C(14)-C(15)-C(20)-C(22)	100.9(2)
C(16)-C(15)-C(20)-C(21)	46.5(3)
C(14)-C(15)-C(20)-C(21)	-134.4(2)
C(18)-C(19)-C(23)-C(25)	-50.3(3)
C(14)-C(19)-C(23)-C(25)	128.7(2)
C(18)-C(19)-C(23)-C(24)	75.5(3)
C(14)-C(19)-C(23)-C(24)	-105.4(2)
N(2)-C(1)-N(1)-C(2)	-136.1(9)
C(7)-C(2)-N(1)-C(1)	-170.7(2)
C(3)-C(2)-N(1)-C(1)	11.0(4)
N(1)-C(1)-N(2)-C(14)	-130.8(9)
C(15)-C(14)-N(2)-C(1)	-130.7(2)
C(19)-C(14)-N(2)-C(1)	53.3(3)

Symmetry transformations used to generate equivalent atoms:

Table 2.12. Crystal data and structure refinement for **38**.

Identification code	**38**	
Empirical formula	C31 H32 B Cl2 N3	
Formula weight	528.31	
Temperature	153(2) K	
Wavelength	0.71069 Å	
Crystal system	Monoclinic	
Space group	P2(1)/c	
Unit cell dimensions	a = 16.925(5) Å	α= 90.000(5)°.
	b = 12.612(5) Å	β= 104.074(5)°.
	c = 16.354(5) Å	γ = 90.000(5)°.
Volume	3386(2) $Å^3$	
Z	4	
Density (calculated)	1.036 Mg/m^3	
Absorption coefficient	0.212 mm^{-1}	
F(000)	1112	
Crystal size	0.35 x 0.35 x 0.25 mm^3	
Theta range for data collection	2.56 to 27.50°.	
Index ranges	-21<=h<=21, -16<=k<=12, -21<=l<=21	
Reflections collected	13089	
Independent reflections	7728 [R(int) = 0.0441]	
Completeness to theta = 27.50°	99.3 %	
Absorption correction	None	
Max. and min. transmission	0.9488 and 0.9294	
Refinement method	Full-matrix least-squares on F^2	
Data / restraints / parameters	7728 / 0 / 340	
Goodness-of-fit on F^2	0.943	
Final R indices [I>2sigma(I)]	R1 = 0.0562, wR2 = 0.1426	
R indices (all data)	R1 = 0.0975, wR2 = 0.1577	
Largest diff. peak and hole	0.378 and -0.295 $e.Å^{-3}$	

Table 2.13. Bond lengths [Å] and angles [°] for **38**.

C(1)-N(3)	1.342(2)
C(1)-N(1)	1.346(3)
C(1)-N(2)	1.353(2)
C(2)-C(7)	1.394(3)
C(2)-C(3)	1.412(3)
C(2)-N(1)	1.434(2)
C(3)-C(4)	1.394(3)
C(3)-C(8)	1.508(3)
C(4)-C(5)	1.389(3)
C(5)-C(6)	1.372(3)
C(5)-C(9)	1.521(3)
C(6)-C(7)	1.395(3)
C(7)-C(10)	1.498(3)
C(11)-C(16)	1.397(3)
C(11)-C(12)	1.398(3)
C(11)-N(2)	1.428(3)
C(12)-C(13)	1.397(3)
C(12)-C(17)	1.498(3)
C(13)-C(14)	1.390(3)
C(14)-C(15)	1.385(3)
C(14)-C(18)	1.510(3)
C(15)-C(16)	1.391(3)
C(16)-C(19)	1.512(3)
C(20)-C(25)	1.386(3)
C(20)-C(21)	1.389(3)
C(20)-N(3)	1.443(3)
C(21)-C(22)	1.388(3)
C(22)-C(23)	1.376(3)
C(23)-C(24)	1.378(3)
C(24)-C(25)	1.386(3)
C(26)-C(31)	1.381(3)
C(26)-C(27)	1.382(3)
C(26)-N(3)	1.448(2)
C(27)-C(28)	1.386(3)

C(28)-C(29)	1.373(4)
C(29)-C(30)	1.383(3)
C(30)-C(31)	1.382(3)
N(1)-B	1.559(3)
N(2)-B	1.566(3)
Cl(1)-B	1.833(3)
Cl(2)-B	1.837(3)

N(3)-C(1)-N(1)	129.00(17)
N(3)-C(1)-N(2)	129.84(18)
N(1)-C(1)-N(2)	101.15(16)
C(7)-C(2)-C(3)	121.14(18)
C(7)-C(2)-N(1)	117.57(18)
C(3)-C(2)-N(1)	121.18(17)
C(4)-C(3)-C(2)	117.42(19)
C(4)-C(3)-C(8)	120.14(19)
C(2)-C(3)-C(8)	122.44(18)
C(5)-C(4)-C(3)	122.5(2)
C(6)-C(5)-C(4)	118.2(2)
C(6)-C(5)-C(9)	120.7(2)
C(4)-C(5)-C(9)	121.1(2)
C(5)-C(6)-C(7)	122.3(2)
C(2)-C(7)-C(6)	118.4(2)
C(2)-C(7)-C(10)	121.11(19)
C(6)-C(7)-C(10)	120.5(2)
C(16)-C(11)-C(12)	121.19(19)
C(16)-C(11)-N(2)	117.80(18)
C(12)-C(11)-N(2)	120.91(18)
C(13)-C(12)-C(11)	117.68(19)
C(13)-C(12)-C(17)	120.0(2)
C(11)-C(12)-C(17)	122.35(19)
C(14)-C(13)-C(12)	122.7(2)
C(15)-C(14)-C(13)	117.7(2)
C(15)-C(14)-C(18)	120.6(2)
C(13)-C(14)-C(18)	121.7(2)
C(14)-C(15)-C(16)	122.0(2)

C(15)-C(16)-C(11)	118.7(2)
C(15)-C(16)-C(19)	119.8(2)
C(11)-C(16)-C(19)	121.46(19)
C(25)-C(20)-C(21)	120.70(19)
C(25)-C(20)-N(3)	119.10(18)
C(21)-C(20)-N(3)	120.20(18)
C(22)-C(21)-C(20)	119.31(19)
C(23)-C(22)-C(21)	120.1(2)
C(22)-C(23)-C(24)	120.2(2)
C(23)-C(24)-C(25)	120.6(2)
C(20)-C(25)-C(24)	118.9(2)
C(31)-C(26)-C(27)	120.44(19)
C(31)-C(26)-N(3)	120.84(18)
C(27)-C(26)-N(3)	118.56(18)
C(26)-C(27)-C(28)	119.7(2)
C(29)-C(28)-C(27)	119.8(2)
C(28)-C(29)-C(30)	120.6(2)
C(31)-C(30)-C(29)	119.8(2)
C(26)-C(31)-C(30)	119.7(2)
C(1)-N(1)-C(2)	130.00(16)
C(1)-N(1)-B	87.86(15)
C(2)-N(1)-B	131.77(16)
C(1)-N(2)-C(11)	131.87(17)
C(1)-N(2)-B	87.31(15)
C(11)-N(2)-B	133.07(16)
C(1)-N(3)-C(20)	121.60(16)
C(1)-N(3)-C(26)	120.19(16)
C(20)-N(3)-C(26)	118.10(15)
N(1)-B-N(2)	83.69(14)
N(1)-B-Cl(1)	117.56(16)
N(2)-B-Cl(1)	113.36(16)
N(1)-B-Cl(2)	112.95(15)
N(2)-B-Cl(2)	116.84(17)
Cl(1)-B-Cl(2)	110.40(12)

Symmetry transformations used to generate equivalent atoms:

Table 2.14. Torsion angles [°] for **38**.

C(7)-C(2)-C(3)-C(4)	-0.1(3)
N(1)-C(2)-C(3)-C(4)	175.86(18)
C(7)-C(2)-C(3)-C(8)	-179.89(19)
N(1)-C(2)-C(3)-C(8)	-3.9(3)
C(2)-C(3)-C(4)-C(5)	0.8(3)
C(8)-C(3)-C(4)-C(5)	-179.4(2)
C(3)-C(4)-C(5)-C(6)	-0.6(3)
C(3)-C(4)-C(5)-C(9)	178.6(2)
C(4)-C(5)-C(6)-C(7)	-0.5(3)
C(9)-C(5)-C(6)-C(7)	-179.7(2)
C(3)-C(2)-C(7)-C(6)	-0.9(3)
N(1)-C(2)-C(7)-C(6)	-176.97(18)
C(3)-C(2)-C(7)-C(10)	177.9(2)
N(1)-C(2)-C(7)-C(10)	1.8(3)
C(5)-C(6)-C(7)-C(2)	1.2(3)
C(5)-C(6)-C(7)-C(10)	-177.6(2)
C(16)-C(11)-C(12)-C(13)	0.2(3)
N(2)-C(11)-C(12)-C(13)	176.40(17)
C(16)-C(11)-C(12)-C(17)	-179.34(19)
N(2)-C(11)-C(12)-C(17)	-3.1(3)
C(11)-C(12)-C(13)-C(14)	-0.7(3)
C(17)-C(12)-C(13)-C(14)	178.9(2)
C(12)-C(13)-C(14)-C(15)	1.0(3)
C(12)-C(13)-C(14)-C(18)	-178.5(2)
C(13)-C(14)-C(15)-C(16)	-0.9(3)
C(18)-C(14)-C(15)-C(16)	178.6(2)
C(14)-C(15)-C(16)-C(11)	0.5(3)
C(14)-C(15)-C(16)-C(19)	-178.8(2)
C(12)-C(11)-C(16)-C(15)	-0.1(3)
N(2)-C(11)-C(16)-C(15)	-176.42(18)
C(12)-C(11)-C(16)-C(19)	179.2(2)
N(2)-C(11)-C(16)-C(19)	2.8(3)
C(25)-C(20)-C(21)-C(22)	2.5(3)
N(3)-C(20)-C(21)-C(22)	-177.50(18)

C(20)-C(21)-C(22)-C(23)	-2.1(3)
C(21)-C(22)-C(23)-C(24)	0.5(3)
C(22)-C(23)-C(24)-C(25)	0.7(3)
C(21)-C(20)-C(25)-C(24)	-1.4(3)
N(3)-C(20)-C(25)-C(24)	178.69(18)
C(23)-C(24)-C(25)-C(20)	-0.3(3)
C(31)-C(26)-C(27)-C(28)	-1.8(3)
N(3)-C(26)-C(27)-C(28)	-177.2(2)
C(26)-C(27)-C(28)-C(29)	1.6(4)
C(27)-C(28)-C(29)-C(30)	-0.2(4)
C(28)-C(29)-C(30)-C(31)	-1.1(4)
C(27)-C(26)-C(31)-C(30)	0.5(3)
N(3)-C(26)-C(31)-C(30)	175.83(19)
C(29)-C(30)-C(31)-C(26)	0.9(3)
N(3)-C(1)-N(1)-C(2)	34.3(3)
N(2)-C(1)-N(1)-C(2)	-146.86(19)
N(3)-C(1)-N(1)-B	-178.7(2)
N(2)-C(1)-N(1)-B	0.15(17)
C(7)-C(2)-N(1)-C(1)	-137.8(2)
C(3)-C(2)-N(1)-C(1)	46.2(3)
C(7)-C(2)-N(1)-B	89.1(3)
C(3)-C(2)-N(1)-B	-87.0(3)
N(3)-C(1)-N(2)-C(11)	27.6(4)
N(1)-C(1)-N(2)-C(11)	-151.3(2)
N(3)-C(1)-N(2)-B	178.7(2)
N(1)-C(1)-N(2)-B	-0.15(17)
C(16)-C(11)-N(2)-C(1)	-133.5(2)
C(12)-C(11)-N(2)-C(1)	50.2(3)
C(16)-C(11)-N(2)-B	87.8(3)
C(12)-C(11)-N(2)-B	-88.5(3)
N(1)-C(1)-N(3)-C(20)	-168.75(19)
N(2)-C(1)-N(3)-C(20)	12.7(3)
N(1)-C(1)-N(3)-C(26)	15.1(3)
N(2)-C(1)-N(3)-C(26)	-163.43(19)
C(25)-C(20)-N(3)-C(1)	-131.9(2)
C(21)-C(20)-N(3)-C(1)	48.2(3)

C(25)-C(20)-N(3)-C(26)	44.4(2)
C(21)-C(20)-N(3)-C(26)	-135.60(19)
C(31)-C(26)-N(3)-C(1)	56.0(3)
C(27)-C(26)-N(3)-C(1)	-128.7(2)
C(31)-C(26)-N(3)-C(20)	-120.3(2)
C(27)-C(26)-N(3)-C(20)	55.1(2)
C(1)-N(1)-B-N(2)	-0.13(15)
C(2)-N(1)-B-N(2)	145.9(2)
C(1)-N(1)-B-Cl(1)	112.96(17)
C(2)-N(1)-B-Cl(1)	-101.0(2)
C(1)-N(1)-B-Cl(2)	-116.64(17)
C(2)-N(1)-B-Cl(2)	29.4(3)
C(1)-N(2)-B-N(1)	0.13(14)
C(11)-N(2)-B-N(1)	150.7(2)
C(1)-N(2)-B-Cl(1)	-117.21(16)
C(11)-N(2)-B-Cl(1)	33.3(3)
C(1)-N(2)-B-Cl(2)	112.69(17)
C(11)-N(2)-B-Cl(2)	-96.8(2)

Symmetry transformations used to generate equivalent atoms:

Table 2.15. Crystal data and structure refinement for **39**.

Identification code	**39**	
Empirical formula	C37 H44 B Cl2 N3	
Formula weight	612.46	
Temperature	153(2) K	
Wavelength	0.71069 Å	
Crystal system	Monoclinic	
Space group	Pc	
Unit cell dimensions	a = 12.258(5) Å	α= 90.000(6)°.
	b = 10.481(5) Å	β= 124.90(2)°.
	c = 16.149(5) Å	γ = 90.000(5)°.
Volume	1701.5(12) $Å^3$	
Z	2	
Density (calculated)	1.195 Mg/m^3	
Absorption coefficient	0.220 mm^{-1}	
F(000)	652	
Crystal size	0.10 x 0.06 x 0.06 mm^3	
Theta range for data collection	1.94 to 27.49°.	
Index ranges	-15<=h<=15, -12<=k<=13, -20<=l<=20	
Reflections collected	6943	
Independent reflections	6934 [R(int) = 0.0258]	
Completeness to theta = 27.49°	99.3 %	
Absorption correction	None	
Max. and min. transmission	0.9869 and 0.9783	
Refinement method	Full-matrix least-squares on F^2	
Data / restraints / parameters	6934 / 2 / 389	
Goodness-of-fit on F^2	1.077	
Final R indices [I>2sigma(I)]	R1 = 0.0568, wR2 = 0.1203	
R indices (all data)	R1 = 0.1433, wR2 = 0.1745	
Absolute structure parameter	0.53(8)	
Largest diff. peak and hole	0.536 and -0.583 e.$Å^{-3}$	

Table 2.16. Bond lengths [Å] and angles [°] for **39**.

C(1)-N(1)	1.341(6)
C(1)-N(3)	1.353(6)
C(1)-N(2)	1.360(5)
C(2)-C(7)	1.401(6)
C(2)-C(3)	1.409(6)
C(2)-N(1)	1.440(6)
C(3)-C(4)	1.393(7)
C(3)-C(8)	1.522(6)
C(4)-C(5)	1.376(7)
C(5)-C(6)	1.388(7)
C(6)-C(7)	1.388(7)
C(7)-C(11)	1.516(6)
C(8)-C(10)	1.518(7)
C(8)-C(9)	1.546(7)
C(11)-C(12)	1.528(7)
C(11)-C(13)	1.530(7)
C(14)-C(15)	1.400(7)
C(14)-C(19)	1.419(6)
C(14)-N(2)	1.441(6)
C(15)-C(16)	1.385(7)
C(15)-C(20)	1.531(7)
C(16)-C(17)	1.388(7)
C(17)-C(18)	1.376(8)
C(18)-C(19)	1.392(7)
C(19)-C(23)	1.517(7)
C(20)-C(21)	1.518(7)
C(20)-C(22)	1.539(7)
C(23)-C(24)	1.521(8)
C(23)-C(25)	1.522(8)
C(26)-C(31)	1.382(7)
C(26)-C(27)	1.387(7)
C(26)-N(3)	1.449(6)
C(27)-C(28)	1.373(8)
C(28)-C(29)	1.375(8)

C(29)-C(30)	1.367(8)
C(30)-C(31)	1.377(7)
C(32)-C(37)	1.387(7)
C(32)-C(33)	1.387(7)
C(32)-N(3)	1.440(6)
C(33)-C(34)	1.398(7)
C(34)-C(35)	1.375(8)
C(35)-C(36)	1.377(9)
C(36)-C(37)	1.384(7)
B-N(2)	1.570(7)
B-N(1)	1.578(6)
B-Cl(1)	1.833(6)
B-Cl(2)	1.833(5)

N(1)-C(1)-N(3)	131.6(4)
N(1)-C(1)-N(2)	101.6(4)
N(3)-C(1)-N(2)	126.8(4)
C(7)-C(2)-C(3)	121.9(4)
C(7)-C(2)-N(1)	121.4(4)
C(3)-C(2)-N(1)	116.7(4)
C(4)-C(3)-C(2)	117.5(4)
C(4)-C(3)-C(8)	119.8(4)
C(2)-C(3)-C(8)	122.5(4)
C(5)-C(4)-C(3)	121.8(5)
C(4)-C(5)-C(6)	119.1(4)
C(7)-C(6)-C(5)	122.0(5)
C(6)-C(7)-C(2)	117.5(4)
C(6)-C(7)-C(11)	117.6(4)
C(2)-C(7)-C(11)	124.8(4)
C(10)-C(8)-C(3)	113.7(4)
C(10)-C(8)-C(9)	110.5(4)
C(3)-C(8)-C(9)	109.1(4)
C(7)-C(11)-C(12)	112.0(4)
C(7)-C(11)-C(13)	110.7(4)
C(12)-C(11)-C(13)	109.8(4)
C(15)-C(14)-C(19)	121.6(4)

C(15)-C(14)-N(2)	121.6(4)
C(19)-C(14)-N(2)	116.8(4)
C(16)-C(15)-C(14)	118.1(5)
C(16)-C(15)-C(20)	118.2(4)
C(14)-C(15)-C(20)	123.4(4)
C(15)-C(16)-C(17)	121.2(5)
C(18)-C(17)-C(16)	120.1(5)
C(17)-C(18)-C(19)	121.4(5)
C(18)-C(19)-C(14)	117.4(4)
C(18)-C(19)-C(23)	120.9(4)
C(14)-C(19)-C(23)	121.5(4)
C(21)-C(20)-C(15)	114.2(4)
C(21)-C(20)-C(22)	108.3(4)
C(15)-C(20)-C(22)	109.3(4)
C(19)-C(23)-C(24)	109.1(4)
C(19)-C(23)-C(25)	114.1(5)
C(24)-C(23)-C(25)	109.8(4)
C(31)-C(26)-C(27)	120.2(5)
C(31)-C(26)-N(3)	120.2(4)
C(27)-C(26)-N(3)	119.6(4)
C(28)-C(27)-C(26)	118.8(5)
C(27)-C(28)-C(29)	121.4(5)
C(30)-C(29)-C(28)	119.2(5)
C(29)-C(30)-C(31)	120.9(5)
C(30)-C(31)-C(26)	119.5(5)
C(37)-C(32)-C(33)	119.8(5)
C(37)-C(32)-N(3)	119.9(5)
C(33)-C(32)-N(3)	120.4(4)
C(32)-C(33)-C(34)	119.3(5)
C(35)-C(34)-C(33)	120.8(5)
C(34)-C(35)-C(36)	119.3(5)
C(35)-C(36)-C(37)	120.8(5)
C(36)-C(37)-C(32)	119.9(5)
N(2)-B-N(1)	83.4(3)
N(2)-B-Cl(1)	112.4(3)
N(1)-B-Cl(1)	118.1(3)

N(2)-B-Cl(2)	117.1(3)
N(1)-B-Cl(2)	112.4(3)
Cl(1)-B-Cl(2)	111.2(3)
C(1)-N(1)-C(2)	128.2(4)
C(1)-N(1)-B	87.7(3)
C(2)-N(1)-B	137.5(3)
C(1)-N(2)-C(14)	126.2(4)
C(1)-N(2)-B	87.4(3)
C(14)-N(2)-B	137.9(4)
C(1)-N(3)-C(32)	121.0(4)
C(1)-N(3)-C(26)	120.0(4)
C(32)-N(3)-C(26)	118.9(4)

Symmetry transformations used to generate equivalent atoms:

Table 2.17. Torsion angles [°] for **39**.

C(7)-C(2)-C(3)-C(4)	-4.0(7)
N(1)-C(2)-C(3)-C(4)	174.4(4)
C(7)-C(2)-C(3)-C(8)	171.0(4)
N(1)-C(2)-C(3)-C(8)	-10.6(6)
C(2)-C(3)-C(4)-C(5)	0.1(7)
C(8)-C(3)-C(4)-C(5)	-175.1(5)
C(3)-C(4)-C(5)-C(6)	3.2(8)
C(4)-C(5)-C(6)-C(7)	-2.7(8)
C(5)-C(6)-C(7)-C(2)	-1.0(7)
C(5)-C(6)-C(7)-C(11)	174.3(5)
C(3)-C(2)-C(7)-C(6)	4.5(7)
N(1)-C(2)-C(7)-C(6)	-173.8(4)
C(3)-C(2)-C(7)-C(11)	-170.5(4)
N(1)-C(2)-C(7)-C(11)	11.2(7)
C(4)-C(3)-C(8)-C(10)	-44.1(6)
C(2)-C(3)-C(8)-C(10)	141.1(5)
C(4)-C(3)-C(8)-C(9)	79.7(5)
C(2)-C(3)-C(8)-C(9)	-95.2(5)

C(6)-C(7)-C(11)-C(12)	59.3(6)
C(2)-C(7)-C(11)-C(12)	-125.7(5)
C(6)-C(7)-C(11)-C(13)	-63.6(6)
C(2)-C(7)-C(11)-C(13)	111.3(5)
C(19)-C(14)-C(15)-C(16)	5.5(7)
N(2)-C(14)-C(15)-C(16)	-174.4(4)
C(19)-C(14)-C(15)-C(20)	-167.9(4)
N(2)-C(14)-C(15)-C(20)	12.2(7)
C(14)-C(15)-C(16)-C(17)	-1.1(8)
C(20)-C(15)-C(16)-C(17)	172.6(5)
C(15)-C(16)-C(17)-C(18)	-3.2(9)
C(16)-C(17)-C(18)-C(19)	3.1(9)
C(17)-C(18)-C(19)-C(14)	1.2(8)
C(17)-C(18)-C(19)-C(23)	-173.0(5)
C(15)-C(14)-C(19)-C(18)	-5.5(7)
N(2)-C(14)-C(19)-C(18)	174.4(4)
C(15)-C(14)-C(19)-C(23)	168.6(5)
N(2)-C(14)-C(19)-C(23)	-11.5(7)
C(16)-C(15)-C(20)-C(21)	60.9(6)
C(14)-C(15)-C(20)-C(21)	-125.8(5)
C(16)-C(15)-C(20)-C(22)	-60.7(6)
C(14)-C(15)-C(20)-C(22)	112.7(5)
C(18)-C(19)-C(23)-C(24)	85.7(6)
C(14)-C(19)-C(23)-C(24)	-88.2(5)
C(18)-C(19)-C(23)-C(25)	-37.6(7)
C(14)-C(19)-C(23)-C(25)	148.5(5)
C(31)-C(26)-C(27)-C(28)	-1.0(8)
N(3)-C(26)-C(27)-C(28)	-178.8(5)
C(26)-C(27)-C(28)-C(29)	0.6(9)
C(27)-C(28)-C(29)-C(30)	1.0(9)
C(28)-C(29)-C(30)-C(31)	-2.1(8)
C(29)-C(30)-C(31)-C(26)	1.6(8)
C(27)-C(26)-C(31)-C(30)	0.0(7)
N(3)-C(26)-C(31)-C(30)	177.7(4)
C(37)-C(32)-C(33)-C(34)	1.2(7)
N(3)-C(32)-C(33)-C(34)	-179.6(4)

C(32)-C(33)-C(34)-C(35)	-1.1(8)
C(33)-C(34)-C(35)-C(36)	-0.4(8)
C(34)-C(35)-C(36)-C(37)	1.8(8)
C(35)-C(36)-C(37)-C(32)	-1.7(8)
C(33)-C(32)-C(37)-C(36)	0.1(7)
N(3)-C(32)-C(37)-C(36)	-179.1(4)
N(3)-C(1)-N(1)-C(2)	23.2(7)
N(2)-C(1)-N(1)-C(2)	-156.0(4)
N(3)-C(1)-N(1)-B	178.1(5)
N(2)-C(1)-N(1)-B	-1.1(4)
C(7)-C(2)-N(1)-C(1)	51.0(6)
C(3)-C(2)-N(1)-C(1)	-127.4(5)
C(7)-C(2)-N(1)-B	-90.2(7)
C(3)-C(2)-N(1)-B	91.3(6)
N(2)-B-N(1)-C(1)	0.9(3)
Cl(1)-B-N(1)-C(1)	112.8(4)
Cl(2)-B-N(1)-C(1)	-115.7(4)
N(2)-B-N(1)-C(2)	151.4(5)
Cl(1)-B-N(1)-C(2)	-96.7(6)
Cl(2)-B-N(1)-C(2)	34.8(7)
N(1)-C(1)-N(2)-C(14)	-151.4(4)
N(3)-C(1)-N(2)-C(14)	29.4(7)
N(1)-C(1)-N(2)-B	1.1(4)
N(3)-C(1)-N(2)-B	-178.2(5)
C(15)-C(14)-N(2)-C(1)	49.9(6)
C(19)-C(14)-N(2)-C(1)	-130.0(5)
C(15)-C(14)-N(2)-B	-86.5(6)
C(19)-C(14)-N(2)-B	93.6(6)
N(1)-B-N(2)-C(1)	-0.9(3)
Cl(1)-B-N(2)-C(1)	-118.6(3)
Cl(2)-B-N(2)-C(1)	110.9(4)
N(1)-B-N(2)-C(14)	145.3(5)
Cl(1)-B-N(2)-C(14)	27.6(6)
Cl(2)-B-N(2)-C(14)	-102.9(5)
N(1)-C(1)-N(3)-C(32)	22.8(7)
N(2)-C(1)-N(3)-C(32)	-158.1(4)

N(1)-C(1)-N(3)-C(26)	-154.2(4)
N(2)-C(1)-N(3)-C(26)	24.8(7)
C(37)-C(32)-N(3)-C(1)	-145.5(4)
C(33)-C(32)-N(3)-C(1)	35.3(6)
C(37)-C(32)-N(3)-C(26)	31.6(6)
C(33)-C(32)-N(3)-C(26)	-147.7(4)
C(31)-C(26)-N(3)-C(1)	51.8(6)
C(27)-C(26)-N(3)-C(1)	-130.4(5)
C(31)-C(26)-N(3)-C(32)	-125.3(5)
C(27)-C(26)-N(3)-C(32)	52.5(6)

Symmetry transformations used to generate equivalent atoms:

CHAPTER 3: Photovoltaics: A Seeded Growth Approach

INTRODUCTION

In ongoing efforts to relieve the increasing global energy crisis, the use of solar energy has recently become an attractive alternative source of energy. The potential implications for a 'carbon neutral' global energy strategy of solar energy conversion are wide-ranging, but none is perhaps as promising as the direct conversion of sunlight into electricity, a process facilitated by devices called photovoltaics. Currently, achieving this lofty goal has been somewhat hampered by the high cost and low efficiency inherent in the available materials. Nevertheless, the allure of this research has led to a blossoming photovoltaic research community. However, despite intense efforts, the results thus far are limited to a few interesting systems, which have ultimately fallen short of the requirements for commercially viable photovoltaics.

Over the last decade organic-based solar cells have been increasingly studied as cheap and flexible alternatives to more traditional inorganic materials [1-5] such as those based on silicon. More conventional heterocomposite materials are typically based upon physical mixtures of inorganic nanoparticles and organic polymers and thus suffer from serious interface problems. Through utilization of well-defined chemical means it is possible to grow the requisite semiconducting nanoparticles within a polymer matrix and hence achieve an intimate contact between the two active components of a photovoltaic device. More specifically, the synthesis of a monomer containing metal-centers which is

also readily electropolymerizable affords a conducting polymer with molecular 'seed' points at well defined locations along the polymer backbone.

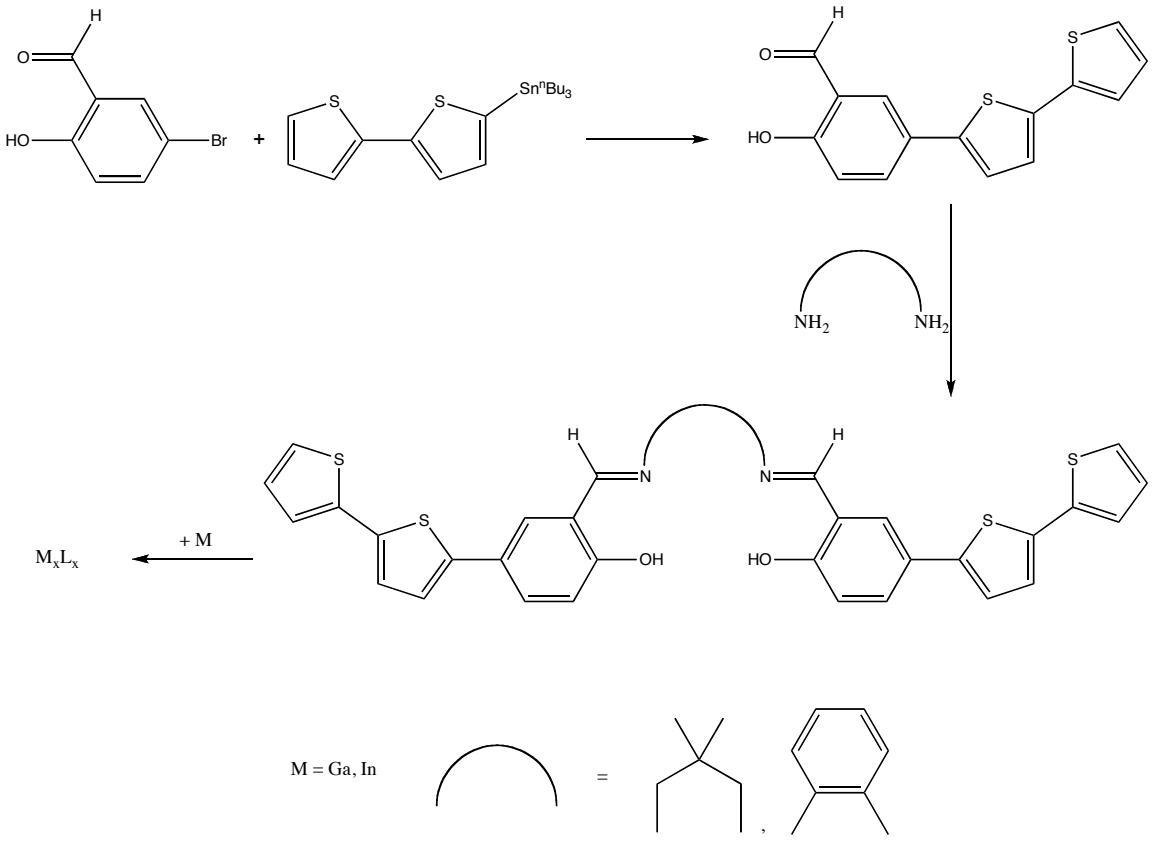

Scheme 3.1. Proposed syntheses of target compounds.

In choosing an appropriate ligand scaffold one must first consider the restrictions imposed upon the ultimate design requirements, namely molecules which have metal binding sites in addition to functional groups which allow subsequent electropolymerization of the monomers. The "salen" class of Schiff-base (SB) ligands was chosen for a number of reasons. Firstly, they are inexpensive, easily prepared and many variations in their metal binding properties can be achieved (Scheme 3.1). Furthermore, since a large number of SB ligands are known to complex Cd^{2+}, Ga^{3+} and

Pb^{2+} metal ions [6-8] it was anticipated that the target materials could be readily accessed by ligand manipulation, metal complex formation and electropolymerization. Indeed, several promising systems of this type have already been realized [9].

The appending of polymerizable groups such as bithiophene to the Schiff base metal complexes permits the formation of conducting polymer films by means of potentiodynamic electropolymerization which is a well precedented process [10]. The metal centers in these conducting polymer films are strongly bound by the ligand framework and thus provide excellent electrical contact with the conducting polymer. Furthermore, these centers will also act as nucleation sites for the subsequent growth of inorganic semiconducting nanoparticles. In this regard the resulting inorganic nanocrystals may be considered as being "directly wired" into the polymer matrix thus avoiding the formation of an undesirable interface between the organic and inorganic components. The nature of the interface is often a problematic issue and can represent a serious drawback in the performance of such heterocomposite based photovoltaic devices [11].

The general approach to the seeded growth of nanoparticles within these polymer matrices is illustrated in Figure 3.1. In the case of the monomeric metal SB complexes (Scheme 3.1), the ligand environments can be characterized by techniques such as NMR, UV-Vis, and fluorescence spectroscopies, mass spectrometry, and single crystal X-ray crystallography. The metal-containing complexes will then be electrodeposited on a variety of conducting substrates utilizing well established electrochemical techniques [12] to track film growth and to characterize the resulting materials with regard to the kinetics of charge transport and overall conductivity both *in situ* and as bulk materials.

Finally, the hybrid materials may be prepared in which semiconductor nanoparticles were incorporated into the conducting polymer matrix. The electronic properties of these materials can then be probed by using a battery of techniques such as TEM, XPS, electrochemistry and UV-Vis spectroscopy.

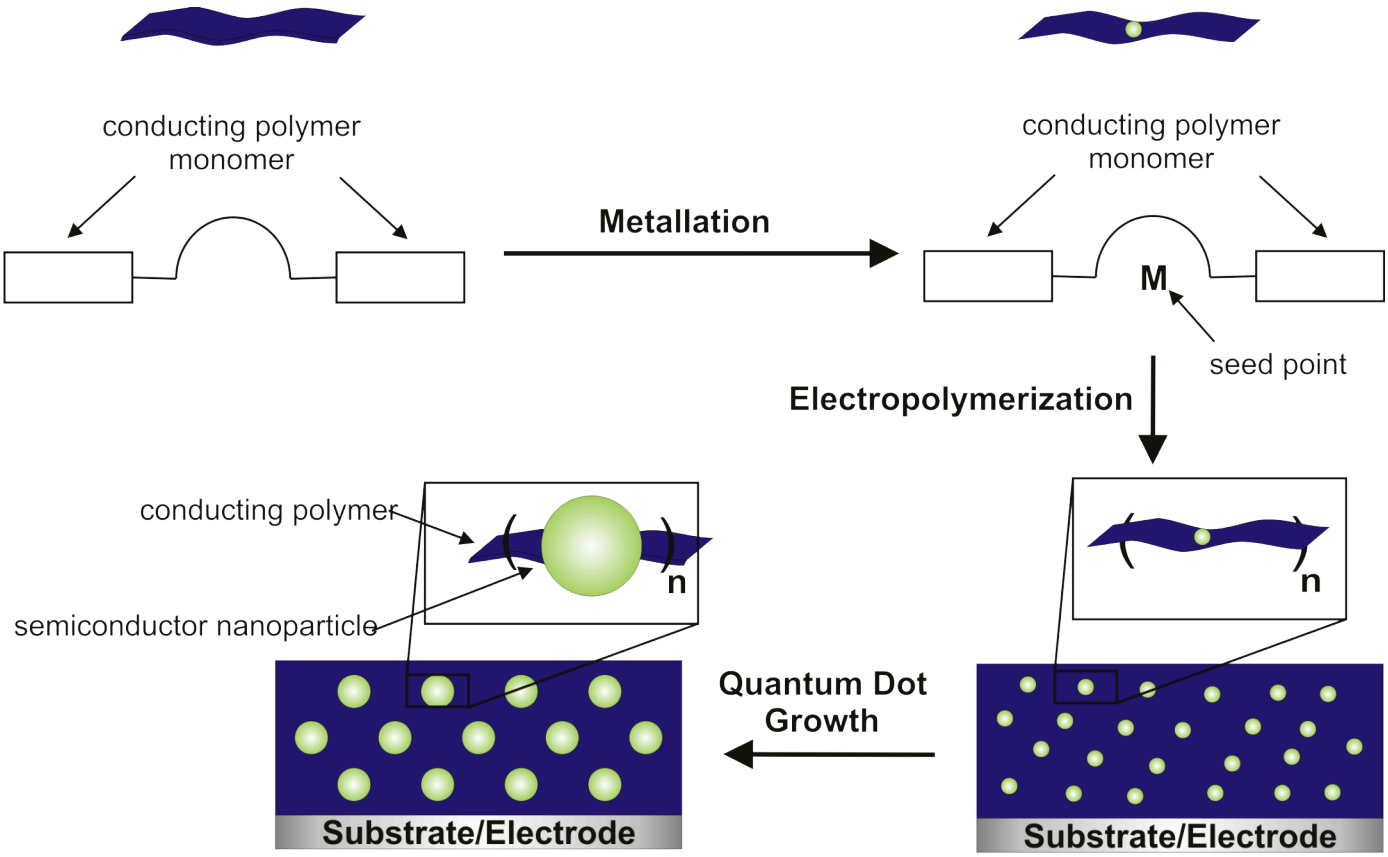

Figure 3.1. Formation of new hybrid electronic materials. Reproduced with permission from Bradley J. Holliday.

The Group III sulfides are an interesting class of materials, which show promise as the active materials in photovoltaic and optoelectronic applications. In particular, such

materials have possible application in solar cells [13]. For example, In_2S_3 thin film solar cells have been reported with efficiencies as high as 16.4% [14]. Binary III/VI materials exhibit a number of stoichiometric forms including M_2E_3 (M = Ga, In; E = S) and have a range of mid- to wide-optical band gaps (e.g., In_2S_3 ~2.00–2.20 eV and Ga_2S_3 ~3.4 eV) [15, 16]. The preparation of thin films of the Group III sulfides has been widely reported. However, the synthetic routes to GaS nanoparticles have been somewhat neglected in the literature. Similarly, despite the increased attention paid to viable synthetic routes to nanocrystalline Group III/V semiconductors in the past few years [17-21], relatively little work has been published regarding the formation of nanocrystalline indium phosphide (InP). These Group III/V compound semiconductors represent promising materials for optoelectronic devices due to their bandgaps (~1.34 eV), which are narrower than that of gallium arsenide and can be tailored depending on size of the nanocrystallites employed [22]. Prompted by the initial success of the seeded growth approach for the development of CdS and CdSe systems, it became important to develop viable approaches to the production materials based on Ga_2S_3 and InP nanparticles. This aspect of the program is now discussed.

Results and Discussion

Model Complexes Synthesis and Characterization

The initial phase of the work involved the synthesis and characterization of model Schiff base complexes of Ga^{3+}, ligands that lack polymerizable bithiophene substituents. Such complexes were intended to provide key information regarding the coordination environments and geometries required by SB ligands that feature electropolymerizable bithiophene groups. Moreover, it was anticipated that these complexes would provide valuable insights in terms of their spectroscopic properties from which useful comparisons could be made with the metal-containing conducting polymer films.

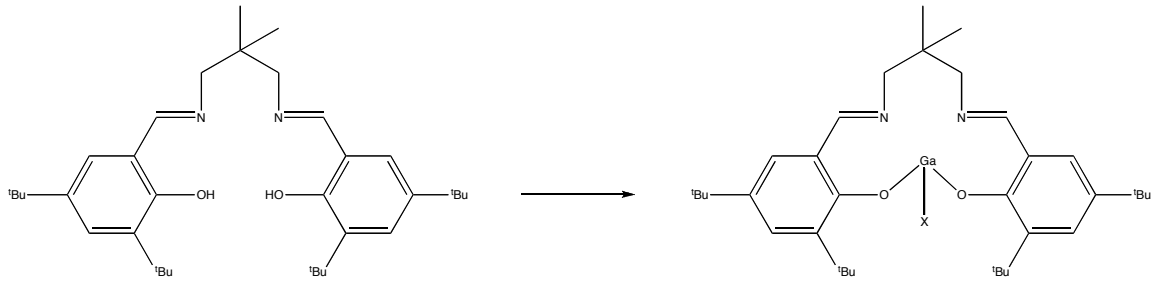

40

41: X = NO_3
42: X = Cl

Scheme 3.2. Synthesis of SB-Ga model complexes.

Despite the wide variation possible in terms of the ligand backbone (Scheme 3.1), the dimethylpropane derivative illustrated in Scheme 3.2 was chosen because it was anticipated that it would result in increased solubility in comparison with the conjugated analogues. Treatment of **40** with an equimolar quantity of gallium nitrate in refluxing methanol solution afforded in virtually quantitative yield the product of the HNO_3 elimination, product **41**. Crystals suitable for study by X-ray diffraction methods were

grown from a concentrated toluene solution. Compound **41** crystallizes in the monoclinic space group C2/c and the solid state consists of individual molecules with no unusually short intermolecular contacts (Figure 3.2). The asymmetric unit contains a half molecule of toluene. The geometry at the gallium center is best described as distorted octahedral and the bond angles O1-Ga1-O3 (150.39(15)º), O2-Ga1-N1 (176.10(15)º), and O4-Ga1-N2 (152.94º) all deviate significantly from linearity. As expected, the greatest deviations are encountered with those atoms comprising the nitrate ligand. This 'inequivalence' is also evident in the significant discrepancy in the average Ga-O bond lengths, Ga-O_{SB} 1.867 Å and Ga-$O_{nit.}$ 2.160 Å.

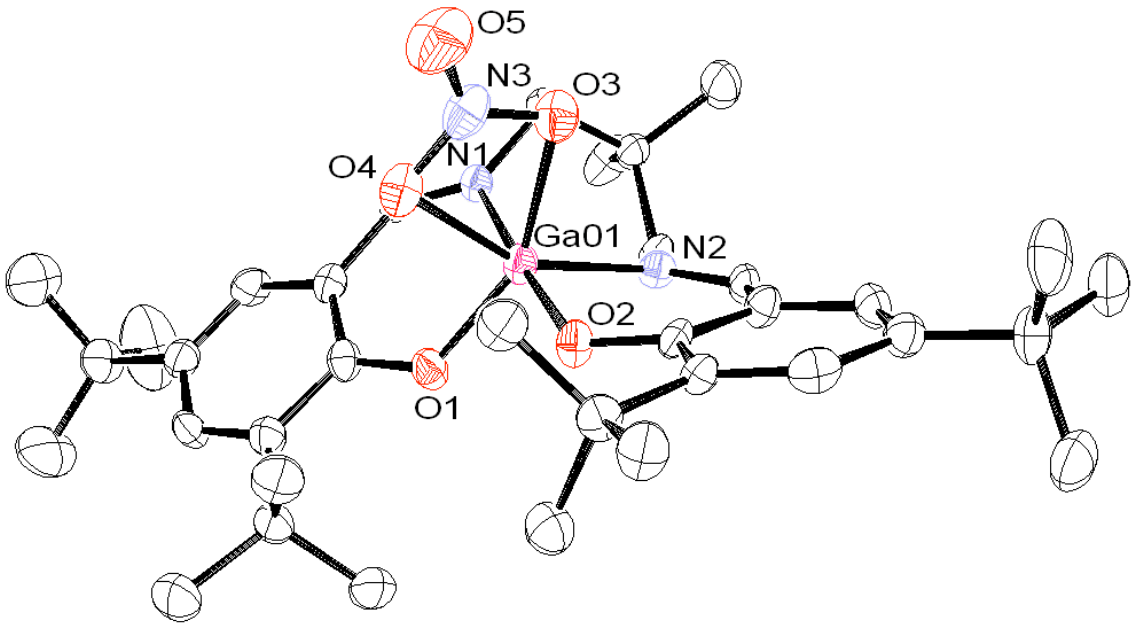

Figure 3.2. Molecular structure of **41**, with thermal ellipsoids shown at the 40% probability level.

While this initial result was very promising, the appended nitrate functionality was regarded as undesirable, particularly in view of the necessity of using toxic hydride sources such as H_2S, AsH_3 and PH_3 in subsequent growth steps. As a consequence, attention was turned to the chemistry of the chloro-substituted derivative **42**. Addition of $GaCl_3$ to the sodium salt of **40** (Scheme 3.2) resulted, after workup, in the gallium chloride Schiff base complex **42**. The molecular structure of **42** was elucidated on the basis of single-crystal X-ray diffraction experiments. Suitable single crystals suitable for such studies were grown by slow diffusion of *n*-hexane into a concentrated chloroform solution of **42**. In contrast to **41**, the gallium center of **42** is five-coordinate and features a square-based pyramidal geometry (Figure 3.3). The angles O(1)-Ga(1)-O(2), O(1)-Ga(1)-N(1), and O(2)-Ga(1)-N(2) are all close to 90°, being 86.90(7)°, 89.40(7)°, and 88.97(7)° respectively. There is however some evidence of distortion within this framework, namely the widely varying angles for O(1)-Ga(1)-N(2) and O(2)-Ga(1)-N(1), 126.41(8)° and 169.71(7)° respectively. The average Ga-O bond distance is 1.8772 Å and the average Ga-N bond distance is 2.0307 Å. The Ga-Cl bond distance for the apical chloride ligand is 2.2135(7) Å. These distances are in close agreement with a similar structure reported by Darensbourg *et al.* for a SB complex with a cyclohexyl backbone rather than the dimethylpropane SB ligand reported here [7e].

The analogous indium halide species were synthesized in a similar manner to that described for the gallium chloride discussed above (Scheme 3.3). Thus, treatment of the sodium salt of **40** with indium chloride or bromide at ambient temperature in THF solution afforded the desired products in good yield (**43** and **44** respectively in Scheme 3.3).

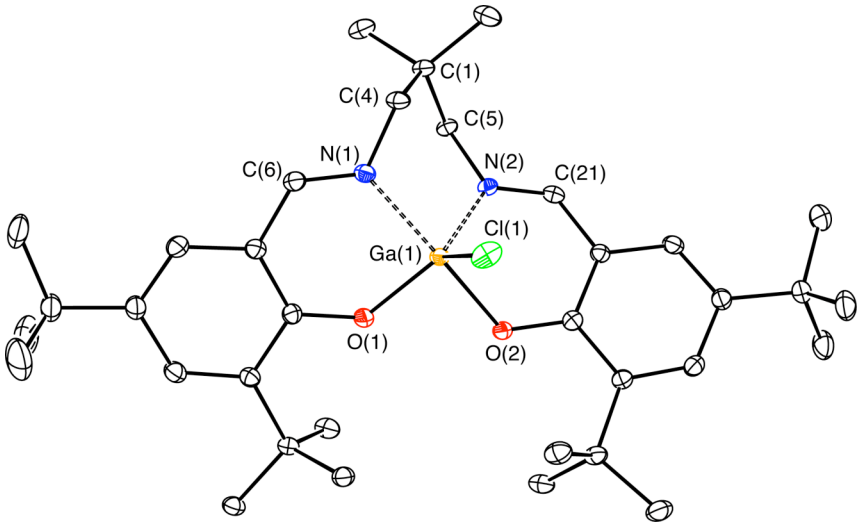

Figure 3.3. Molecular structure of **42**, with thermal ellipsoids shown at the 40% probability level.

Compounds **43** and **44** both crystallize in the monoclinic space group $P2_1/c$ and the solid state consists of an ensemble of monomers that features no unusually short intermolecular contacts. The molecular structure of **43** is illustrated in Figure 3.4.

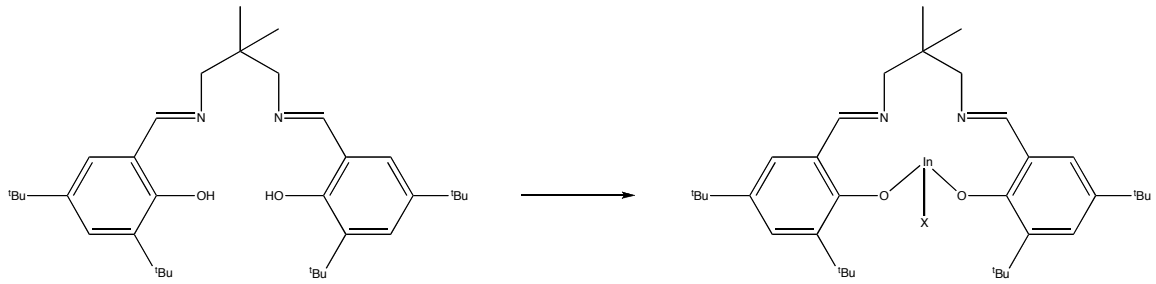

Scheme 3.3. Synthesis of SB-In model complexes.

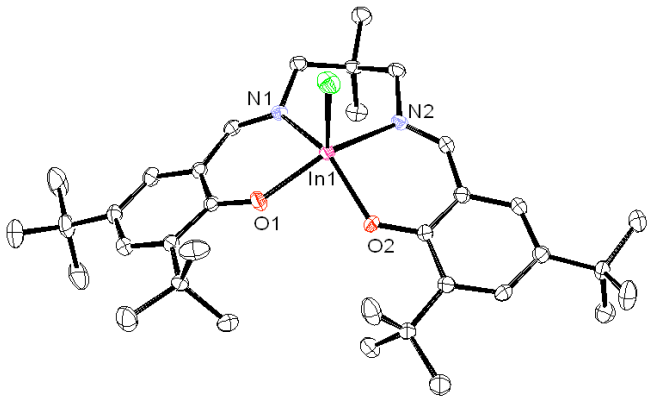

Figure 3.4. Molecular structure of **43**, with thermal ellipsoids shown at 40% probability level.

The overall structures of both **43** and **44** are similar to that of the gallium chloride analogue, **42**, in the sense that all three structures display a distorted square based pyramidal geometry in which several important bond angles are distorted from their ideal values (see Table 3.1).

Table 3.1. Important metrical parameters for **43** and **44**.

	43	**44**
In-O_{av} (Å)	2.0699	2.064
In-N_{av} (Å)	2.2040	2.200
In-X (Å)	2.3975	2.5337
O(1)-In(1)-O(2) (°)	85.59	85.82
O(1)-In(1)-N(1) (°)	86.39	86.39
O(2)-In(1)-N(2) (°)	84.59	84.71
O(1)-In(1)-N(2) (°)	158.07	158.22
O(2)-In(1)-N(1) (°)	138.7	138.83

Bithiophene Complexes Synthesis and Characterization

Although the study of model complexes was very useful for the development of viable synthetic routes to the desired SB-metal complexes and for gleaning information about their patterns of reactivity (*vide infra*), such compounds lacked the ability to be polymerized. Accordingly, it was necessary to append polymerizable bithiophene moieties to the SB complexes. This was achieved as shown in Scheme 3.4 using the method described by Holliday *et al.* Thus, the Stille coupling of tri-n-butyltin bithiophene with p-bromosalicylaldehyde resulted in moderate yields (50-70%) of the desired aldehyde precursor **45**. In turn, condensation of **45** with 2,2-dimethylpropanediamine in methanol solution afforded the polymerizable Schiff base compound **46** in essentially quantitative yield.

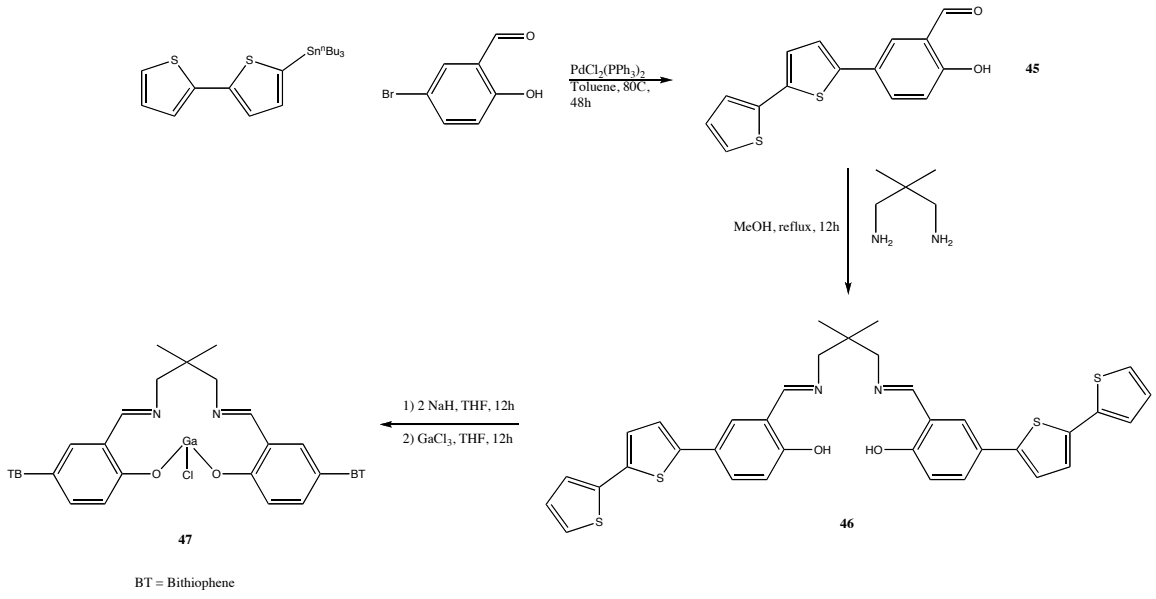

Scheme 3.4. Synthesis of polymerizable Schiff Base gallium complex **47**.

Subsequent treatment of **46** with two equivalents of sodium hydride, followed by the addition of gallium trichloride resulted in a good yield of the desired gallium chloride substituted Schiff Base complex **47**. Crystals suitable for single crystal X-ray diffraction experiments were grown by slow diffusion of hexane into a concentrated methylene chloride solution of **47**. Compound **47** crystallizes in the triclinic space group P-1 and the solid state comprises individual molecules of **47** (Figure 3.5) with no unusually short intermolecular contacts.

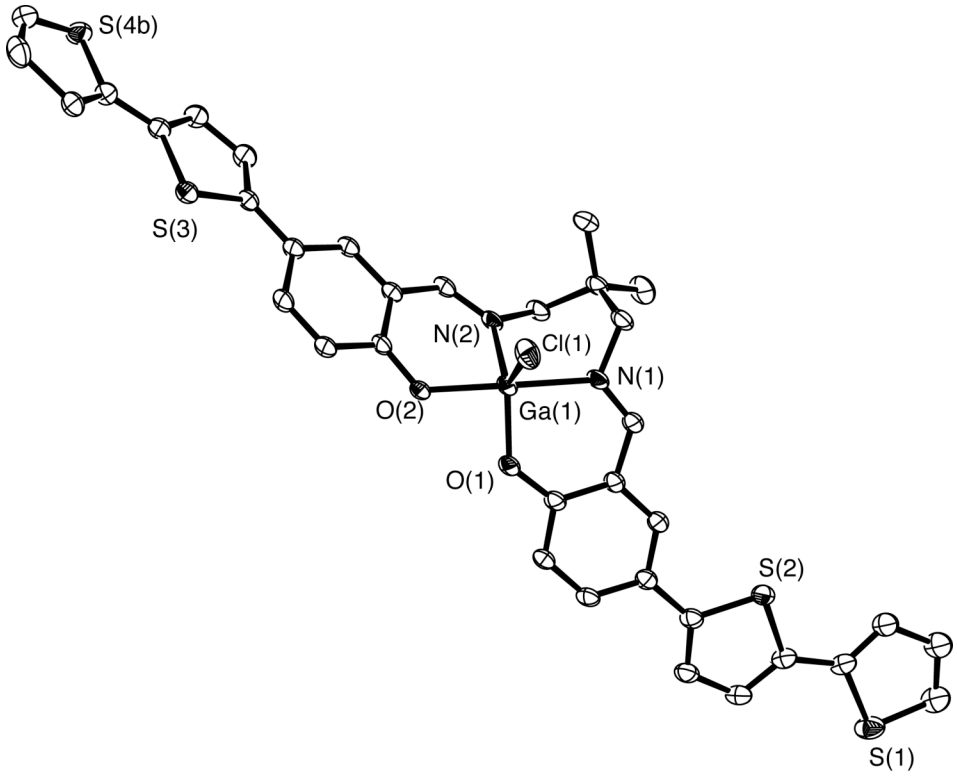

Figure 3.5. Molecular structure of **47**, with thermal ellipsoids shown at 40% probability level. Atoms S(4) and C(33) are disordered over two positions with site occupancy factors of 48% for S(4b) and C(33b).

As previously observed in the case of model-GaCl species, **42**, the bonding at the gallium center is best described as that of a distorted square-based pyramid. The bond angles O(1)-Ga(1)-O(2), O(1)-Ga(1)-N(1), and O(2)-Ga(1)-N(2) of 87.65(10)°, 90.64(11)°, and 80.41(10)° respectively all deviate from the ideal value of 90°. Moreover, further evidence of structural distortion is found in the bond angles O(1)-Ga(1)-N(2) and O(2)-Ga(1)-N(1), which have the values of 124.27(12)° and 170.40(11)°, respectively. The average Ga-O bond distance is 1.889 Å and the average Ga-N bond distance is 2.013 Å. The Ga-Cl bond distance for the apical chloride ligand is 2.4436(13) Å and thus appreciably longer than the corresponding value of 2.2135(7) Å for **42**. As is common in the solid-state structures of bithiophene containing molecules, there is considerable disorder in one of the thiophene rings. Complex **47** is sparingly soluble in CH_2Cl_2 and, as a consequence, the ^{13}C NMR spectrum could not be recorded. The solution phase ^{1}H NMR spectrum and both the low- and high-resolution mass spectra are consistent with the solid-state structure.

The corresponding indium chloride complex, **48**, was synthesized by Joe Rivers, a collaborator in the research group of Professor Richard Jones, and was found to exist as a dimer in the solid state. Interestingly, the indium atom is six-coordinate and exhibits distorted octahedral geometry around the group 13 element center. This expansion of the coordination sphere is doubtless the result of the larger size of the indium atom in comparison with that of the gallium atom in **47**.

It was envisioned that **47** would prove an ideal starting material for the construction of the desired polymer-embedded semiconducting gallium sulfide nanoparticles as summarized pictorially in Figure 3.1. However, despite showing well-

behaved electrochemical polymerization characteristics, no nanoparticle growth was observed when this polymer was treated with methylene chloride solutions of H_2S. Thus, it was decided to make use of model complex **42** in an effort to explore the inherent reactivity of gallium chloride Schiff Base complexes of this type.

Reactivity studies of Gallium Chloride Schiff Base Complexes

The continued reluctance of the bithiophene substituted complex **47** to undergo nanoparticle formation prompted an examination of the chemistry of the model complex **42**. The hope was that a better understanding of the fundamental chemistry of the gallium species would permit satisfactory nanoparticle growth. However, as in the case of **47**, treatment of **42** with H_2S over extended periods of time and with a variety of reaction temperatures resulted in no detectable Ga-S bond formation.

Turning to the silyl halide elimination route, which has previously been successfully employed for the production of GaAs nanoparticles [23], complex **42** was treated with equimolar amounts of $P(SiMe_3)$, $As(SiMe_3)_3$ and $S(SiMe_3)_2$ in toluene solution at ambient temperatures. In one instance, block crystals of the hydrolysis product SB-Ga(OTMS) was isolated in good yield and characterized by single-crystal X-ray diffraction. However, no evidence was found for the formation of the desired Ga-P, Ga-As or Ga-S bonds. Further insight into this seeming lack of reactivity came from closer examination of the indium complex **48**. As noted above, the indium complex undergoes an increase in coordination number from five to six, while the corresponding gallium complex **47** does not. Reasoning that the gallium atom is coordinatively saturated in **47**, the next logical step was to increase the reactivity at the gallium center by abstraction of

the appended chloride ligand to afford a four-coordinate 'active' cationic moiety. Accordingly, treatment of a methylene chloride / acetonitrile solution of **42** with one equivalent of $AgPF_6$ afforded a pale yellow powder which was identified as the desired cation-anion complex **49**, as shown in Scheme 3.5.

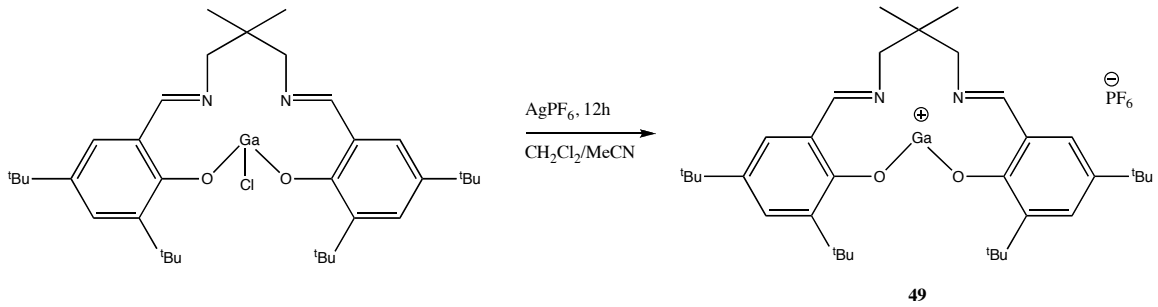

49

Scheme 3.5. Synthesis of four-coordinate gallium Schiff Base complex, **49**.

Fortunately, on one occasion it was possible to isolate crystals suitable for X-ray diffraction experiments. However, the data obtained were of poor quality, thus precluding any meaningful discussion of metrical parameters. Nevertheless, the connectivity of the structure was clearly established. As illustrated in Figures 3.6 (a) and (b), the chloride anion was successfully abstracted and, in the solid state, there is intimate contact between a fluoride atom of the PF_6 ligand and the gallium center. Moreover, a closer examination of the extended structure of **49** (Figure 3.6 (b)), reveals that the PF_6^- anion forms a bridge between the layers of Schiff Base complexes in a one-dimensional polymeric fashion.

NMR spectroscopic assays showed, however, that this structure is not retained in solution. Specifically, in the ^{19}F NMR spectrum only a doublet centered at δ -73.33, with

a J_{P-F} of 706 Hz was observed. The ^{31}P NMR spectrum comprised a septet centered at δ -149.37, with a J_{P-F} value of 706 Hz. Clearly, only one F and one P environment is present in the solution phase.

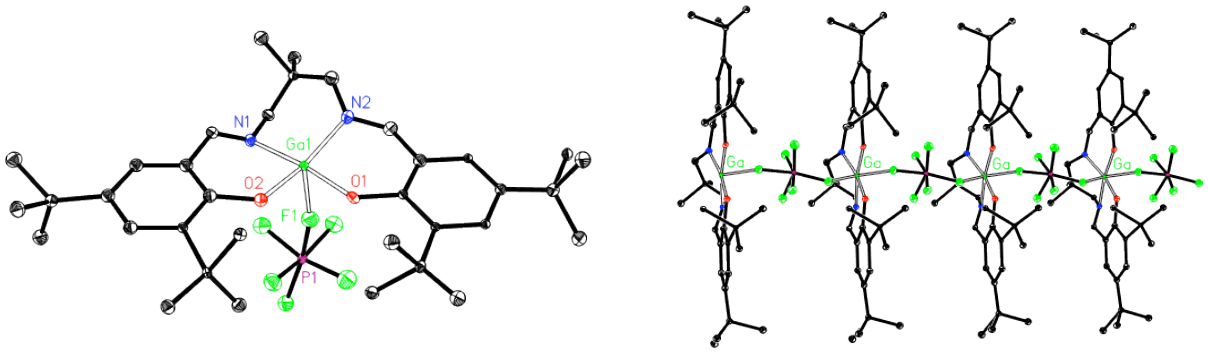

Figure 3.6. (a) Molecular structure of **49** showing the connectivity; (b) Extended solid-state structure of **49**.

Having successfully demonstrated the ability to abstract an appended halide, the halide ion abstraction method was applied to the bithiophene-derivative **47** in order to form the chloride-abstracted Schiff Base complex, **50**. Unfortunately, repeated efforts to obtain crystals suitable for X-ray diffraction from a variety of solvents and crystallization techniques failed hence it was necessary to rely on NMR spectroscopy. As observed in the case of the halide-abstracted model species **49**, the ^{19}F and ^{31}P NMR of **50** were

indicative of the presence of a halide-abstracted species in solution (δ -69.39, doublet, J_{P-F} of 710 Hz and δ -139.19, septet, J_{P-F} of 710 Hz respectively). Unfortunately, the low solubility of **50** and the relatively low NMR sensitivity of the ^{69}Ga and ^{71}Ga nuclei proved to be a hindrance in complete characterization of the discrete monomer **50**.

Despite the incomplete characterization of **50** it was decided to carry out further investigation of the potential utility of **50** to serve as a scaffold for the construction of polymer / nanoparticle hybrid systems. This work was carried out in collaboration with Michelle Mejia in the research group of Professor Bradley Holliday and as such, only the salient details of these results will be presented here. Through careful potentiodynamic electropolymerization of **50** in a methylene chloride / acetonitrile medium, a thin film of the corresponding polymer of **50** was deposited onto an ITO slide. The cyclic voltammograms obtained, which are displayed in Figure 3.7, exhibit the characteristic oxidative and reductive cycles expected in the polymerization of bithiophene derivatives. Additionally, by plotting the applied current against the number of scans (Figure 3.8), a linear progression is evident, thus indicating a well-behaved system. Note, however, that the relatively shallow slope is indicative of a somewhat 'sluggish' polymerization.

With readily polymerized films of **50** in hand, these substrates were then exposed to nanoparticle growth conditions. These conditions involve exposure of the film to methylene chloride solutions of H_2S and $Ga(NO_3)_3$ on an alternating basis. Characterization of the resulting embedded gallium sulfide nanoparticles was accomplished by using XPS and TEM, the results of which are illustrated in Figures 3.9 and 3.10.

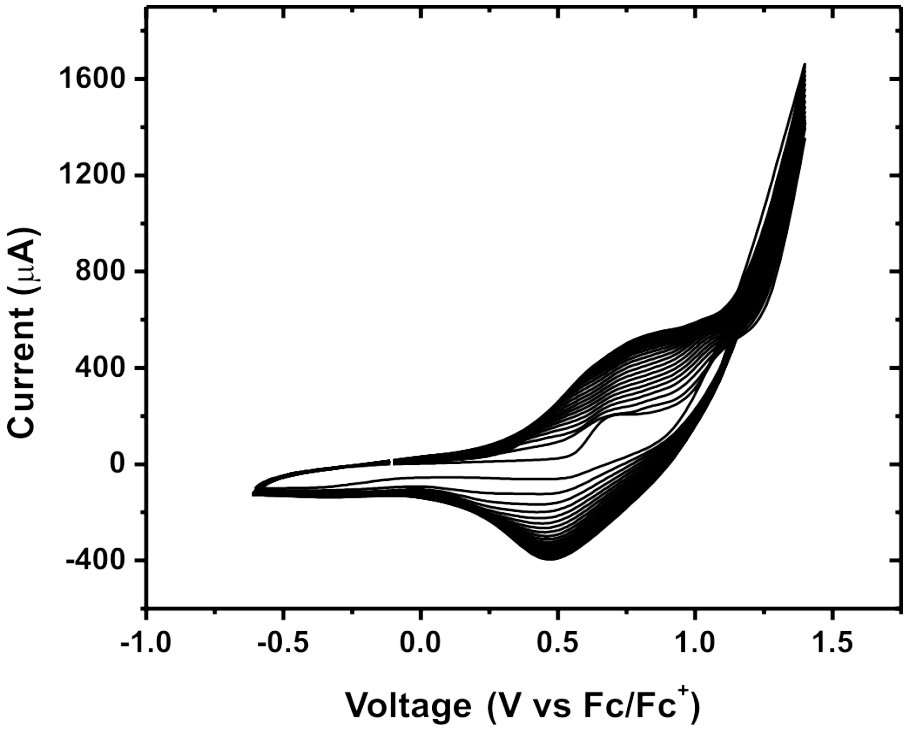

Figure 3.7. Cyclic voltammogram for the electropolymerization of **50**.

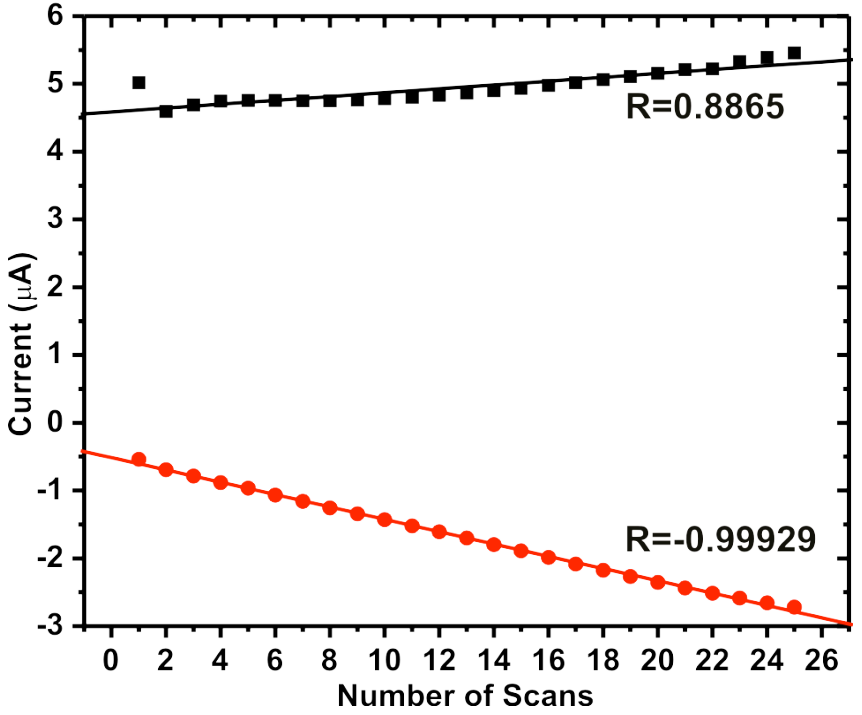

Figure 3.8. Linear relationship of current with number of scans in the electropolymerization of **50**.

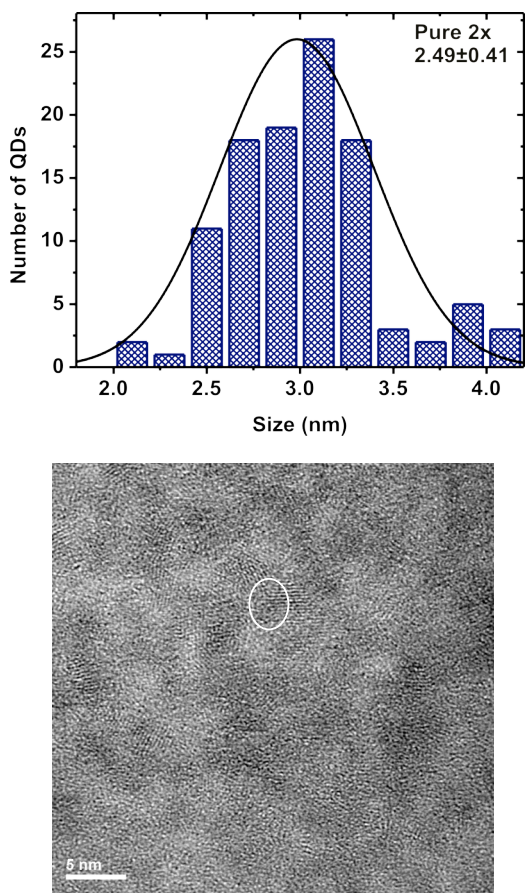

Figure 3.9. Size distribution of, and TEM image of GaS nanoparticles embedded within polymer of **50**, after exposure to two treatments of growth conditions.

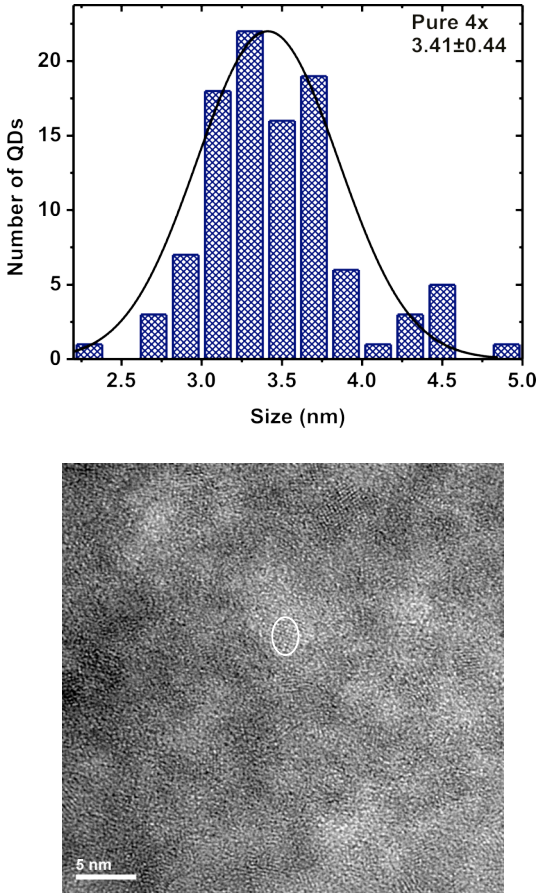

Figure 3.10. Size distribution of, and TEM image of GaS nanoparticles embedded within polymer of **50**, after exposure to four treatments of growth conditions.

The relatively narrow size distribution of the GaS nanoparticles is clearly evident in Figures 3.9 and 3.10. This is a remarkable achievement given the underlying simplicity of the growth technique. Moreover, with no 'specialized' treatments, the production of nanocrystals is also achieved during the growth process.

Reactivity studies of Indium substituted Schiff Base complexes

In an effort to gain access to a broader swathe of the solar spectrum, synthetic access to semiconductors with band gaps of varying size is necessary. In order to explore the ability of Schiff base ligands to support important III-V semiconductors such as InP, work is underway to test the reactivity of the indium –substituted model complexes **43** and **44** with a variety of phosphorus-containing reagents.

As noted previously, the indium chloride analogue, **48**, of the gallium chloride bithiophene-Schiff Base **47** forms a dimer in the solid state in which the indium centers are six-coordinate and the geometry is best described as distorted octahedral. It is noteworthy that the model indium halide complexes **43** and **44**, are square-based pyramidal in nature and do not form dimers in the solid state. This difference is undoubtedly the result of the increased steric loading at the aryl position *ortho*- to the phenol with a bulky *tert*-butyl group. In an effort to provide access to alternative semiconducting nanoparticles based upon an appropriately substituted indium precursor was desirable for the twin purposes of proving the generality of the seeded growth approach and, more importantly, gaining access to a broader range of the solar spectrum for solar energy conversion. In turn, the key to preparing such a precursor appeared to be

the substitution of the originally targeted ligand with a bulky *tert*-butyl group in a position akin to that of the model complexes **43** and **44**.

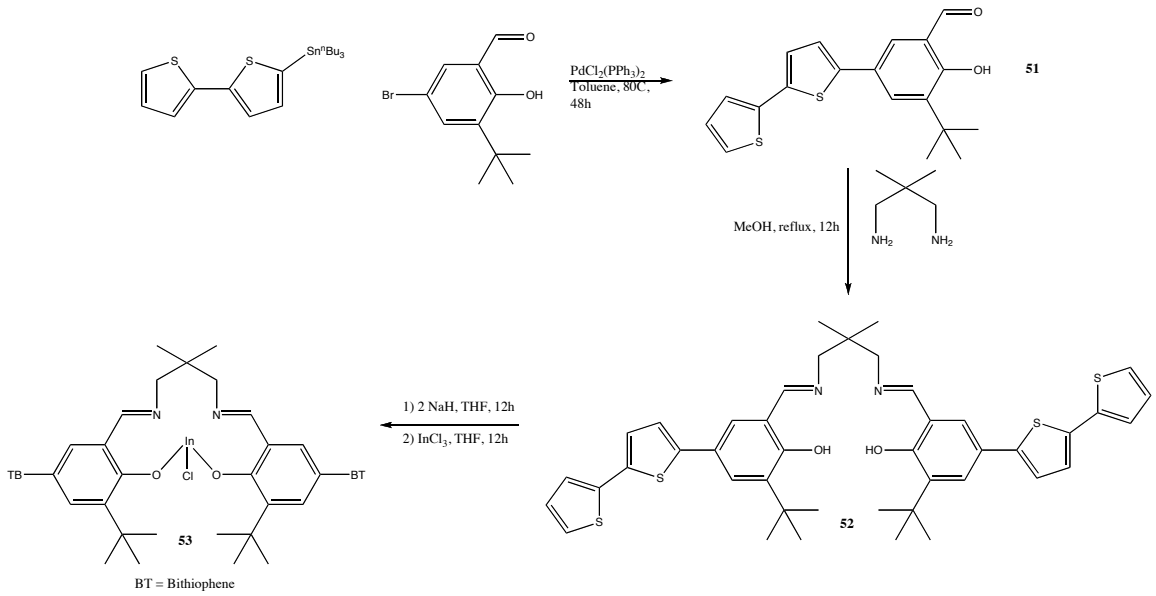

Scheme 3.6. Proposed synthesis of polymerizable indium chloride substituted Schiff base complex **53**.

The precursor bromo-substituted *tert*-butylsalicylaldehyde was synthesized according to the literature method in high yield from commercially available products [23]. The bulky SB compound, **52**, was prepared in an analogous fashion to that employed for the synthesis of **46**. Unfortunately, current studies have not progressed to the final metallation step at the time of writing. However, the synthetic methodology proposed is entirely consistent with previous syntheses and is expected to proceed as planned. Preliminary data are, however, available for a discussion of the reactivity patterns of the model complex **44**.

Treatment of **44** with $AgBF_4$ in methylene chloride solution afforded, after stirring overnight, the BF_4^- salt of the desired indium cation as outlined in Scheme 3.7. After removal of material by filtration, the solvent was removed under reduced pressure and the resulting yellow residue was re-dissolved in toluene. To this toluene solution was added $(THF)_2 \rightarrow LiP(SiMe_3)_2$ [24] at ambient temperature and the reaction mixture was stirred overnight. Work up of this reaction mixture involved removal of the solvent and subsequent extraction of the residue with hexane. Crystals suitable for single crystal X-ray diffraction study were grown from a toluene solution of **54** layered with hexane.

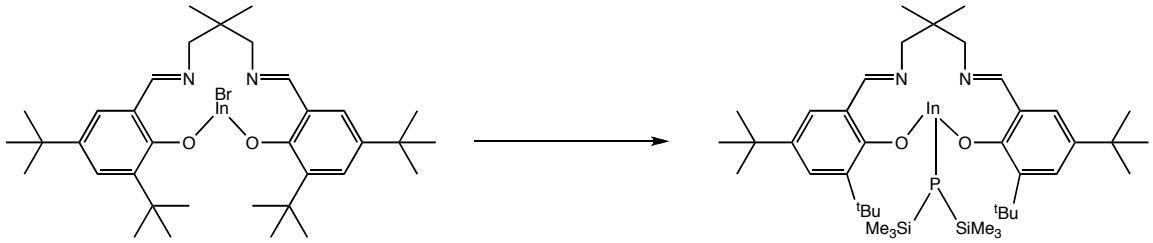

Scheme 3.7. Synthesis of **54**, a phosphorus-substituted indium-SB complex.

Despite low- and high-resolution mass spectral evidence for the formation of the desired complex **54**, the isolated crystals proved to be the dimeric structure **55**, shown in Figure 3.11. Clearly, the formation of **55** results from the reaction of **54** with a further equivalent of the indium cation, or perhaps starting material **44**. Complex **55** crystallizes in the triclinic space group P-1 as an ensemble of monomers with no unusually short intermolecular contacts. Interestingly, the indium centers of **55** display two different five-coordinate bonding geometries, namely trigonal bipyramidal at In(1) and square-based

pyramidal at In(2). The bond angles O(3)-In(2)-O(4), O(3)-In(2)-N(3), and O(4)-In(2)-N(4) are all close (albeit somewhat acute) to 90°, being 83.32(13)°, 83.17(14)°, and 81.02(14)° respectively. The distortion within this framework, namely the acute nature of the bond angles, is clearly the result of the second sterically demanding SB ligand within the coordination sphere. The trigonal bipyramidal geometry about In(1) is also appreciably distorted, the indium-oxygen and indium-nitrogen bonds displaying a tendency to splay away from the direction of the phosphorus atom. This distortion is most evident in the bond angles P(1)-In(1)-O(1), P(1)-In(1)-N(2), O(1)-In(1)-N(2), and O(2)-In(1)-N(1) which all exhibit values which deviate from the ideal values, being 135.91(10)°, 110.00(11)°, 112.97(14)° and 153.11(13)° respectively. The average In-O bond distance is 2.115(3) Å and the average In-N bond distance is 2.265(4) Å. The In-P bond distances for In(1)-P(1) and In(2)-P(1) are 2.4720(14) Å, and 2.4863(13) Å respectively.

Conclusions

A range of Schiff base gallium complexes, with and without polymerizable bithiophene substituents, have been prepared. The complexes bearing bithiophene substituents can be electropolymerized to give conducting thin films containing Ga. However, initial attempts to grow gallium sulfide within the polymer matrices by sequential treatment with H_2S and $Ga(NO_3)_3$ were unsuccessful. The reason for this lack of reactivity was probed using the newly synthesized model complex, **42**.

Since it seemed reasonable to assume that the electropolymerized film featured a five-coordinate gallium center, the lack of reactivity was most likely due to coordinative

saturation at the metal center. It was discovered that treatment of the SB-Ga-Cl complexes, with or without bithiophene moieties, with $AgPF_6$ in CH_3CN/CH_2Cl_2 solution resulted in chloride anion abstraction and generation of a four-coordinate cationic center at gallium accompanied by a weakly coordinating PF_6 anion. The solid-state structure of **49** consists of a one-dimensional coordination polymer of cationic gallium moieties bridged by PF_6 anions.

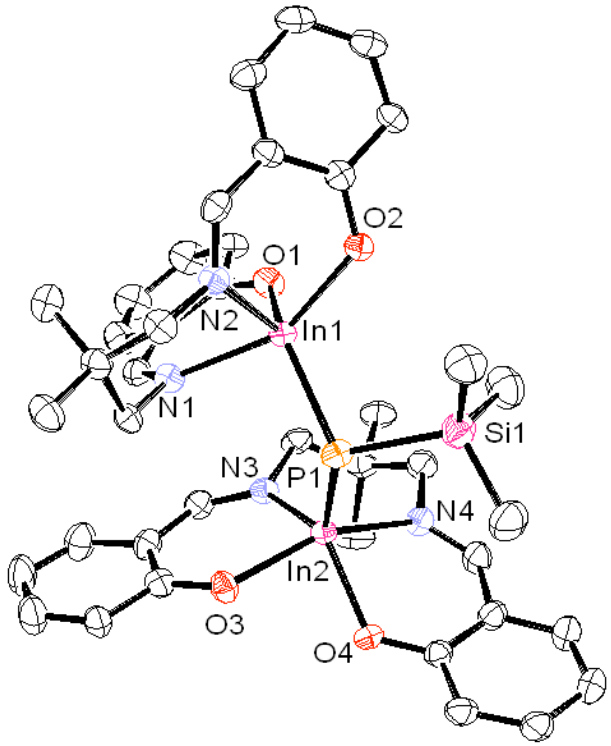

Figure 3.11. Molecular structure of **55**, with thermal ellipsoids shown at the 40% probability level. The tert-butyl substituents have been omitted for clarity.

Treatment of the electropolymerized thin film of **50** with $AgPF_6$ followed by $H_2S/Ga(NO_3)_3$ nanoparticle growth conditions resulted in excellent Ga_2S_3 nanoparticle

growth within the polymer matrix. This result is particularly significant because it shows that nanoparticle formation must originate at the pre-designed seed point – in this case an activated Ga center. If this center is not present then formation of polymer bound nanoparticles does not occur.

The preparation of InP nanocrystals *via* low temperature growth techniques is of significant technological importance. Initial efforts have focused on the use of the appended halide as a functional group to help initiate the growth of the semiconductor nanoparticle and thus anchor it to the polymer matrix. Preliminary results suggest that this is possible by a salt metathesis reaction of the indium halide complex with a suitable metallated phosphorus reagent. Current studies are focused on the preparation of a bulky bithiophene-substituted SB indium complex in an effort to disfavor unwanted dimer by using the steric crowding afforded by appropriately placed tert-butyl groups. The isolation of the In-P-In dimer, **55**, while an unwanted by-product, does indicate the reactivity of the P-$SiMe_3$ bonds and their potential utility to serve as appropriate growth points for nanoparticle formation.

Experimental Section

(a) General procedures

All manipulations and reactions were performed under a dry, oxygen-free, catalyst-scrubbed argon atmosphere using a combination of standard Schlenk techniques or in an M-Braun or Vacuum Atmospheres drybox. All glassware was oven-dried and vacuum- and argon flow-degassed before use. All solvents were distilled over sodium benzophenone ketyl, except dichloromethane, which was distilled over CaH_2, and degassed prior to use. Unless specified, all starting materials were obtained commercially and used without further purification.

(b) Physical measurements

Low-resolution CI mass spectra were obtained on a Finnigan MAT TSQ-700 mass spectrometer and high-resolution CI mass spectra recorded on a VG Analytical ZAB-VE sector instrument. All MS analyses were performed on samples that had been sealed in glass capillaries under an argon atmosphere. ^{1}H, $^{13}C\{^{1}H\}$, ^{11}B, ^{19}F and $^{31}P\{^{1}H\}$ NMR spectra were recorded at 295 K in C_6D_6 solutions on a GE EQ-300 instrument (^{1}H, 300 MHz; ^{13}C, 75 MHz, ^{11}B, 96 MHz, ^{19}F, 282 MHz, ^{31}P, 121 MHz) immediately following removal of the sample from the drybox. ^{1}H and $^{13}C\{^{1}H\}$ chemical shift values are reported in parts per million (ppm) relative to $SiMe_4$ (δ 0.00), using residual solvent resonances as internal standards. ^{11}B NMR data are referenced to $BF_3{:}OEt_2$ (δ 0.00). Melting points (uncorrected) were obtained on a Fisher-Johns apparatus after flame-sealing the samples in glass capillaries under argon.

(c) X-ray crystallography

For compounds **41**, **42**, **43**, **44**, **47**, and **55**, a crystal of suitable quality was removed from a Schlenk flask under positive argon pressure, covered immediately with degassed hydrocarbon oil and mounted on a glass fiber. The X-ray diffraction data were collected at 153 K on a Nonius Kappa CCD diffractometer equipped with an Oxford Cryostream low-temperature device and a graphite-monochromated Mo Kα radiation source (λ = 0.71073 Å). Corrections were applied for Lorentz and polarization effects. All structures were solved by direct methods [25] and refined by full-matrix least-squares cycles on F^2. All non-hydrogen atoms were allowed anisotropic thermal motion, and hydrogen atoms were placed in fixed, calculated positions using a riding model (C-H 0.96 Å).

(d) Syntheses

Synthesis of Model Schiff Base-$GaNO_3$ (**41**). In a round-bottom flask, **40** (535 mg, 1 mmol), gallium nitrate (390 mg, 1 mmol) and an ethanol : methanol (1:1, 50 mL) solution were mixed. This mixture was heated to reflux temperature and stirred overnight. After concentration of the crude mixture to half-volume the flask was stored at -40°C for 12h at which point the desired product was obtained as pale yellow crystals (mg, %). ^{1}H NMR (CD_2Cl_2): δ 8.24 (s, 2H, C(H)=N), 7.55 (m, 1H, Ar-H), 7.15 (m, 1H, Ar-H), 3.58 (br m, 4H, N-CH_2), 1.42 (s, 18H, $C(CH_3)_3$), 1.38 (s, 18H, $C(CH_3)_3$), 1.11 (s, 6H, CH_3); ^{13}C NMR (CD_2Cl_2): δ 172.71 (C=N), 165.87 (Ar), 141.68 (Ar), 139.16 (Ar), 131.72 (Ar), 128.65 (Ar), 117.19 (Ar), 67.441 (N-CH_2), 35.69 ($\underline{C}Me_3$), 34.30 ($\underline{C}Me_3$), 31.38 ($C\underline{Me}_3$), 29.48 ($C\underline{Me}_3$), 29.34 (CH_3). MS (CI^+, CH_4): *m/z* 666 (M+H); 604 (M-NO_3). HRMS (CI, CH_4) calcd. for $C_{35}H_{52}N_3O_5Ga^{69}$ 663.3163; found 663.3166.

Synthesis of Model Schiff Base-GaCl (**42**). A solution of **40** (1.000 g, 1.87 mmol) in THF (50 mL) was added slowly to a suspension of KH (0.150 g, 3.74 mmol) in THF (10 mL) at ambient temperature. The mixture was allowed to stir for 12h. The resulting yellow solution was added to a solution if $GaCl_3$ (0.329 g, 1.87 mmol) in THF (20 mL) and stirred for a further 12h. All volatiles were subsequently removed at reduced pressure and the yellow residue extracted with methylene chloride to afford the product as a yellow powder (1.04 g, 90%). ^{1}H NMR (CD_2Cl_2): δ 8.38 (s, 2H, C(H)=N), 7.40 (m, 1H, Ar-H), 7.12 (m, 1H, Ar-H), 3.13 (br m, 4H, N-CH_2), 1.47 (s, 18H, $C(CH_3)_3$), 1.35 (s, 18H, $C(CH_3)_3$), 1.11 (s, 6H, CH_3). MS (CI^+, CH_4): *m/z* 637 (M+H); 601 (M-Cl). HRMS (CI, CH_4) calcd. for $C_{37}H_{44}BCl_2N_3$ 611.3131; found 611.3123.

Synthesis of Model Schiff Base-InCl (**43**). A solution of **40** (1.000 g, 1.87 mmol) in THF (50 mL) was added slowly to a suspension of NaH (0.090 g, 3.74 mmol) in THF (10 mL) at ambient temperature. The mixture was allowed to stir for 12h. The resulting yellow solution was added to a solution if $InCl_3$ (0.414 g, 1.87 mmol) in THF (20 mL) and stirred for a further 12h. All volatiles were subsequently removed at reduced pressure and the yellow residue extracted with methylene chloride to afford the product as a yellow powder (1.27 g, 99%). ^{1}H NMR (CD_2Cl_2): δ 8.42 (s, 2H, C(H)=N), 7.42 (m, 1H, Ar-H), 7.17 (m, 1H, Ar-H), 3.53 (br m, 4H, N-CH_2), 1.48 (s, 18H, $C(CH_3)_3$), 1.34 (s, 18H, $C(CH_3)_3$), 1.12 (s, 6H, CH_3). MS (CI^+, CH_4): *m/z* 683 (M+H); 647 (M-Cl). HRMS (CI, CH_4) calcd. for $C_{35}H_{53}N_2O_2ClIn$ 683.2834; found 683.2829.

Synthesis of Model Schiff Base-InBr (**44**). Pale yellow plate-like, crystals of **44** were prepared in 90% yield from **40** using the same procedure that was described for **43**. ^{1}H NMR ($CDCl_3$): δ. MS (CI^+, CH_4): *m/z* 728 (M+H). HRMS (CI, CH_4) calcd. for $C_{35}H_{53}N_2O_2BrIn$ 727.2329; found 727.2328.

Synthesis of N,N'-((2,2'-dimethyl)propyl)-bis(5-(2,2'-bithiophene-5-yl)salicylidenimine) (**47**). A solution of **46** (250 mg, 0.32 mmol) in THF (50 mL) was added to a slurry of NaH (19 mg, 0.78 mmol) in THF (50 mL) and this mixture stirred for 12 hours at ambient temperature. Filtration of the slightly cloudy solution yielded a clear solution which was subsequently added to a solution of $GaCl_3$ (69 mg, 0.32 mmol) in THF (30 mL). After stirring overnight the mixture was filtered and all volatiles removed from the filtrate at reduced pressure. The yellow residue obtained was recrystallized from a THF/hexane mixture to afford a yellow microcrystalline solid (236 mg, 97%). ^{1}H NMR (CD_2Cl_2): δ 8.28 (s, 2H, HC=N), 7.69 (dd, 2H, Ar-H), 7.53 (d, 2H, Ar-H), 7.28 (m, 2H, Ar-H), 7.23 (m, 2H, Ar-H), 7.17 (m, 4H, Ar-H), 7.06-7.09 (m, 4H, Ar-H), 4.06 (d, 2H, CH_2), 3.40 (d, 2H, CH_2), 1.22 (s, 3H, CH_3), 1.09 (s, 3H, CH_3). MS (CI^+, CH_4): *m/z* 741 (M+H), 707 (M-Cl). HRMS (CI, CH_4) calcd. for $C_{35}H_{29}N_2O_2S_4ClGa^{69}$ 741.0056; found 741.0054.

Synthesis of Abstracted [Model Schiff Base-Ga][PF_6] (**49**). To a stirred solution of **42** (32 mg, 0.05 mmol) in a methylene chloride : acetonitrile (1:1, 10 mL) was added in one portion silver hexafluorophosphate (13 mg, 0.05 mmol) at ambient temperature. The mixture was allowed to stir for 12h. The resulting yellow solution was

filtered and all volatiles were removed at reduced pressure to give a yellow residue, which was crystallized from methylene chloride to afford the product as a yellow solid (30 mg, 80%). ^{1}H NMR (CD_2Cl_2): δ 8.54 (s, 2H, C(H)=N), 7.66 (d, 2H, Ar-H), 7.42 (d, 2H, Ar-H), 3.76 (br s, 4H, N-CH_2), 1.47 (s, 18H, C(CH_3)$_3$), 1.36 (s, 18H, C(CH_3)$_3$), 1.24 (br s, 6H, CH_3). ^{13}C NMR (CD_2Cl_2): δ 169.36 (HC=N), 157.02 (Ar), 142.94 (Ar), 136.54 (Ar), 131.69 (Ar), 131.69 (Ar), 129.16 (Ar) 116.19 (Ar), 64.15 (N-CH_2), 36.34 ($\underline{C}Me_3$), 34.22 ($\underline{C}Me_3$), 30.73 ($C\underline{Me}_3$), 29.24 ($C\underline{Me}_3$), 23.18 (CH_3). ^{19}F NMR (CD_2Cl_2): δ -73.32 (d, PF_6). ^{31}P NMR (CD_2Cl_2): δ -149.37 (sept, PF_6). MS (CI^+, CH_4): *m/z* 602 (M+H). HRMS (CI, CH_4) calcd. for $C_{35}H_{52}N_2O_2Ga$ 601.3285; found 601.3283.

Synthesis of Abstracted [Bithiophene Schiff Base-Ga][PF_6] (**50**). To a stirred solution of **47** (32 mg, 0.05 mmol) in a methylene chloride : acetonitrile (1:1, 10 mL) was added in one portion silver hexafluorophosphate (13 mg, 0.05 mmol) at ambient temperature. The mixture was allowed to stir for 12h. The resulting yellow solution was filtered and all volatiles were removed at reduced pressure to give a yellow residue, which was crystallized from methylene chloride to afford the product as a yellow solid (30 mg, 80%). ^{1}H NMR (CD_2Cl_2): δ 8.60 (s, 2H, C(H)=N), 7.76 (m, 4H, Ar-H), 7.23 (m, 4H, Ar-H), 7.14 (m, 4H, Ar-H), 6.98 (m, 4H, Ar-H), 3.84 (br s, 4H, N-CH_2), 1.20 (br s, 6H, CH_3). ^{19}F NMR (CD_2Cl_2): δ -69.39 (d, PF_6). ^{31}P NMR (CD_2Cl_2): δ -139.19 (sept, PF_6). MS (CI^+, CH_4): *m/z* 705 (M+H). HRMS (CI, CH_4) calcd. for $C_{35}H_{28}N_2O_2S_4Ga$ 705.0289; found 705.0284.

Synthesis of 5-(2,2'-bithiophene-5-yl)-2-hydroxy-3-tertbutylbenzaldehyde (**51**). To a 100 mL Schlenk flask equipped with a reflux condenser was added the palladium catalyst, $PdCl_2(PPh_3)_2$, (5 mol %) and the tributyltin-bithiophene (1.05 eq.). The flask was then evacuated and refilled three times before addition of toluene (~30 mL), followed by subsequent addition of the bromo-salicylaldehyde (1 eq.). The stirred reaction mixture was then warmed to 80 °C at which point the mixture began to noticeably darken. After 48h the reaction was cooled to room temperature, the solvent removed in vacuuo and the brown/black residue redissolved in methylene chloride. Residual palladium was removed via filtration through a silica plug and the filtrate treated with a saturate ammonium chloride solution. After drying with magnesium sulfate, the solvent was removed and the product isolated as a yellow powder. Further purification may be achieved by trituration in petroleum ether, though this results in a dramatic drop in product yield. ^{1}H-NMR (CD_2Cl_2): δ 11.87 (s, 1H, OH), 9.95 (s, 1H, *H*C=O), 7.78 (s, 1H, H_{arom}), 7.66 (s, 1H, H_{arom}), 7.12-7.25 (m, 4H, H_{arom}), 7.01 (m, 1H, H_{arom}), 1.47 (s, 9H, ^{t}Bu). ^{13}C NMR (CD_2Cl_2): δ 197.06 (<u>C</u>(O)H) 160.53 (Arom-OH), 138.80 (Arom), 135.80 (Arom), 131.32 (Arom), 128.31 (Arom), 124.25 (Arom), 123.10 (Arom),. 120.47 (Arom), 34.69 (<u>C</u>(Me)$_3$), 26.63 (C(<u>Me</u>)$_3$). LRMS (CI+ m/z) (%): 343 (100%, MH+). HRMS (CI+ CH_4) calcd. for: $C_{19}H_{19}O_2S_2$ 343.0826 ; Found 343.0827.

Synthesis of N,N'-((2,2'-dimethyl)propyl)-bis(5-(2,2'-bithiophene-5-yl) -2-hydroxy-3-tertbutylsalicylidenimine) (52). To a methanol solution (50 mL) of the salicylaldehyde was added the diamine (0.5 eq) as a solution in methanol (5 mL). The yellow mixture was heated to reflux and stirred overnight. The mixture was stirred for a further 12 hours at

room temperature and the product was isolated via filtration, yielding a yellow solid. ^{1}H-NMR (CD_2Cl_2) δ: 1.51 [s, 18H, ^{t}Bu], 3.53 [m, 2H, N-CH_2], 7.03-7.19 [m, 10H, H_{arom}], 7.37 [s, 2H, H_{arom}], 7.58 [s, 2H, H_{arom}], 8.40 [s, 2H, *H*C=N], 14.33 [s, 2H, OH]. ^{13}C NMR (CD_2Cl_2) δ: 24.58 [CH_3], 29.42 [C(Me)$_3$], 35.29 [C(Me)$_3$], 68.47 [N-CH_2], 119.10 [Arom], 122.76 [Arom], 123.65 [Arom], 124.31 [Arom], 124.50 [Arom], 124.91 [Arom], 127.00 [Arom], 127.47 [Arom], 128.25 [Arom], 135.68 [Arom], 137.86 [Arom], 138.53 [Arom], 143.71 [Arom], 161.03 [Arom-OH], 166.79 [N=CH]. LRMS (CI+ m/z) (%): 752 (M+H, 100%) HRMS (CI+ CH_4) calcd. for: $C_{43}H_{46}N_2O_2S_4$ 751.2520; Found 751.25149.

Reaction of 44 with $(THF)_2$→Li-P$(SiMe_3)_2$ (54 and 55). To a methylene chloride (10 mL) solution of **44** (g, mmol) was added $AgBF_4$ (g, mmol) at ambient temperature. This reaction mixture was then stirred overnight and insoluble materials removed by filtration. Removal of solvent at reduced pressure afforded a yellow residue which was redissolved in toluene and $(THF)_2$→Li-P$(SiMe_3)_2$ (g, mmol) added as a solid at room temperature. This mixture was stirred overnight, the solvent was removed at reduced pressure and the yellow residue obtained extracted with hexanes to afford, after solvent stripping a yellow oily residue. Crystals of **55** were isolated from a toluene solution of the obtained residue. Mass spectral data were obtained for both **54** and **55** in addition to ^{31}P NMR data for **55**. **54**: LRMS (CI+ m/z): 824 (M+H). HRMS (CI+ CH_4) calcd. for: $C_{41}H_{70}N_2O_2Si_2PIn$ 824.3752; Found 824.3748. **55**: ^{31}P NMR (C_6D_6): δ -304.01 (s). LRMS (CI+ m/z): 1399 (M+H). HRMS (CI+ CH_4) calcd. for: $C_{73}H_{114}N_4O_4SiPIn_2$ 1399.6425; Found 1399.6423.

References

1 C. Brabec, V. Dyakonov, J. Parisi and N. S. Sariciftci (Eds.), *Organic Photovoltaics*: *Concepts and Realization*, Springer Press, 2000.

2 J. Nelson, *Cur. Opin. Solid State, Mater. Sci.*, 2002, **6**, 87.

3 J. Xue, S. Uchida, B. R. Rand and S. R. Forrest, *Appl. Phys. Lett.*, 2004, **85**, 5757.

4 J. M. Marshall and D. Dimova-Malinovska (Eds.), *Photovoltaic and Photoactive Materials: Properties, Technology, and Applications*, 2001, p. 197, NATO Science Series, Kluwer Academic Publishers, Dordecht.

5 S.-S. Sun, *Solar Energy Mater. And Solar Cells*, 2003, **79**, 257.

6 (a) M. R. Ganjali, T. Poursaberi, F. Basiripour, M. S. Niassari, M. Yousefi and M. Shamsipur, *Fresenius J. Anal. Chem*., 2001, **370**, 1091; (b) M. L. Duran, A. Rodriguez, J. Romero and A. Sousa, *Synth. React. Inorg. Met. Org. Chem.*, 1987, **17**, 681; (c) H. Keypour, S. Salehzadeh, R. G. Pritchard and R. V. Parish, *Polyhedron*, 2000, **19**, 1633; (d) L. F. Lindoy, D. H. Busch and V. Goedken, *J. Chem. Soc. Chem. Comm.*, 1972, 683; (e) A. Jantti, M. Wagner, R. Suontamo, E. Kolehmainen and K. Rissanen, *Eur. J. Inorg. Chem.*, 1998, 1555.

7 (a) R. N. Prasad and J. P. Tandon, *J. Less-Common Met.*, 1974, **37**, 141; (b) R. N. Prasad and J. P. Tandon, *J. Inorg. Nucl. Chem.*, 1975, **37**, 35; (c) M.-A. Munoz-Hernandez, T. S. Keizer, S. Parkin, B. Patrick and D. A. Atwood, *Organometallics*, 2000, **19**, 4416; (d) J. Qiao, L. D. Wang, L. Duan, Y. Li, D. Q. Zhang and Y. Qui, *Inorg. Chem.*, 2004, **43**, 5096; (e) D. J. Darensbourg

and D. R. Billodeaux, *Comp. Rend. Chim.*, 2004, **7**, 755; (f) M. S. Hill and D. A. Atwood, *Eur. J. Inorg. Chem.*, 1998, **1**, 67; (g) M. S. Hill, A. Hutchinson, T. S. Keizer, S. Parkin, M. VanAelstyn and D. A. Atwood, *J. Organomet. Chem.*, 2001, **628**, 71; (h) D. A. Atwood, J. A. Jeiger and D. Rutherford, *Bull. Chem. Soc. Jpn.*, 1997, **70**, 2093; (i) M. S. Hill and D. A. Atwood, *Main Group Chem.*, 1998, **2**, 191.

8 (a) J. Parr, A. T. Ross and A. M. Z. Slawin, *J. Chem. Soc. Dalton Trans.*, 1996, 1509; (b) J. Parr, A. T. Ross and A. M. Z. Slawin, *Polyhedron*, 1997, **16**, 1509; (c) P. Bhattacharyya, J. Parr, A. T. Ross and A. M. Z. Slawin, *J. Chem. Soc. Dalton Trans.*, 1998, 3149.

9 See for example: (a) X.-P. Yang, R. A. Jones, V. Lynch, M. M. Oye and A. L. Holmes, *Dalton Trans.*, 2005, 849; (b) X.-P. Yang, R. A. Jones and M. J. Wiester, *Dalton Trans.*, 2004, 1787; (c) R. A. Jones and X.-P. Yang, *J. Am. Chem. Soc.*, 2005, **127**, 7686.

10 A. Voituriez, M. Mella and E. Schulz, *Synth. Met.*, 2006, **156**, 166.

11 (a) W. U. Huynh, J. J. Dittmer and A. P. Alivisatos, *Science*, 2002, **295**, 2425; (b) W. U. Huynh, J. J. Dittmer and A. P. Alivisatos, *Adv. Mater.*, 2005, **17**, 66.

12 Ref 29

13 J. Sterner, J. Malstrom and L. Stolt, *Prog. Photovoltaics*, 2005, **13**, 179.

14 N. Naghavi, S. Spiering, M. Powalla, B. Cavana and D. Lincot, *Prog. Photovoltaics*, 2003, **11**, 437.

15 P. O'Brien and A. C. Jones, *CVD of Compound Semiconductors*, VCH, Weidlein, 1997, Chapter 1.

16 N. N. Greenwood and A. Earnshaw, *Chemistry of the Elements*, Pergamon Press, Oxford, 1984, Chapter 7.

17 E. K. Byrne, L. Parkyani and K. H. Theopold, *Science*, 1988, **241**, 64.

18 (a) R. L. Wells, C. G. Pitt, A. T. McPhail, A. P. Purdy, S. Shafieezad and R. B. Hallock, *Chem. Mater.*, 1989, **1**, 4; (b) R. L. Wells, R. B. Hallock, A. T. McPhail, C. G. Pitt and J. D. Johansen, *Chem. Mater.*, 1991, **3**, 381; (c) S. S. Kher and R. L. Wells, *Chem. Mater.*, 1994, **6**, 2056.

19 M. A. Olshavsky, A. N. Goldstein and A. P. Alivisatos, *J. Am. Chem. Soc.*, 1990, **112**, 9438.

20 (a) H. Uchida, C. J. Curtis and A. Nozik, *J. Phys. Chem.*, 1991, **95**, 5382; (b) H. Uchida, C. J. Curtis, P. V. Kamat, K. M. Jones and A. J. Nozik, *J. Phys. Chem.*, 1992, **96**, 1156.

21 L. Butler, G. Redmond and D. Fitzmaurice, *J. Phys. Chem.*, 1993, **97**, 10750.

22 H. Uchida, T. Matsunaga, H. Yoneyama, T. Sakata, H. Mori and T. Sasaki, *Chem. Mater.*, 1993, **5**, 716.

23 C. Baleizao, B. Gigante, H. Garcia and A. Corma, *Tetrahedron*, 2004, **60**, 10461.

24 G. Becker, H. Schmidt, G. Uhl and W. Uhl, *Inorg. Syntheses*, 1990, **27**, 243.

25 G. M. Sheldrick, SHELL-PC Version 5;03, Siemens Analytical X-ray Instruments, Inc., Madison, WI, USA, 1994

Tables of Crystallographic Data

Table 3.2. Crystal data and structure refinement for **41**.

Identification code	**41**	
Empirical formula	C38.50 H56 Ga N3 O5	
Formula weight	710.58	
Temperature	153(2) K	
Wavelength	0.71073 Å	
Crystal system	Monoclinic	
Space group	C 1 2/c 1	
Unit cell dimensions	a = 30.798(6) Å	α= 90°.
	b = 12.114(2) Å	β= 118.67(3)°.
	c = 23.235(5) Å	γ = 90°.
Volume	7606(3) $Å^3$	
Z	8	
Density (calculated)	1.241 Mg/m^3	
Absorption coefficient	0.768 mm^{-1}	
F(000)	3032	
Crystal size	0.15 x 0.10 x 0.10 mm^3	
Theta range for data collection	1.51 to 27.45°.	
Index ranges	-39<=h<=39, -15<=k<=14, -30<=l<=30	
Reflections collected	13373	
Independent reflections	8488 [R(int) = 0.0878]	
Completeness to theta = 27.45°	97.7 %	
Absorption correction	None	
Max. and min. transmission	0.9272 and 0.8935	
Refinement method	Full-matrix least-squares on F^2	
Data / restraints / parameters	8488 / 0 / 442	
Goodness-of-fit on F^2	1.015	
Final R indices [I>2sigma(I)]	R1 = 0.0675, wR2 = 0.1406	
R indices (all data)	R1 = 0.1868, wR2 = 0.2037	
Largest diff. peak and hole	0.770 and -0.987 $e.Å^{-3}$	

Table 3.3. Bond lengths [Å] and angles [°] for **41**.

C(1)-O(1)	1.329(6)
C(15)-N(1)	1.298(6)
C(16)-N(1)	1.466(6)
C(18)-N(2)	1.483(6)
C(19)-N(2)	1.295(6)
C(22)-O(2)	1.327(6)
N(1)-Ga(01)	2.021(4)
N(2)-Ga(01)	2.001(4)
N(3)-O(5)	1.209(5)
N(3)-O(3)	1.257(5)
N(3)-O(4)	1.297(6)
O(1)-Ga(01)	1.855(3)
O(2)-Ga(01)	1.878(3)
O(3)-Ga(01)	2.165(4)
O(4)-Ga(01)	2.156(3)
C(15)-N(1)-C(16)	119.8(4)
C(15)-N(1)-Ga(01)	123.2(3)
C(16)-N(1)-Ga(01)	116.8(3)
C(19)-N(2)-C(18)	119.5(4)
C(19)-N(2)-Ga(01)	122.7(3)
C(18)-N(2)-Ga(01)	117.8(3)
O(5)-N(3)-O(3)	124.2(5)
O(5)-N(3)-O(4)	121.4(5)
O(3)-N(3)-O(4)	114.3(4)
C(1)-O(1)-Ga(01)	127.9(3)
C(22)-O(2)-Ga(01)	126.9(3)
N(3)-O(3)-Ga(01)	93.4(3)
N(3)-O(4)-Ga(01)	92.6(3)
O(1)-Ga(01)-O(2)	91.01(15)
O(1)-Ga(01)-N(2)	116.31(16)
O(2)-Ga(01)-N(2)	90.03(15)
O(1)-Ga(01)-N(1)	91.60(15)
O(2)-Ga(01)-N(1)	176.10(15)

N(2)-Ga(01)-N(1)	86.22(15)
O(1)-Ga(01)-O(4)	90.73(15)
O(2)-Ga(01)-O(4)	90.33(14)
N(2)-Ga(01)-O(4)	152.94(16)
N(1)-Ga(01)-O(4)	92.53(14)
O(1)-Ga(01)-O(3)	150.29(15)
O(2)-Ga(01)-O(3)	89.67(14)
N(2)-Ga(01)-O(3)	93.39(15)
N(1)-Ga(01)-O(3)	89.49(15)
O(4)-Ga(01)-O(3)	59.56(14)

Symmetry transformations used to generate equivalent atoms:

#1 -x,y,-z+3/2

Table 3.4. Torsion angles [°] for **41**.

C(27)-C(19)-N(2)-C(18)	-176.5(4)
C(27)-C(19)-N(2)-Ga(01)	4.6(7)
C(17)-C(18)-N(2)-C(19)	-108.6(5)
C(17)-C(18)-N(2)-Ga(01)	70.4(5)
C(6)-C(1)-O(1)-Ga(01)	27.6(7)
C(2)-C(1)-O(1)-Ga(01)	-154.5(3)
C(27)-C(22)-O(2)-Ga(01)	-27.9(6)
C(23)-C(22)-O(2)-Ga(01)	155.4(3)
O(5)-N(3)-O(3)-Ga(01)	174.5(5)
O(4)-N(3)-O(3)-Ga(01)	-4.0(4)
O(5)-N(3)-O(4)-Ga(01)	-174.5(4)
O(3)-N(3)-O(4)-Ga(01)	4.0(4)
C(1)-O(1)-Ga(01)-O(2)	155.1(4)
C(1)-O(1)-Ga(01)-N(2)	-114.4(4)
C(1)-O(1)-Ga(01)-N(1)	-27.8(4)
C(1)-O(1)-Ga(01)-O(4)	64.7(4)
C(1)-O(1)-Ga(01)-O(3)	64.0(5)
C(22)-O(2)-Ga(01)-O(1)	151.7(4)
C(22)-O(2)-Ga(01)-N(2)	35.4(4)
C(22)-O(2)-Ga(01)-N(1)	20(2)

C(22)-O(2)-Ga(01)-O(4)	-117.5(4)
C(22)-O(2)-Ga(01)-O(3)	-58.0(4)
C(19)-N(2)-Ga(01)-O(1)	-114.3(4)
C(18)-N(2)-Ga(01)-O(1)	66.7(3)
C(19)-N(2)-Ga(01)-O(2)	-23.2(4)
C(18)-N(2)-Ga(01)-O(2)	157.8(3)
C(19)-N(2)-Ga(01)-N(1)	155.8(4)
C(18)-N(2)-Ga(01)-N(1)	-23.2(3)
C(19)-N(2)-Ga(01)-O(4)	67.6(5)
C(18)-N(2)-Ga(01)-O(4)	-111.4(4)
C(19)-N(2)-Ga(01)-O(3)	66.5(4)
C(18)-N(2)-Ga(01)-O(3)	-112.5(3)
C(15)-N(1)-Ga(01)-O(1)	14.1(4)
C(16)-N(1)-Ga(01)-O(1)	-160.7(3)
C(15)-N(1)-Ga(01)-O(2)	146(2)
C(16)-N(1)-Ga(01)-O(2)	-29(2)
C(15)-N(1)-Ga(01)-N(2)	130.4(4)
C(16)-N(1)-Ga(01)-N(2)	-44.5(3)
C(15)-N(1)-Ga(01)-O(4)	-76.7(4)
C(16)-N(1)-Ga(01)-O(4)	108.5(3)
C(15)-N(1)-Ga(01)-O(3)	-136.2(4)
C(16)-N(1)-Ga(01)-O(3)	49.0(3)
N(3)-O(4)-Ga(01)-O(1)	178.0(3)
N(3)-O(4)-Ga(01)-O(2)	87.0(3)
N(3)-O(4)-Ga(01)-N(2)	-3.7(5)
N(3)-O(4)-Ga(01)-N(1)	-90.4(3)
N(3)-O(4)-Ga(01)-O(3)	-2.5(3)
N(3)-O(3)-Ga(01)-O(1)	3.4(5)
N(3)-O(3)-Ga(01)-O(2)	-88.0(3)
N(3)-O(3)-Ga(01)-N(2)	-178.0(3)
N(3)-O(3)-Ga(01)-N(1)	95.8(3)
N(3)-O(3)-Ga(01)-O(4)	2.5(3)

Symmetry transformations used to generate equivalent atoms:

#1 -x,y,-z+3/2

Table 3.5. Crystal data and structure refinement for **42**.

Identification code	**42**	
Empirical formula	C35 H52 Cl Ga N2 O2	
Formula weight	637.96	
Temperature	153(2) K	
Wavelength	0.71069 Å	
Crystal system	orthorhombic	
Space group	Pbma	
Unit cell dimensions	a = 12.1280(2) Å	$\alpha = 90°$.
	b = 22.6490(3) Å	$\beta = 90°$.
	c = 25.8340(5) Å	$\gamma = 90°$.
Volume	7096.3(2) $Å^3$	
Z	8	
Density (calculated)	1.194 Mg/m^3	
Absorption coefficient	0.881 mm^{-1}	
F(000)	2720	
Crystal size	0.21 x 0.18 x 0.18 mm^3	
Theta range for data collection	2.30 to 27.46°.	
Index ranges	-15<=h<=15, -29<=k<=29, -33<=l<=33	
Reflections collected	15270	
Independent reflections	8090 [R(int) = 0.0466]	
Completeness to theta = 27.46°	99.6 %	
Max. and min. transmission	0.8575 and 0.8366	
Refinement method	Full-matrix least-squares on F^2	
Data / restraints / parameters	8090 / 0 / 384	
Goodness-of-fit on F^2	1.028	
Final R indices [I>2sigma(I)]	R1 = 0.0430, wR2 = 0.0936	
R indices (all data)	R1 = 0.0864, wR2 = 0.1099	
Largest diff. peak and hole	0.595 and -0.687 $e.Å^{-3}$	

Table 3.6. Bond lengths [Å] and angles [°] for **42**.

C(4)-N(1)	1.466(3)
C(5)-N(2)	1.464(3)
C(6)-N(1)	1.279(3)
C(12)-O(1)	1.326(3)
C(21)-N(2)	1.294(3)
C(27)-O(2)	1.319(3)
N(1)-Ga(1)	2.0613(19)
N(2)-Ga(1)	2.0001(18)
O(1)-Ga(1)	1.8448(16)
O(2)-Ga(1)	1.9096(15)
Cl(1)-Ga(1)	2.2135(7)
C(6)-N(1)-Ga(1)	125.16(15)
C(4)-N(1)-Ga(1)	114.36(15)
C(21)-N(2)-C(5)	119.06(18)
C(21)-N(2)-Ga(1)	121.41(15)
C(5)-N(2)-Ga(1)	119.53(14)
C(12)-O(1)-Ga(1)	132.83(14)
C(27)-O(2)-Ga(1)	122.34(13)
O(1)-Ga(1)-O(2)	86.90(7)
O(1)-Ga(1)-N(2)	126.41(8)
O(2)-Ga(1)-N(2)	88.97(7)
O(1)-Ga(1)-N(1)	89.40(7)
O(2)-Ga(1)-N(1)	169.71(7)
N(2)-Ga(1)-N(1)	85.51(7)
O(1)-Ga(1)-Cl(1)	120.71(6)
O(2)-Ga(1)-Cl(1)	96.12(5)
N(2)-Ga(1)-Cl(1)	112.86(6)
N(1)-Ga(1)-Cl(1)	94.02(6)

Symmetry transformations used to generate equivalent atoms:

Table 3.7. Torsion angles [°] for **42**.

C(7)-C(12)-O(1)-Ga(1)	13.4(4)
C(11)-C(12)-O(1)-Ga(1)	-167.22(17)
C(22)-C(27)-O(2)-Ga(1)	-38.4(3)
C(26)-C(27)-O(2)-Ga(1)	145.64(17)
C(12)-O(1)-Ga(1)-O(2)	174.7(2)
C(12)-O(1)-Ga(1)-N(2)	-98.9(2)
C(12)-O(1)-Ga(1)-N(1)	-14.9(2)
C(12)-O(1)-Ga(1)-Cl(1)	79.4(2)
C(27)-O(2)-Ga(1)-O(1)	173.16(17)
C(27)-O(2)-Ga(1)-N(2)	46.61(17)
C(27)-O(2)-Ga(1)-N(1)	104.1(4)
C(27)-O(2)-Ga(1)-Cl(1)	-66.27(16)
C(21)-N(2)-Ga(1)-O(1)	-115.43(18)
C(5)-N(2)-Ga(1)-O(1)	64.68(18)
C(21)-N(2)-Ga(1)-O(2)	-30.05(18)
C(5)-N(2)-Ga(1)-O(2)	150.06(16)
C(21)-N(2)-Ga(1)-N(1)	158.64(19)
C(5)-N(2)-Ga(1)-N(1)	-21.25(16)
C(21)-N(2)-Ga(1)-Cl(1)	66.16(18)
C(5)-N(2)-Ga(1)-Cl(1)	-113.73(15)
C(6)-N(1)-Ga(1)-O(1)	9.8(2)
C(4)-N(1)-Ga(1)-O(1)	-172.44(16)
C(6)-N(1)-Ga(1)-O(2)	78.7(4)
C(4)-N(1)-Ga(1)-O(2)	-103.6(4)
C(6)-N(1)-Ga(1)-N(2)	136.4(2)
C(4)-N(1)-Ga(1)-N(2)	-45.84(15)
C(6)-N(1)-Ga(1)-Cl(1)	-110.93(19)
C(4)-N(1)-Ga(1)-Cl(1)	66.81(15)

Symmetry transformations used to generate equivalent atoms:

Table 3.8. Crystal data and structure refinement for **43**.

Identification code	**43**	
Empirical formula	C35 H52 Cl In N2 O2	
Formula weight	683.06	
Temperature	293(2) K	
Wavelength	0.71069 Å	
Crystal system	monoclinic	
Space group	p21/c	
Unit cell dimensions	a = 17.436(5) Å	α= 90.000(5)°.
	b = 11.666(5) Å	β= 112.646(5)°.
	c = 18.613(5) Å	γ = 90.000(5)°.
Volume	3494(2) $Å^3$	
Z	4	
Density (calculated)	1.298 Mg/m^3	
Absorption coefficient	0.784 mm^{-1}	
F(000)	1432	
Crystal size	0.20 x 0.20 x 0.20 mm^3	
Theta range for data collection	2.11 to 27.48°.	
Index ranges	-22<=h<=22, -15<=k<=13, -24<=l<=24	
Reflections collected	12850	
Independent reflections	7932 [R(int) = 0.0254]	
Completeness to theta = 27.48°	99.0 %	
Absorption correction	None	
Max. and min. transmission	0.8590 and 0.8590	
Refinement method	Full-matrix least-squares on F^2	
Data / restraints / parameters	7932 / 0 / 393	
Goodness-of-fit on F^2	1.054	
Final R indices [I>2sigma(I)]	R1 = 0.0305, wR2 = 0.0669	
R indices (all data)	R1 = 0.0456, wR2 = 0.0742	
Extinction coefficient	0.00043(17)	
Largest diff. peak and hole	1.332 and -0.524 $e.Å^{-3}$	

Table 3.9 Bond lengths [Å] and angles [°] **43**.

C(1)-N(1)	1.478(3)
C(3)-N(2)	1.476(3)
C(6)-N(1)	1.297(3)
C(12)-O(1)	1.317(2)
C(21)-N(2)	1.290(3)
C(27)-O(2)	1.320(3)
N(1)-In(1)	2.1921(18)
N(2)-In(1)	2.2158(18)
O(1)-In(1)	2.0712(15)
O(2)-In(1)	2.0625(16)
Cl(1)-In(1)	2.3975(10)
C(6)-N(1)-C(1)	116.02(18)
C(6)-N(1)-In(1)	123.51(14)
C(1)-N(1)-In(1)	120.15(13)
C(21)-N(2)-C(3)	116.84(18)
C(21)-N(2)-In(1)	123.51(15)
C(3)-N(2)-In(1)	118.92(13)
C(12)-O(1)-In(1)	132.84(14)
C(27)-O(2)-In(1)	131.59(14)
O(2)-In(1)-O(1)	85.59(6)
O(2)-In(1)-N(1)	138.77(7)
O(1)-In(1)-N(1)	86.39(6)
O(2)-In(1)-N(2)	84.59(6)
O(1)-In(1)-N(2)	158.07(7)
N(1)-In(1)-N(2)	88.15(7)
O(2)-In(1)-Cl(1)	118.56(5)
O(1)-In(1)-Cl(1)	105.71(5)
N(1)-In(1)-Cl(1)	102.55(5)
N(2)-In(1)-Cl(1)	96.21(5)

Symmetry transformations used to generate equivalent atoms:

Table 3.10. Crystal data and structure refinement for **44**.

Identification code	**44**	
Empirical formula	C35 H52 Br In N2 O2	
Formula weight	727.52	
Temperature	153(2) K	
Wavelength	0.71069 Å	
Crystal system	Monoclinic	
Space group	p21/c	
Unit cell dimensions	a = 17.479(5) Å	α= 90.000(5)º.
	b = 11.691(5) Å	β= 112.703(5)º.
	c = 18.638(5) Å	γ = 90.000(5)º.
Volume	3514(2) $Å^3$	
Z	4	
Density (calculated)	1.375 Mg/m^3	
Absorption coefficient	1.841 mm^{-1}	
F(000)	1504	
Crystal size	0.20 x 0.20 x 0.20 mm^3	
Theta range for data collection	2.11 to 27.57º.	
Index ranges	-22<=h<=20, -12<=k<=15, -23<=l<=24	
Reflections collected	20908	
Independent reflections	7866 [R(int) = 0.0772]	
Completeness to theta = 27.57∞	96.8 %	
Absorption correction	None	
Max. and min. transmission	0.7097 and 0.7097	
Refinement method	Full-matrix least-squares on F^2	
Data / restraints / parameters	7866 / 0 / 379	
Goodness-of-fit on F^2	1.054	
Final R indices [I>2sigma(I)]	R1 = 0.0476, wR2 = 0.0989	
R indices (all data)	R1 = 0.0884, wR2 = 0.1174	
Extinction coefficient	0.0014(2)	
Largest diff. peak and hole	0.887 and -1.070 e.$Å^{-3}$	

Table 3.11. Bond lengths [Å] and angles [°] for **44**.

C(1)-N(1)	1.477(5)
C(3)-N(2)	1.484(5)
C(6)-N(1)	1.300(5)
C(12)-O(1)	1.317(5)
C(21)-N(2)	1.304(5)
C(27)-O(2)	1.330(5)
N(1)-In(1)	2.193(3)
N(2)-In(1)	2.208(3)
O(1)-In(1)	2.064(3)
O(2)-In(1)	2.063(3)
Br(1)-In(1)	2.5337(10)
C(6)-N(1)-C(1)	116.0(4)
C(6)-N(1)-In(1)	123.3(3)
C(1)-N(1)-In(1)	120.3(2)
C(21)-N(2)-C(3)	117.0(3)
C(21)-N(2)-In(1)	122.9(3)
C(3)-N(2)-In(1)	119.4(2)
C(12)-O(1)-In(1)	133.1(3)
C(27)-O(2)-In(1)	131.1(3)
O(2)-In(1)-O(1)	85.82(11)
O(2)-In(1)-N(1)	138.33(12)
O(1)-In(1)-N(1)	86.39(12)
O(2)-In(1)-N(2)	84.71(12)
O(1)-In(1)-N(2)	158.22(12)
N(1)-In(1)-N(2)	87.73(12)
O(2)-In(1)-Br(1)	118.17(8)
O(1)-In(1)-Br(1)	105.52(8)
N(1)-In(1)-Br(1)	103.36(9)
N(2)-In(1)-Br(1)	96.24(9)

Symmetry transformations used to generate equivalent atoms:

Table 3.12. Torsion angles [°] for **44**.

C(7)-C(6)-N(1)-In(1)	0.1(6)
C(2)-C(1)-N(1)-In(1)	55.0(4)
C(22)-C(21)-N(2)-In(1)	6.5(6)
C(2)-C(3)-N(2)-In(1)	-58.3(4)
C(7)-C(12)-O(1)-In(1)	-0.5(6)
C(11)-C(12)-O(1)-In(1)	179.6(3)
C(22)-C(27)-O(2)-In(1)	-22.2(5)
C(26)-C(27)-O(2)-In(1)	160.4(3)
C(27)-O(2)-In(1)-O(1)	-173.8(3)
C(27)-O(2)-In(1)-N(1)	106.4(3)
C(27)-O(2)-In(1)-N(2)	25.8(3)
C(27)-O(2)-In(1)-Br(1)	-68.4(3)
C(12)-O(1)-In(1)-O(2)	-134.4(3)
C(12)-O(1)-In(1)-N(1)	4.6(3)
C(12)-O(1)-In(1)-N(2)	-70.0(5)
C(12)-O(1)-In(1)-Br(1)	107.5(3)
C(6)-N(1)-In(1)-O(2)	75.4(4)
C(1)-N(1)-In(1)-O(2)	-112.1(3)
C(6)-N(1)-In(1)-O(1)	-4.2(3)
C(1)-N(1)-In(1)-O(1)	168.3(3)
C(6)-N(1)-In(1)-N(2)	154.8(3)
C(1)-N(1)-In(1)-N(2)	-32.7(3)
C(6)-N(1)-In(1)-Br(1)	-109.3(3)
C(1)-N(1)-In(1)-Br(1)	63.2(3)
C(21)-N(2)-In(1)-O(2)	-16.9(3)
C(3)-N(2)-In(1)-O(2)	173.4(3)
C(21)-N(2)-In(1)-O(1)	-81.5(4)
C(3)-N(2)-In(1)-O(1)	108.9(4)
C(21)-N(2)-In(1)-N(1)	-155.9(3)
C(3)-N(2)-In(1)-N(1)	34.5(3)
C(21)-N(2)-In(1)-Br(1)	100.9(3)
C(3)-N(2)-In(1)-Br(1)	-68.7(3)

Symmetry transformations used to generate equivalent atoms:

Table 3.13. Crystal data and structure refinement for **47**.

Identification code	**47**	
Empirical formula	C37 H32 Cl5 Ga N2 O2 S4	
Formula weight	911.86	
Temperature	153(2) K	
Wavelength	0.71069 Å	
Crystal system	Triclinic	
Space group	p-1	
Unit cell dimensions	a = 9.418(5) Å	α= 92.035(5)°.
	b = 13.039(5) Å	β= 97.726(5)°.
	c = 17.289(5) Å	γ = 97.726(5)°.
Volume	2081.6(15) $Å^3$	
Z	2	
Density (calculated)	1.455 Mg/m^3	
Absorption coefficient	1.217 mm^{-1}	
F(000)	928	
Crystal size	0.20 x 0.15 x 0.08 mm^3	
Theta range for data collection	1.92 to 27.50°.	
Index ranges	-11<=h<=12, -16<=k<=15, -22<=l<=21	
Reflections collected	12554	
Independent reflections	8199 [R(int) = 0.0288]	
Completeness to theta = 27.50∞	85.7 %	
Absorption correction	Semi-empirical from equivalents	
Max. and min. transmission	0.907 and 0.803	
Refinement method	Full-matrix least-squares on F^2	
Data / restraints / parameters	8199 / 0 / 469	
Goodness-of-fit on F^2	1.020	
Final R indices [I>2sigma(I)]	R1 = 0.0480, wR2 = 0.1145	
R indices (all data)	R1 = 0.0762, wR2 = 0.1326	
Largest diff. peak and hole	0.649 and -0.818 $e.Å^{-3}$	

Table 3.14. Bond lengths [Å] and angles [°] for **47**.

C(2)-N(1)	1.443(4)
C(3)-N(2)	1.387(4)
C(6)-N(1)	1.281(4)
C(8)-O(1)	1.331(4)
C(13)-N(2)	1.323(5)
C(15)-O(2)	1.323(4)
C(20)-S(2)	1.715(4)
C(23)-S(2)	1.735(4)
C(24)-S(1)	1.736(4)
C(27)-S(1)	1.676(5)
C(28)-S(3)	1.656(3)
C(31)-S(3)	1.733(4)
C(32)-S(4A)	1.613(4)
C(32)-S(4B)	1.669(6)
C(34)-S(4B)	1.484(10)
C(35)-S(4A)	1.578(8)
N(1)-Ga(1)	2.031(3)
N(2)-Ga(1)	1.994(3)
O(1)-Ga(1)	1.841(2)
O(2)-Ga(1)	1.937(2)
Cl(1)-Ga(1)	2.4436(13)
C(6)-N(1)-C(2)	119.7(3)
C(6)-N(1)-Ga(1)	126.3(2)
C(2)-N(1)-Ga(1)	114.1(2)
C(13)-N(2)-C(3)	117.5(3)
C(13)-N(2)-Ga(1)	127.4(2)
C(3)-N(2)-Ga(1)	115.0(3)
C(8)-O(1)-Ga(1)	130.7(2)
C(15)-O(2)-Ga(1)	126.7(2)
O(1)-Ga(1)-O(2)	87.65(10)
O(1)-Ga(1)-N(2)	124.27(12)
O(2)-Ga(1)-N(2)	80.41(10)
O(1)-Ga(1)-N(1)	90.64(11)

O(2)-Ga(1)-N(1)	170.40(11)
N(2)-Ga(1)-N(1)	92.80(11)
O(1)-Ga(1)-Cl(1)	118.78(9)
O(2)-Ga(1)-Cl(1)	104.35(8)
N(2)-Ga(1)-Cl(1)	116.92(9)
N(1)-Ga(1)-Cl(1)	84.74(9)

Symmetry transformations used to generate equivalent atoms:

Table 3.15. Torsion angles [°] for **47**.

C(8)-O(1)-Ga(1)-O(2)	171.3(3)
C(8)-O(1)-Ga(1)-N(2)	94.6(3)
C(8)-O(1)-Ga(1)-N(1)	0.8(3)
C(8)-O(1)-Ga(1)-Cl(1)	-83.6(3)
C(15)-O(2)-Ga(1)-O(1)	-169.3(3)
C(15)-O(2)-Ga(1)-N(2)	-44.0(3)
C(15)-O(2)-Ga(1)-Cl(1)	71.5(3)
C(13)-N(2)-Ga(1)-O(1)	110.6(3)
C(3)-N(2)-Ga(1)-O(1)	-72.5(3)
C(13)-N(2)-Ga(1)-O(2)	30.2(3)
C(3)-N(2)-Ga(1)-O(2)	-153.0(3)
C(13)-N(2)-Ga(1)-N(1)	-156.7(3)
C(3)-N(2)-Ga(1)-N(1)	20.1(2)
C(13)-N(2)-Ga(1)-Cl(1)	-71.2(3)
C(3)-N(2)-Ga(1)-Cl(1)	105.7(2)
C(6)-N(1)-Ga(1)-O(1)	-1.4(3)
C(2)-N(1)-Ga(1)-O(1)	179.4(3)
C(6)-N(1)-Ga(1)-N(2)	-125.8(3)
C(2)-N(1)-Ga(1)-N(2)	55.1(3)
C(6)-N(1)-Ga(1)-Cl(1)	117.4(3)
C(2)-N(1)-Ga(1)-Cl(1)	-61.7(2)

Symmetry transformations used to generate equivalent atoms:

Table 3.16. Crystal data and structure refinement for **55**.

Identification code	**55**	
Empirical formula	C73 H113 In2 N4 O4 P Si	
Formula weight	1399.37	
Temperature	153(2) K	
Wavelength	0.71069 Å	
Crystal system	triclinic	
Space group	p-1	
Unit cell dimensions	a = 16.312(5) Å	α= 110.272(5)°.
	b = 17.743(5) Å	β= 99.924(5)°.
	c = 19.652(5) Å	γ = 109.571(5)°.
Volume	4752(2) $Å^3$	
Z	2	
Density (calculated)	0.978 Mg/m^3	
Absorption coefficient	0.551 mm^{-1}	
F(000)	1476	
Crystal size	0.20 x 0.20 x 0.20 mm^3	
Theta range for data collection	1.40 to 27.58°.	
Index ranges	-21<=h<=21, -23<=k<=22, -20<=l<=25	
Reflections collected	31487	
Independent reflections	21357 [R(int) = 0.0296]	
Completeness to theta = 27.58°	97.0 %	
Absorption correction	None	
Max. and min. transmission	0.8977 and 0.8977	
Refinement method	Full-matrix least-squares on F^2	
Data / restraints / parameters	21357 / 0 / 806	
Goodness-of-fit on F^2	1.087	
Final R indices [I>2sigma(I)]	R1 = 0.0661, wR2 = 0.1993	
R indices (all data)	R1 = 0.0976, wR2 = 0.2194	
Extinction coefficient	0.0089(6)	
Largest diff. peak and hole	2.608 and -0.938 $e.Å^{-3}$	

Table 3.17. Bond lengths [Å] and angles [°] for **55**.

C(1)-N(1)	1.465(6)
C(3)-N(2)	1.472(6)
C(6)-N(1)	1.289(6)
C(12)-O(1)	1.320(6)
C(21)-N(2)	1.287(6)
C(27)-O(2)	1.323(6)
C(36)-Si(1)	1.873(7)
C(37)-Si(1)	1.862(7)
C(38)-Si(1)	1.871(6)
C(39)-N(3)	1.469(6)
C(41)-N(4)	1.463(6)
C(43)-N(3)	1.293(6)
C(50)-O(3)	1.294(6)
C(59)-N(4)	1.288(6)
C(65)-O(4)	1.321(6)
N(1)-In(1)	2.269(4)
N(2)-In(1)	2.238(4)
N(3)-In(2)	2.247(4)
N(4)-In(2)	2.305(4)
Si(1)-P(1)	2.225(2)
P(1)-In(1)	2.4720(14)
P(1)-In(2)	2.4863(13)
In(1)-O(1)	2.104(3)
In(1)-O(2)	2.131(3)
In(2)-O(4)	2.102(3)
In(2)-O(3)	2.123(3)
Si(1)-P(1)-In(1)	105.49(7)
Si(1)-P(1)-In(2)	110.58(7)
In(1)-P(1)-In(2)	104.23(5)
O(1)-In(1)-O(2)	88.01(14)
O(1)-In(1)-N(2)	112.97(14)
O(2)-In(1)-N(2)	81.78(13)
O(1)-In(1)-N(1)	82.17(14)

O(2)-In(1)-N(1)	153.11(13)
N(2)-In(1)-N(1)	79.19(14)
O(1)-In(1)-P(1)	135.91(10)
O(2)-In(1)-P(1)	107.58(10)
N(2)-In(1)-P(1)	110.00(11)
N(1)-In(1)-P(1)	96.73(11)
O(4)-In(2)-O(3)	83.32(13)
O(4)-In(2)-N(3)	127.63(14)
O(3)-In(2)-N(3)	83.17(14)
O(4)-In(2)-N(4)	81.02(14)
O(3)-In(2)-N(4)	147.32(14)
N(3)-In(2)-N(4)	84.00(15)
O(4)-In(2)-P(1)	112.06(10)
O(3)-In(2)-P(1)	100.66(10)
N(3)-In(2)-P(1)	120.11(10)
N(4)-In(2)-P(1)	111.77(11)

Symmetry transformations used to generate equivalent atoms:

CHAPTER 4: Loose Ends and Future Directions

Transition Metal Chemistry

Chromium and Molybdenum Metal Complexes

In the course of attempts to access new boron-transition metal complexes with boron-metal multiple bonds, it was necessary to synthesize $(Me_3N)M(CO)_5$ [M = Cr (**56**); Mo (**57**)] since these complexes are useful sources of the corresponding anions $[M(CO)_5]^{2-}$. Although **56** and **57** are well known compounds [1], no X-ray crystallographic data were available in the literature. Both compounds crystallize in the monoclinic space group $P2_1/n$ with $Z = 4$. There are no unusually short contacts. As expected, the molecular structures are essentially octahedral (Figure 4.1) but slight deviations from idealized 90° angles are evident in both structures (Table 4.1) due to the steric demands of the Me_3N ligand. Since amines are good σ-donors and poor π-acceptors, the metal-CO distance *trans* to the amine ligand is shorter than the other metal-CO bond distances in both complexes (Table 4.1). The chromium-nitrogen and molybdenum-nitrogen bond distances are comparable to those of a number of related $(amine)M(CO)_5$ (M = Cr, Mo) complexes. For example, the Mo-N bond distance of 2.377(3) Å is comparable to those found previously $(N(CH_2)_6N)Mo(CO)_5$ (2.367(3) Å) [2] and $((CH_2)_6N_4)Mo(CO)_5$) (2.337(3) Å) [3]. There are more reported examples of chromium pentacarbonyl complexes with coordinated amine ligands in comparison with their molybdenum analogues. The Cr-N bond distance of 2.2472(17) Å, compares well with those reported for similar complexes, e.g. 2.236(5) Å for $Cr(CO)_5(C_5H_3(NH_2)_2)$ [4],

2.222(7) Å for $Cr(CO)_5(C_9H_{10}NH)$ [5], 2.195(4) Å for $Cr(CO)_5(NHMe_2)$ [6], 2.249(5) Å for quinuclide-$Cr(CO)_5$ [7], 2.197(4) Å for morpholine-$Cr(CO)_5$ [8] and 2.204(3) Å for $Cr(CO)_5(NHC_5H_{10})$ [9].

Compounds **56** and **57** were synthesized by published methods [1] by the reaction of $M(CO)_6$ with NMe_3 at elevated temperatures. Both compounds were isolated as needle-like yellow crystals from pentane solutions cooled to -40˚C.

Table 4.1. Crystal data and structure refinement for **56** and **57**.

	56	**57**
Formula	$C_8H_9CrNO_5$	$C_8H_9MoNO_5$
Formula weight	251.16	295.10
Crystal system	Monoclinic	Monoclinic
Space group	*P*2(1)/*n*	*P*2(1)/*n*
a/Å	6.8267(14)	6.9494(14)
b/Å	11.269(2)	11.362(2)
c/Å	14.692(3)	14.927(3)
α/°	90	90
β/°	102.89(3)	102.64(3)
γ/°	90	90
V/Å^3	1101.8(4)	1150.0(4)
Z	4	4
P_{calcd}/g cm^{-3}	1.514	1.704
F(000)	512	584
Crystal size/mm	0.25 x 0.15 x 0.15	0.25 x 0.15 x 0.10
θ range/°	2.30 to 25.00	2.27 to 27.53
No. of reflns. Collected	3406	7307
No. of indep reflns.	1932	2653
R1[$I > 2\sigma(I)$]	0.0283	0.0309
*w*R$_2$ (all data)	0.0681	0.0758
Peak and hole/e.Å^{-3}	0.306 and -0.223	1.380 and -0.905

Table 4.2. Selected bond lengths (Å) and angles (˚) for **56** and **57**.		
	56	**57**
N(1)-M(1)	2.2472(17)	2.379(3)
M(1)-C(1)	1.830(2)	1.960(4)
M(1)-C(2)	1.904(2)	2.058(4)
M(1)-C(3)	1.909(2)	2.057(4)
M(1)-C(4)	1.910(2)	2.050(4)
M(1)-C(5)	1.908(2)	2.056(4)
N(1)-M(1)-C(1)	178.16(7)	178.86(12)
N(1)-M(1)-C(2)	91.27(8)	93.97(13)
N(1)-M(1)-C(3)	92.34(8)	93.02(12)
N(1)-M(1)-C(4)	94.14(8)	91.62(12)
N(1)-M(1)-C(5)	93.79(8)	92.69(13)

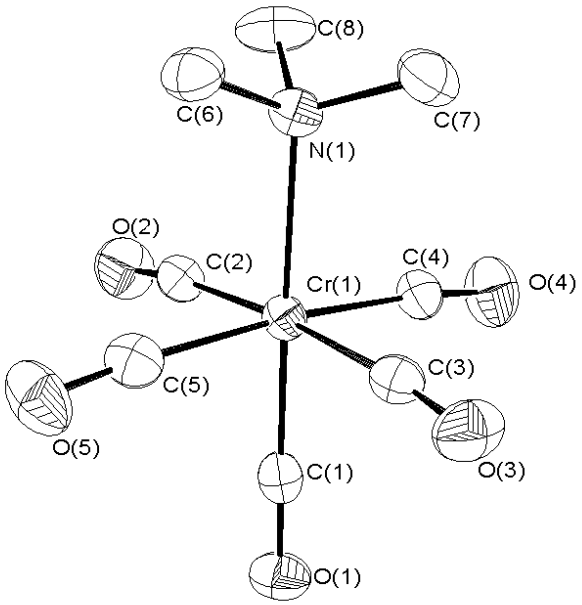

Figure 4.1. ORTEP diagram of **56** with thermal ellipsoids shown at the 40% probability and H-atoms omitted for clarity.

Attempted Synthesis of a Terminal Stibinidene

The recent report of a catalytic dehydrocoupling process, in which a low-valent main group antimony compound plays a key role, has highlighted the importance of this fundamental area of research [10]. The literature contains no report of a terminal stibinidene [11], whereas the lighter congeneric phosphinidene [12] and arsinidene [12] complexes are well known. The success of halide ion abstraction chemistry for the syntheses of the corresponding terminal borylene complexes [13] prompted an investigation of the potential use of this methodology for the preparation of the cationic terminal stibinidene, $[(\eta^5\text{-}C_5H_5)(CO)_2\text{-}FeSb(\eta^5\text{-}C_5Me_5)][AlCl_4]$. As shown in Scheme 4.1, the proposed synthetic route to the multiply-bonded target compound features the abstraction of a chloride anion from the precursor chlorostibine complex, **58**.

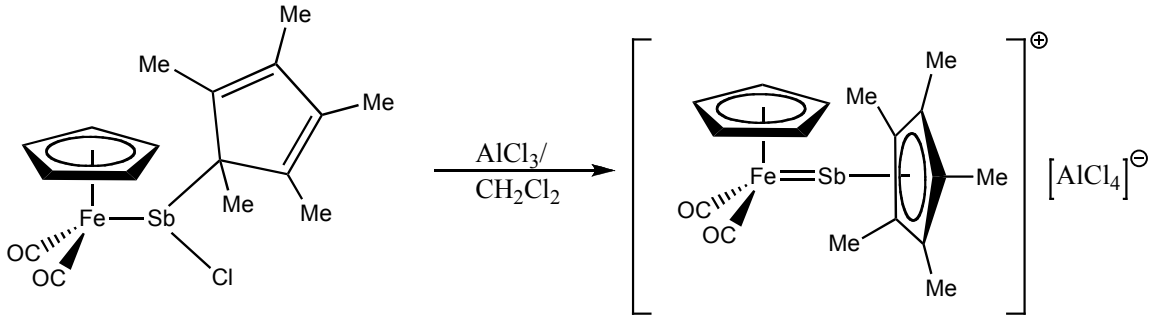

58 **59**

Scheme 4.1. Proposed synthetic route to a terminal stibinidene complex, **59**.

A bright yellow diethyl ether solution of pentamethylcyclopentadienyl antimony dichloride [14] was added to an equimolar quantity of $[(\eta^5\text{-}C_5H_5)Fe(CO)_2]K$ at 0˚C and the reaction mixture was stirred overnight at 25˚C. Removal of the solvent resulted in a brown residue which was extracted with toluene and filtered to remove

the remaining insolubles. After solvent stripping, an orange material was isolated and recrystallized from toluene solution. However, a single crystal X-ray diffraction study revealed that the product is in fact $[\{(\eta^5\text{-}C_5H_5)Fe(CO)_2\}_3SbCl][FeCl_4]$ (**60**) rather than **58**. The fact that **60** also exists in the solution phase was confirmed on the basis of ^1H and $^{13}C\{^1H\}$ NMR data. The tris-iron stibonium salt **60** has been synthesized previously by treatment of three equivalents of $[(\eta^5\text{-}C_5H_5)Fe(CO)_2]Na$ with one equivalent of $SbCl_3$ [15]. Given the foregoing, further efforts to synthesize the targeted stibinidene complex were made by avoiding the isolation of the intermediate halostibyl complex **58**.

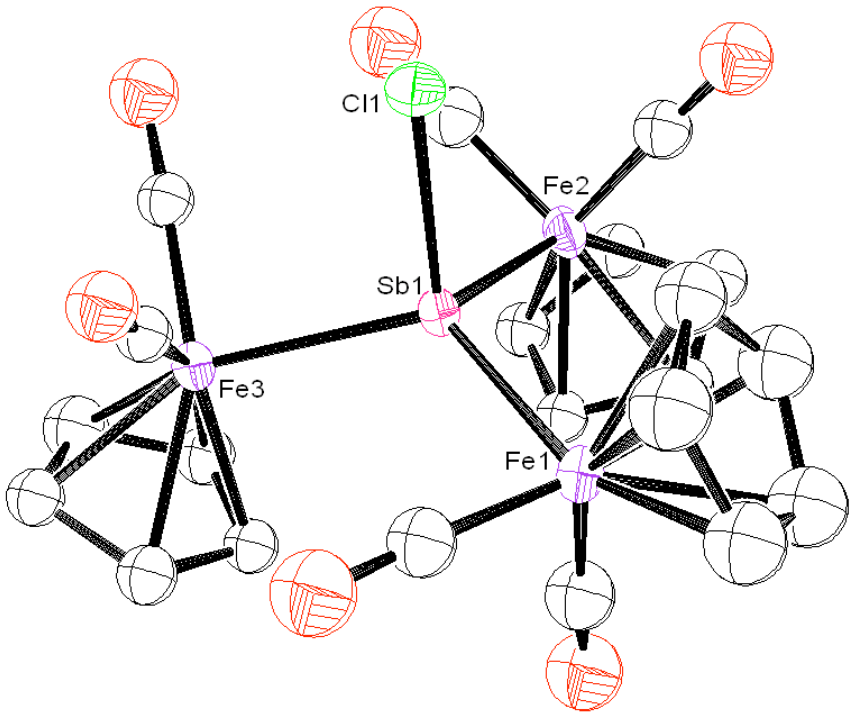

Figure 4.2. Molecular structure of **60** with thermal ellipsoids shown at the 40% probability level. The $[FeCl_4]^-$ anion has been omitted for clarity.

When cold (0°C) solutions of pentamethylcyclopentadienyl antimony dichloride and $[(\eta^5\text{-}C_5H_5)Fe(CO)_2]K$ were allowed to react with an equimolar amount of $AlCl_3$ in CH_2Cl_2 solution at 25˚C a gradual darkening of the solution was observed. A sharp ^{27}Al NMR peak at ~103 ppm diagnostic of the formation of $[AlCl_4]^-$ was detected, thus suggesting that the halide abstraction shown in Scheme 4.1 had taken place. Following solvent removal, recrystallization of the residue from toluene solution resulted in a crop of crystals suitable for examination by single-crystal X-Ray diffraction. The X-ray analysis revealed that the product is the $[AlCl_4]^-$ salt of the bis(cyclopentadienyldicarbonyliron)dichloro stibonium cation **61**. This cation has been reported previously [16] by insertion of $SbCl_3$ into the Fe-Fe bond of the $[(\eta^5\text{-}C_5H_5)Fe(CO)_2]_2$ dimer followed by elimination of Cl^-. A search of the Cambridge Structural Database revealed that **61** is the only crystallographically characterized example of an antimony atom serving as a bridge between two $[(\eta^5\text{-}C_5H_5)Fe(CO)_2]$ units.

The observation that **60** and **61** are formed in preference to the desired products **58** and **59** is indicative of the tendency of pentamethylcyclopentadienyl antimony dichloride to dissociate back to $SbCl_3$ in solution, thus allowing formation of side-products **60** and **61**. Future synthetic efforts should therefore focus on more kinetically and thermodynamically stable $RSbX_2$ derivatives with an emphasis on low-temperature reaction techniques.

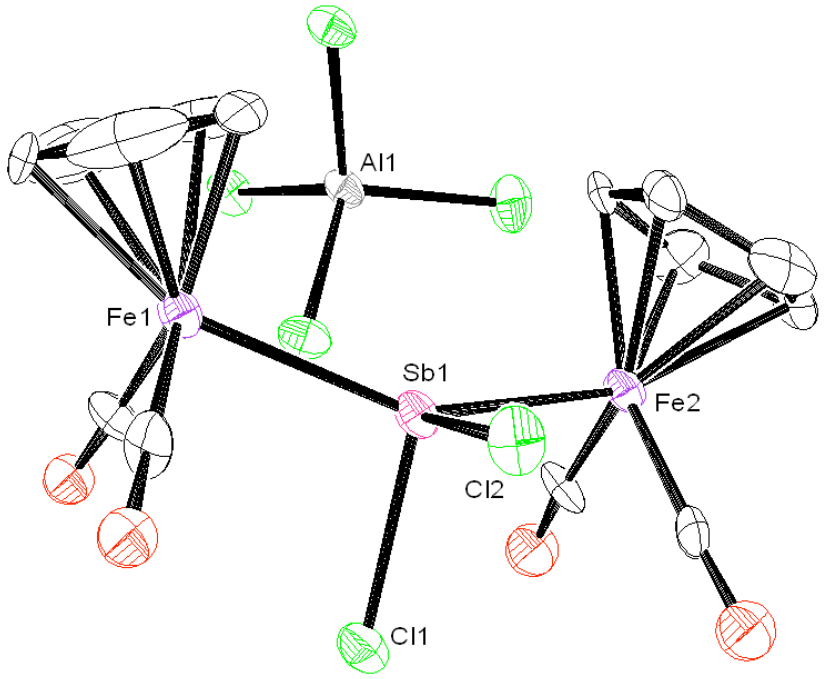

Figure 4.3. Molecular structure of **61** with thermal ellipsoids shown at the 40% probability level.

Group 14 Heterocycles

Silylenes and Germylenes

Two classes of transition metal complexes with a formal metal-carbon double bond are known, both named for those who first synthesized them. Fischer-type carbene complexes [16] which possess a donor-acceptor bond between a low-valent metal fragment L_nM and a carbene ligand CR_1R_2 where one of the ligands R is a π-donor. Conversely, Schrock-type carbene complexes [16] are typically comprised of high oxidation state metals and alkyl-substituted carbenes. The last ten years however has seen the development of a new class of carbene ligand, namely the N-heterocyclic carbene (NHC) [17]. These ligands are formally neutral, two-electron donors with

properties that are very similar to those of tertiary phosphines. Unlike Fischer and Schrock carbenes, the NHCs are best described as effectively pure σ-donors, with only minimal metal-to-ligand back donation.

The first stable carbenes were isolated by Arduengo in 1991 by deprotonation of the corresponding imidazolium salts [17]. The heavier congeneric N-heterocyclic silylenes and germylenes **62** and **63**, first reported in the early 1990s, are thermally stable analogues of the NHCs [18]. The key to the isolation of these highly reactive compounds was the use of a combination of stereo-electronic factors, namely the placement of sterically demanding substituents on the nitrogen atoms and the presence of significant π-delocalization within the five-membered heterocycle.

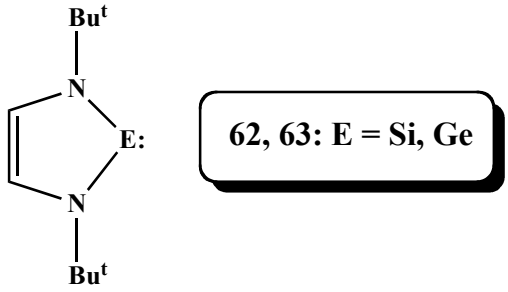

The successful syntheses of **62-63** represent milestones in synthetic main group chemistry; however, the vast majority of subsequent research work has focused mainly on their reactions with simple organic and inorganic compounds. Since **62-63** resemble NHCs in both an electronic and structural sense, they might be expected to display similar patterns of reactivity. However, factors such as ionic radius, electronegativity, and the nature of the frontier molecular orbitals exert a strong influence on the outcomes of reactions, hence major differences between the chemistry of **62-63** and NHCs are anticipated. Furthermore, the readily tunable steric

and electronic properties of **62-63** suggest that their ligation to organometallic fragments and the subsequent reactions of such complexes will differ substantially from those of the isolobal and well-studied Cp*E compounds [19].

Both **62** and **63** are thermally stable, isolable molecules, and thus their metal complexes should be accessible *via* standard synthetic organometallic techniques. Preliminary studies focused upon exploring the reactivity have focused on their reactivity toward both organometallic and main group fragments [20]. Specifically, attempts were made to synthesize both the silylene and germylene analogues of the Grubbs 2nd generation catalyst, to prepare boron polycations by heterolysis of halide atoms from BX_3 precursors using the Lewis basic properties of these heterocycles and to use silylene **62** as a single-source precursor for the formation of silicon films *via* Atomic Layer Epitaxy (ALE).

Attempts to prepare the group 14 ligated ruthenium species shown in Figure 4.4 involved a minor modification of a published procedure, namely displacement of a phosphine ligand from the corresponding 1st generation catalyst [21]. One equivalent of the group 14 carbenoid was added to a toluene solution of the Grubbs 1st generation catalyst at ambient temperature. After the reaction mixture had been stirred overnight, aliquots were taken for analysis by NMR. These assays indicated the desired reaction had not taken place. After stirring the reaction mixture for a further twelve hours under reflux conditions, NMR data suggested that reaction had still not taken place. It seemed clear that this simple displacement approach would not be appropriate to access the heavier analogues of the Grubbs 2nd generation catalyst. Interestingly, recent theoretical studies indicate that the basicity of the carbenoids decreases upon descending the group 14 [22].

This is due, in part, to the increasing aromatic character of the heterocycles in the order Ge > Si > C. Thus, the basicities of the silylene and germylene heterocycles are not sufficiently high to displace a phosphine ligand from this ruthenium complex.

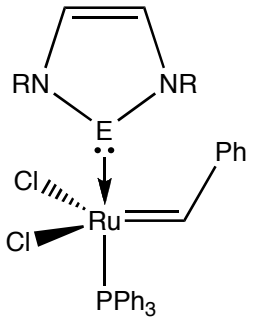

E = Si / Ge; R = t-Bu

Figure 4.4. Ruthenium carbenoid complexes.

The intrinsic electron-deficiency of tricoordinate boron compounds has led to their use as potent Lewis Acids in a diverse range of research areas, ranging from fluoride anion sensors [23] to co-catalysts in olefin polymerization [24]. In general, inducing a cationic charge at the boron center is expected to generate a more potent acceptor than the corresponding neutral species, thus heralding a superior class of reagents and catalysts with greatly enhanced activities. Recently, in an effort to extend the reactivity of boron cations reports on the synthesis and structure of a new class of 'borocation', namely a boron dication have been disclosed [25]. The use of nitrogen-based donors is prevalent in almost all facets of boron chemistry due to the large boron-nitrogen bond enthalpy, a result of efficient overlap of the nitrogen lone pair with the formally vacant boron-based p_z orbital.

The reaction of four equivalents of **63** with one equivalent of BI_3 in toluene solution at ambient temperature afforded, after solvent stripping, a yellowish brown residue. Analysis by NMR spectroscopy revealed a sharp singlet in the ^{11}B spectrum at δ = 5.86 ppm which falls in the range anticipated for a fully saturated, four-coordinate, boron center. Moreover, both the ^{1}H and ^{13}C NMR spectra confirm the presence of only one set of resonances corresponding to germylene **63**. Unfortunately, at this time, no further data are available to confirm the solid-state molecular structure as the (tetragermylene)boron tribromide salt.

In collaboration with the research group of Professor Brian Korgel, the silylene **62** was also examined as a potential precursor for Atomic Layer Epitaxy (ALE) in which a well-defined silicon surface may be deposited onto a substrate. Silicon remains one of the most important materials in modern transistor technology. Silicon films have found applications in microelectronics and photovoltaic cells and as a result, much research has focused on methods involved in producing high quality silicon films on a variety of substrates. An early report by Steigerwald [26] utilized the so-called 'butterfly' compound, **64**, shown in Figure 4.5 (a) in an effort to prepare silicon films. The deposition is proposed to proceed through a transient silylene, generated by elimination of one molecule of butadiene, thus generating a monolayer which subsequently loses a second butadiene molecule to generate the desired silicon film (Figure 4.5 (b)). Clearly, this process could be probed more fully and perhaps prove to be better controlled by utilizing the thermally and kinetically stable silylene **62** in preference to generating an *in-situ* divalent species. Samples of **62** were prepared for this purpose and subjected to the growth conditions typically used in the Korgel laboratory. Unfortunately, subsequent

removal of the butadiene molecules proved incomplete, possibly due to the large nitrogen-silicon bond enthalpy. Current efforts are focused on modification and optimization of this ALE process.

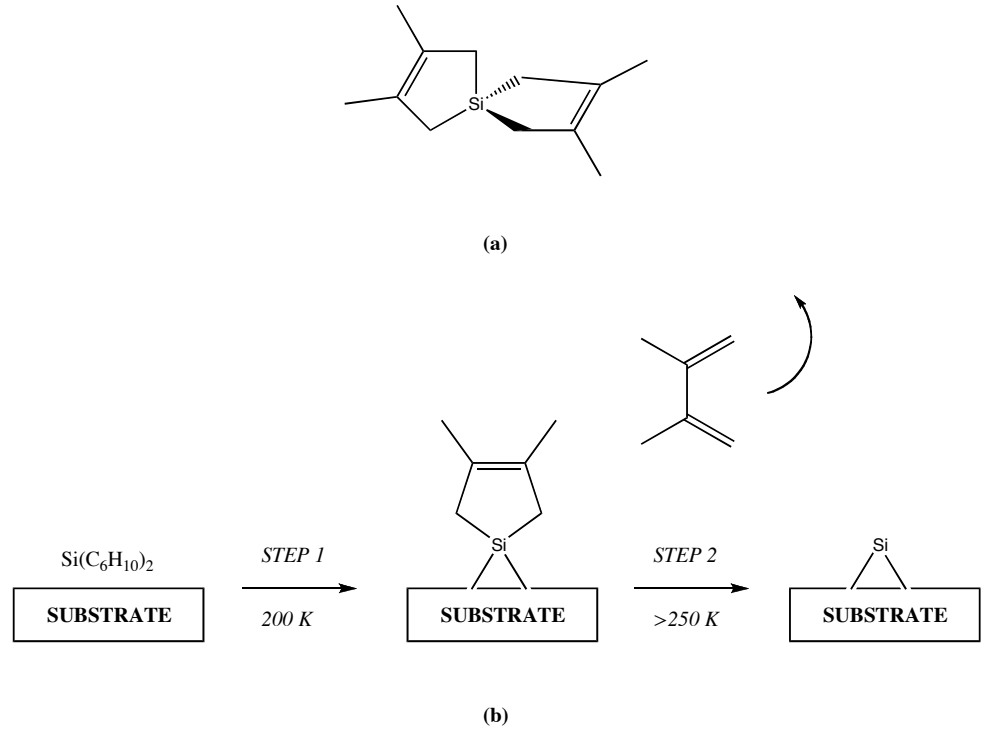

Figure 4.5. (a) 'Butterfly' molecule, **64**. (b) Pictorial representation of ALE deposition process of **64** onto a substrate.

Group 14 Metalloles

The group 14 metallole dianions have generated considerable interest from both the synthetic and theoretical communities as heavier congeners of the cyclopentadienyl anion [27]. The structure of silole and germole dianions has been discussed extensively, and their aromatic character is well established [28, 29]. The reactions of these dianions, however, have been mostly limited to those with simple electrophiles [28, 30], which

were typically used as trapping reagents. There are, however, a few reports of unique reactions by West *et al*. [31] as well as coupling reactions to form oligo-or poly(1,1-metallole)s [32].

The silole dianion, **65**, is conveniently prepared *via* lithium metal reduction of the precursor silicon dichloride or chlorophenylsilane as shown in Scheme 4.2 [33]. Some reactions of this dianion with a variety of boron dihalides were explored in an effort to prepare novel compounds with silicon-boron multiple bonds. Unfortunately, no evidence was found for the desired silicon-boron derivatives. As noted above, the reactivity of patterns of silole dianions have yet to be fully explored and, despite these initial failures, it is anticipated that this will ultimately prove to a fertile field of research.

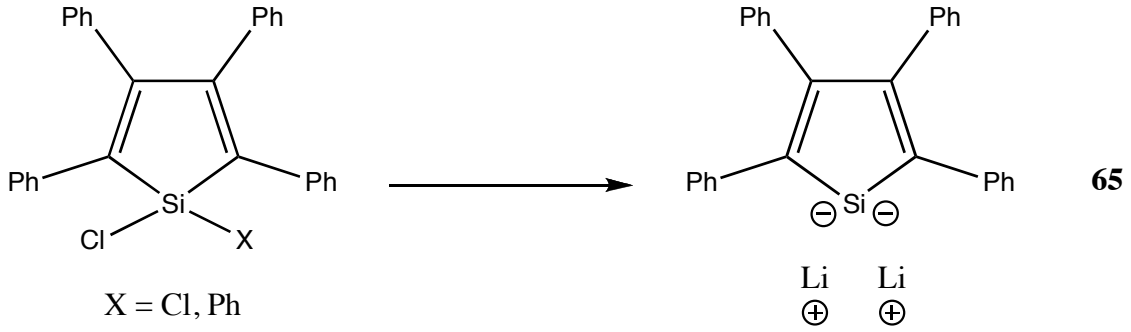

Scheme 4.2. Synthesis of the silole dianion, **65**.

Thiophene Containing Diazabutadienes and Bis(imino)arylacenapthenes

Over the last several decades, the field of conducting polymers has blossomed into a mature and well-understood research area [34]. Since the vast majority of work in this area has focused on all-organic systems, the electron/hole transport in these systems is reasonably well understood. More recently, systems that incorporate transition metals have presented the possibility of greatly expanding the scope and ultimately the applications for such conducting polymers. Early work has focused primarily on the attachment of transition metal fragments to polymer main-chain backbones. However, a more effective, though much less explored, approach would be the incorporation of metal complexes into the polymer backbone directly [35]. Two ligand classes are particularly attractive for the support of polymers of this type. The diazabutadiene (DAB) ligand class has been used extensively in d- and p-block chemistry by virtue of its diversity of coordination modes and interesting redox properties. Interest in the 1,2-bis(arylimino)acenaphthene (aryl-BIAN) ligand class stems from the ability of such ligands to function as both electron and proton sponges. In turn, this desirable combination of properties is attributable to the presence of both a naphthalene ring and a 1,4-diaza-1,3-butadiene moiety. The d-block chemistry of aryl-BIAN ligands is now well established and many transition complexes have been employed as catalysts [36]. Given the foregoing, attempts were made to attach bithiophene groups to both DAB and BIAN ligands in order to generate electropolymerizable monomers with readily available metal coordination sites.

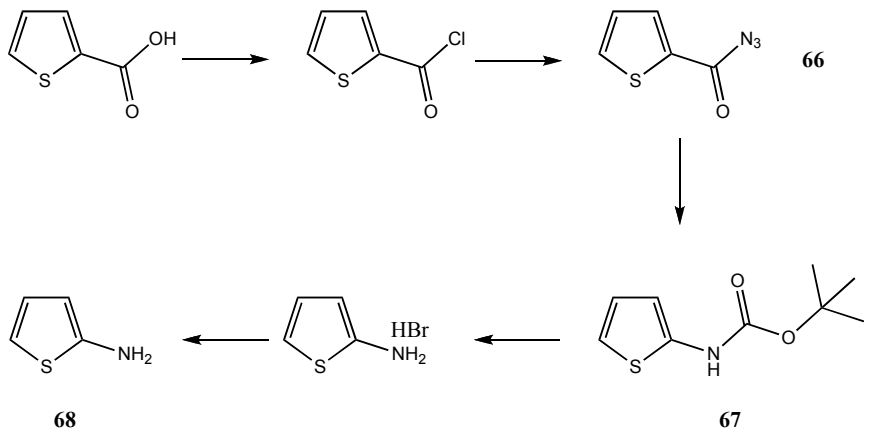

Scheme 4.3. Synthetic pathway to 2-aminothiophene, **68.**

The synthesis of DAB ligands is typically accomplished by means of a simple condensation reaction between an amine and a diketone. However, this approach would necessitate the preparation of the highly reactive 2-aminothiophene, **68**, according to the series of steps outlined in Scheme 4.3. The initial conversion to the acid chloride proceeded smoothly by treatment of thionyl chloride with the thiophene carboxylic acid starting material. In turn, treatment of this acid chloride with sodium azide at ambient temperature afforded the 2-(azidocarbonyl)thiophene (**66**) in moderate to good yields (60-85%) after recrystallization. Crystals of **66** suitable for analysis by single-crystal X-ray diffraction techniques were grown from toluene solution and the molecular structure of this compound is shown in Figure 4.6. The amine-protected carbamate, **67**, was prepared by refluxing a toluene solution of **66** and *tert*-butyl alcohol over a period of 3h. After cooling of the reaction mixture to room temperature, aqueous-organic work-up afforded **67** as an off-white solid. Storage of a concentrated toluene solution of **67** at -40°C overnight resulted in a crop of crystals which were suitable for study by X-ray crystallography (Figure 4.7).

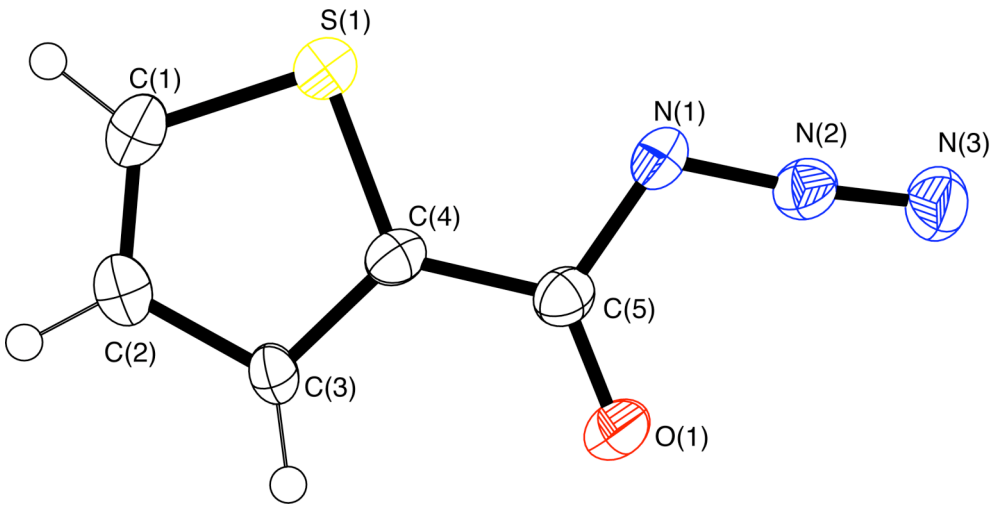

Figure 4.6. Molecular structure of **66** with thermal ellipsoids shown at the 40% probability level.

The hydrobromide salt of **68** was prepared by deprotection of **67** using a 33% HBr solution in acetic acid. This salt was converted, in low yield, to **68** by bubbling ammonia through a slurry of the HBr salt in methylene chloride at low temperature (0°C). Isolation of the yellow oil, **68**, proved difficult due to the extreme air and moisture sensitivity of this product. Furthermore, **68** undergoes facile ring opening to afford more thermodynamically stable acetonitrile derivatives. Repeated efforts to prepare **68** in higher overall yield failed. Accordingly, it was decided to adopt an alternative target monomer, namely one that features a phenyl-spacer between the amino group and the thiophene ring (**69**).

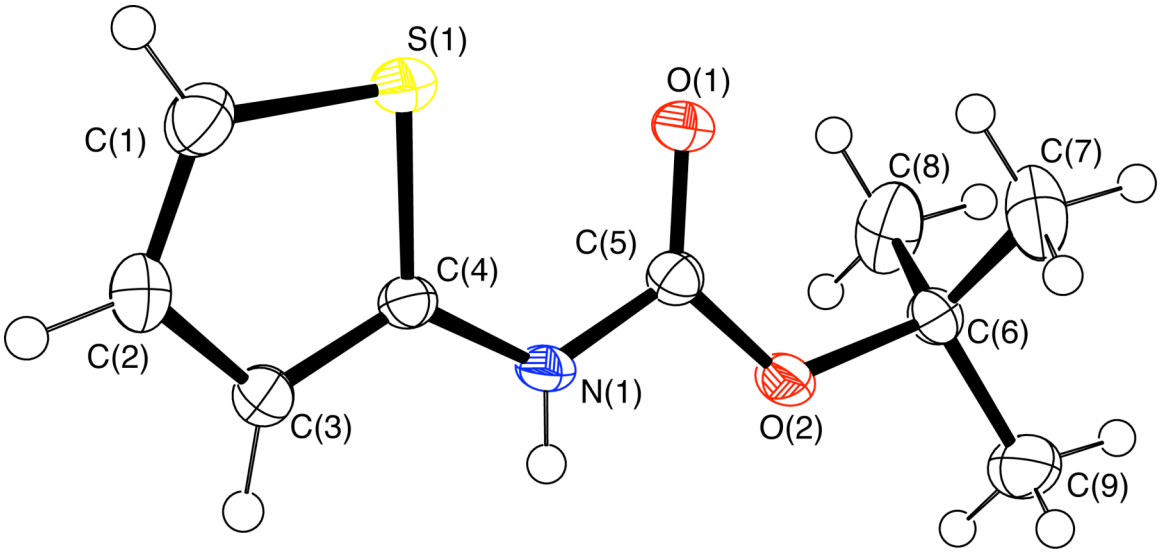

Figure 4.7. Molecular structure of **67** with thermal ellipsoids shown at the 40% probability level.

In stark contrast to the somewhat unreliable synthesis of 2-aminothiophene (**68**), the preparation of the 4-(2-thienyl)benzen-amine (TBA) (**69**) precursor proceeds in good yield from the Suzuki coupling of commercially available 2-thienylboronic acid with 4-bromoaniline. Condensation of two equivalents of **69** with glyoxal (Scheme 4.4) in ethanol solution afforded the anticipated diazabutadiene ligand **70** in virtually quantitative yields. Ligand **70** is sparingly soluble in a variety of organic solvents. Subsequent studies carried out by Clint Hoberg have focused on alkyl subtitution of the phenyl-ring with a view to increasing the solubility of this ligand class and to providing enhanced steric protection of subsequently coordinated metal-containing functionalities.

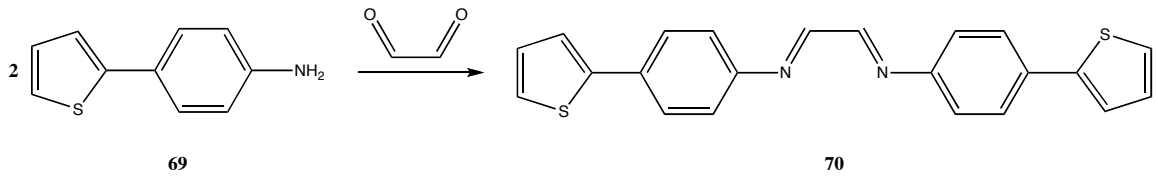

69 70

Scheme 4.4. Synthesis of the thienyl-substituted DAB ligand, **70**.

The reaction of **70** and its alkylated analogues with BI_3 represents an attractive target because if such reactions proceed *via* two-electron reduction of the ligand this could be an important step in the production of polyboroles, a fascinating class of polymer due to their anticipated small band gap.

Turning to the more rigid BIAN ligand class, the synthesis of the bithiophene functionalized ligand **71** proceeds in good yield by palladium-catalyzed Stille coupling of the readily available precursors 2-tributyltin-5,5'-bithiophene and 4-bromophenylBIAN. Red, plate-like crystals of **71** suitable for single-crystal X-ray diffraction experiments were grown from hexane solution. The molecular structure of the new ligand is shown in Figure 4.8. Recent reports by the Cowley group [37] have demonstrated the important role that BIAN-based ligands can play in the support of redox-active lanthanide moieties and the construction of molecular wires. Accordingly, efforts were made to synthesize lanthanide complexes by treatment of **71** with a variety of lanthanocenes. Unfortunately, these reactions have not been successful thus far.

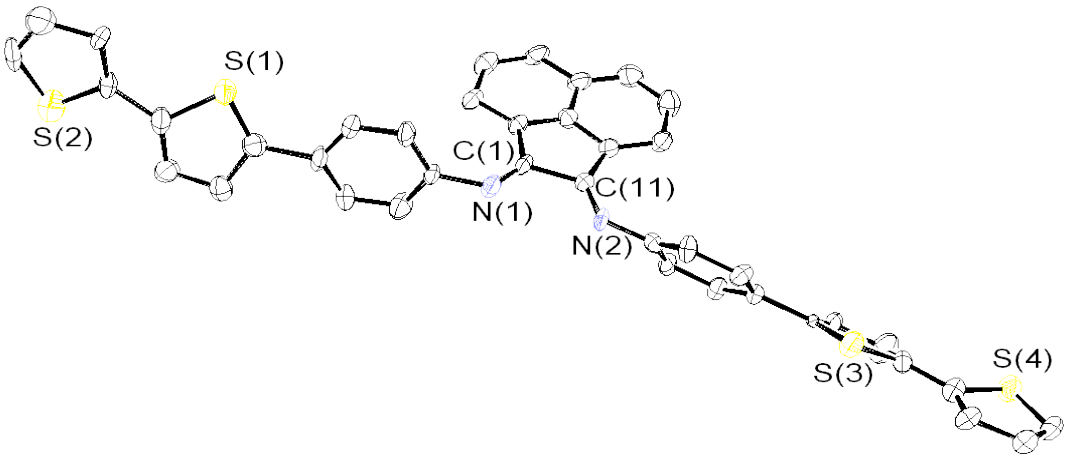

Figure 4.8. Molecular structure of **71** with thermal ellipsoids shown at the 40% probability level.

Further studies of the reactivity patterns of **71** are currently being conducted by Adam Powell. By analogy with the DAB ligand systems described earlier the initial strategy has been to synthesize sterically encumbered derivatives of **71**. These precursors are of significant potential interest for the synthesis of metallopolymers with fascinating opto-electronic properties. Moreover, the DAB skeleton (also present in the BIAN ligand class) is identical to that found within NHCs and, as such, these molecules have the intriguing possibility of providing access to polycarbenes.

Conclusions

In the literature method for the preparation of the 1st generation Grubbs catalyst [38], use is made of the readily available triphenylphosphine ruthenium complex, which is somewhat unstable and contains a labile P→Ru bond. Tricyclohexylphosphine readily

displaces the coordinated triphenylphosphine to form a more stable catalyst. The proposed silylene and germylene analogues of Grubbs-type complexes could be of interest as higher activity metathesis catalysts and are worth exploring.

The initial result of the germylene-promoted, boron-iodine bond heterolysis are both exciting and promising. Future work should focus on unequivocal identification of the germanium-boron cation that is produced and an investigation of the charge distribution in this species. Recent theoretical studies [39] have revealed a substantial charge-quenching effect which serves to lower the overall cationic charge at the boron center. Moreover, further efforts are required to develop non-coordinatively saturated systems which will be capable of more fully realizing the potential of these polycationic boron complexes for affecting important organic transformations and serving as olefin polymerization catalysts.

Finally, the development of the chemistry of the silole dianion, **65**, is still in its infancy. While essentially an unexplored area, the chemistry of this species is ripe for development and represents a very promising area for future work.

The wide variety of projects discussed herein is provided as a 'jumping-off' point for future synthetic and theoretical work.

References

1. Hui K. Y., Wu S. Y. and Mak T. C. W., *Chinese J. Struct. Chem.*, 1985, **4**, 148
2. Hui K. Y., Chan P. C. and Mak T. C. W., *Inorg. Chim. Acta*, 1984, **84**, 25
3. Morkan I. A., Guven K. and Ozkar S., *J. Organometallic Chem.*, 2004, **689**, 2319
4. Lopez C., Munoz-Hernandez M. A., Morales-Morales D., Del-Rio F., Hernandez-Ortega S., Toscano R. A., and Garcia J. J., *J. Organometallic Chem*, 2003, **672**, 58
5. Rogers R. D. and Alt H. G., *J. Crystallographic and Spectroscopic Res.*, 1993, **23**(6), 533
6. Aroney M. J., Clarkson R. M., Hambley T. W. and Pierens R. K., *J. Organometallic Chem.*, 1992, **426**, 331
7. Rodriguez M. L., Brito I. and Rodriguez-Romero F. V., *Acta Crysallogr.*, 1991, **C47**, 858
8. Cotton F. A., Darensbourg D. J., Fang A., Kolthammer B. W. S., Reed D. and Thompson J. L., *Inorg. Chem.*, 1981, **20**, 4090
9. Maher J. M., Beatty R. P. and Cooper N. J., *Organometallics*, 1985, **4**, 1354
10. R. Waterman and T. Don Tilley, *Chem. Commun.*, 2006, **38**, 4030
11. A. H. Cowley, *Acc. Chem. Res.*, 1997, **30**, 445
12. a) D. L. Coombs, S. Aldridge, C. Jones and D. J. Willock, *J. Am. Chem. Soc.*, 2003, **125**, 6356; (b) D. L. Coombs, S. Aldridge, A. Rossin, C. Jones and D. J. Willock, *Organometallics*, 2004, **23**, 2911; (c) D. L. Kay (nee Coombs), J. K. Day, L.-L Ooi and S. Aldridge, *Angew. Chem. Int. Ed.*, 2005, **44**, 7457; (d) S. Aldridge, C. Jones, T. G. Eichler, A. Stasch, D. L. Kay (nee Coombs), N. D. Coombs and D. J. Willock, *Angew. Chem. Int. Ed.*, 2006, **45**, 6118; (e) D. Vidovic, M. Findlater, G. Reeske and A. H. Cowley, *Chem. Commun.*, 2006, **36**, 3786
13. H. Saleske, Ph.D Dissertation, University of Wurzburg, 1983. Synthesized by reaction of Cp*Na with $SbCl_3$ in Et_2O at 0˚C; mp 151˚C; ^1H NMR δ 1.71.
14. Trinh-Toan; Dahl, L.F. *J. Am. Chem. Soc.,* 1971, **93**, 2654

15. Cullen, W. R.; Patmore, D. J.; Sams, J. R.; Newlands, M. J.; Thompson, L. K. *Chem. Commun.*, 1971, 952
16. (a) Maasbol, A; Fischer, E. O. *Angew. Chem.* 1964, **76**, 645. (b) Schrock, R. R. *J. Am. Chem. Soc.* 1974, **96**, 6796
17. Arduengo, A. J. III; Harlow, R. L.; Kline, M. *J. Am. Chem. Soc.*. 1991, **113**, 361
18. (a) Hill, N. J.; West, R. *J. Organomet. Chem*. 2004, **689***,* 4169. (b) Kühl, O. *Coord. Chem. Rev*, 2004, **248**, 411
19. Gemel, C.; Steinke, T.; Cokoja, M.; Kempter, A.; Fischer, R. A. *Eur. J. Inorg. Chem.* 2004, 4161
20. Although isolated examples of metal complexes featuring coordinated **2Si** and **2Ge** have been reported, there have been no sustained, systematic studies of the behavior of carbenoids as ligands
21. C. W. Bielawski and R. H. Grubbs, *Angew. Chem. Int. Ed.* 2000, **39**, 2903.
22. N. Tokitoh and R. Okazaki, *Coord. Chem. Rev.* 2000, **210**, 251 and references therein
23. S. Sole and F. P. Gabbaï, *Chem. Commun.* 2004, 1359
24. E. R. Burkhardt and K. Matos, *Chem. Rev.* 2006, **106**, 2617
25. D. Vidovic, M. Findlater and A. H. Cowley, *Dalton Trans.*, 2007, **129**, 8436
26. C.-M. Chiang, J. E. Rowe, R. A. Malic, A. Sen, M. L. Steigerwald and A. P. Mills, *App. Surface Sci.* 1996, **107**, 189
27. Meunier, In *The Chemistry of Organic Silicon Compounds*; (Eds.: Z. Rappoport, Y. Apeloig), John Wiley and Sons, Chichester, 1998, 1961
28. (a) W.-C. Joo, J.-H. Hong, S.-B. Choi, H.-E. Son and C. H. Kim, *J. Organomet. Chem.* 1990, **391**, 27; (b) J.-H. Hong, P. Boudjouk and S. Castellino, *Organometallics*, 1994, **13**, 3387; (c) J.-H. Hong and P. Boudjouk, *Bull. Soc. Chim. Fr.* 1995, **132**, 495; (d) U. Bankwitz, H. Sohn, D. R. Powell and R. West, *J. Organomet. Chem.* 1995, **499**, C7; (e) R. West, H. Sohn, U. Bankwitz, J. Calabrese, Y. Apeloig and T. Mueller, *J. Am. Chem. Soc.* 1995, **117**, 11608; (f) W. P. Freeman, T. D. Tilley, G. P. A. Yap and A. L. Rheingold, *Angew. Chem. Int. Ed. Engl.* 1996, **35**, 882; (g) R. West, H. Sohn, D. R. Powell, T. Müller and Y. Apeloig, *Angew. Chem. Int. Ed. Engl.* 1996, **35**, 1002

29. (a) B. Goldfuss, P. v. R. Schleyer and F. Hampel, *Organometallics* 1996, **15**, 1755; (b) B. Goldfuss and P. v. R. Schleyer, *Organometallics* 1997, **16**, 1543
30. (a) T. Wakahara and W. Ando, *Chem. Lett.* 1997, **26**, 1179; (b) T. Sanji, T. Sakai, C. Kabuto and H. Sakurai, *J. Am. Chem. Soc.* 1998, **120**, 4552
31. (a) H. Sohn, J. Merritt, D. R. Powell and R. West, *Organometallics* 1997, **16**, 5133; (b) I. S. Toulokhonova, T. C. Stringfellow, S. A. Ivanov, A. Masunov and R. West, *J. Am. Chem. Soc.* 2003, **125**, 5767
32. H. Sohn, M. J. Sailor, D. Magde and W. C. Trogler, *J. Am. Chem. Soc.* 2003, **125**, 3821
33. H. Sohn, *J. Organomet. Chem.* 2004, **689**, 134
34. H. Shirakawa, *Angew. Chem. Int. Ed.* 2001, **40**, 2574
35. P. Lenarets, A. Storms, J. Mullens, J. D'Haen, C. Görller-Walrand, K. Binnemans and K. Driesen, *Chem. Mater.*, 2005, **17**, 5194
36. For recent examples, see: (*a*) P. Preishuber-Pflugl and M. Brookhart, *Macromolecules* 2002, **35**, 6074; (*b*) M. D. Leatherman, S. A. Svedja, L. K. Johnson and M. Brookhart, *J. Am. Chem. Soc.* 2003, **125**, 3068; (*c*) A. E. Cherian, E. M. Lobkovsky and G. W. Coates, *Chem. Commun.* 2003, 2566; (*d*) W. Liu and M. Brookhart, *Organometallics* 2004, **23**, 6099; (*e*) D. H. Camacho, E. V. Salo, J. W. Ziller and Z. Guan, *Angew. Chem., Int. Ed.* 2004, **43**, 1821; (*f*) B. S. Williams, M. D. Leatherman, P. S. White and M. Brookhart, *J. Am. Chem. Soc.* 2005, **127**, 5132; (*g*) A. M. Kluwer, T. S. Koblenz, T. Jonischkeit, K. Woelk and C. J. Elsevier, *J. Am. Chem. Soc.* 2005, **127**, 15470; (*h*) D. H. Camacho and Z. Guan, *Macromolecules* 2005, **38**, 2544; (*i*) J. M. Rose, A. E. Cherian and G. W. Coates, *J. Am. Chem. Soc.* 2006, **128**, 4186
37. K. Vasudevan and A. H. Cowley, *Chem. Commun* 2007, 3464
38. P. Schwab, R. H. Grubbs and J. W. Ziller, *J. Am. Chem. Soc.* 1996, **118**, 100
39. M. Findlater, A. Powell, K. Vasudevan, I. Vargas-Baca and A. H. Cowley, *Dalton Trans*, Manuscript in preparation

VITA

Michael Findlater was born in Bellshill, Scotland in the United Kingdom on June 3, 1980, the son of Alexander and Rosina Findlater. After completing his work at Saint Ambrose High School he entered the chemistry program at The University of Strathclyde in Glasgow, Scotland. He received the degree of Bachelor of Science in June 2003. In August 2003 he entered the Graduate School of the University of Texas at Austin.

Permanent Address: 2 Castle Way, Bargeddie,
Glasgow, G69 7QG, Scotland, UK

This dissertation was typed by the author.